Isoelectric Focusing with Simple Buffers:

Studies of Liver Alcohol Dehydrogenase and Its Complexes with Ligands

by

A. David Hausfeld

A dissertation submitted to the Graduate Faculty in Biomedical Sciences in partial fulfillment of the requirements for the degree of Doctor of Philosophy, The City University of New York

1996

This manuscript has been read and accepted for the Graduate Faculty in Biomedical Sciences in satisfaction of the dissertation requirement for the degree of Doctor of Philosophy.

9/15/96
Date

Prof. A. Cederbaum, Chair of Examining Committee

9/18/96
Date

Prof. T. A. Krulwich, Executive Officer

Prof. J. B. A. Ross

Prof. W. R. Laws

Prof. R. Kohanski

Prof. M. Sassaroli

THE CITY UNIVERSITY OF NEW YORK

Table of Contents

Figures

Tables

Overview

A primary objective of this work was to develop an improved method for isoelectric focusing of proteins. The established methods, carrier ampholyte gels and immobilized pH gradient gels, have been very successful in a range of applications. However, carrier ampholyte methods have several serious problems which include carrier ampholyte binding to focusing proteins, an unstable pH gradient, particularly in alkaline pH ranges, and a low and poorly defined ionic strength environment in which many proteins are insoluble. The immobilized pH gradient methods have problems which include proteins binding to the charged gel matrix. Both methods require that salts be removed from the focusing environment.

The focusing method that was developed as part of this work employs an ion-selective membrane in a manner that establishes a pH gradient with simple buffer systems. This eliminates difficulties with carrier ampholyte binding to proteins, the pH gradient instability, and the low ionic strength environment. Furthermore, this method does not require a charged gel matrix. An important attribute of this new method

that previous methods do not have is that the pH gradient may be formed in the presence of relatively high concentrations of salts. This allows isoelectric focusing to be applied to the study of weak binding of charged ligands to proteins, which requires high concentrations of a charged ligand in the focusing environment.

A second objective of this work was to evaluate one of the current theoretical procedures for calculating protein isoelectric points. This was approached by comparing calculated isoelectric points with experimentally measured isoelectric points. In order to compare theory with experiment it is necessary to have a well-defined ionic strength in the medium in which the protein is isoelectric; this is provided with the focusing method developed as part of this work. The comparison was carried out for a well-characterized protein for which precise structural information is available from x-ray crystallography. The protein selected was alcohol dehydrogenase from horse liver (LADH). This protein forms several well-characterized complexes with ligands; therefore in addition to comparing calculated and measured isoelectric points, calculated shifts in isoelectric point accompanying

complex formation may also be compared with experimental values.

More specifically, it has been hypothesized that the interior of a protein has an effective dielectric constant of approximately 20 that takes into account flexibility in protein structure; this value is significantly higher than what would be expected from dessicated protein powders, i.e, 2 to 4. Accordingly, theoretical calculations of isoelectric points with dielectric constants of both 4 and 20 were carried out and compared with experimentally measured isoelectric points to determine which dielectric constant is more appropriate.

A final objective of this work was to employ the new isoelectric focusing method to gain new and important information about a biologically important protein. The protein chosen was again LADH. Improved characterization of this enzyme would have a direct bearing on the all important understanding of alcohol metabolism. Additionally, a better understanding of this enzyme and its catalytic mechanisms may lead to important insights involving a large class of

dehydrogenases.

Specifically, it has been found that the association rates for both oxidized and reduced coenzyme decrease with increasing pH even though at equilibrium oxidized coenzyme binds more tightly with increasing pH whereas reduced coenzyme binds more weakly with increasing pH. A hypothesis proposed by others to account for this is as follows: the protein undergoes a pH-dependent conformational change such that access to the coenzyme binding site is more restricted at higher pH. This pH-dependent conformational change is proposed to occur in a range where the protein is isoelectric. Evidence that would support this hypothesis would be a finding that LADH and/or one or more of its complexes with coenzyme, substrate or known inhibitors have more than one isoelectric point. From the theory of protein titration curves one conformation of a protein should have only one isoelectric point. Isoelectric focusing experiments have therefore been carried out in search of multiple isoelectric points.

Part 1. The Membrane Isoelectric Focusing Method (MIEF).

Introduction

Isoelectric Point

The isoelectric point which reflects the surface charge properties of a protein is an ideal parameter to further characterize the conformational states of a protein in solution. The effective dissociation constants (pKa's) of acid dissociating groups substantially determine the value of the isoelectric point. The effective pKa's of these groups depend upon their microenvironments. The proximity of an acid dissociating group to other charged groups may affect the pKa; the effective dielectric constant, resulting from surrounding polar or hydrophobic moieties, also may influence the pKa. Some acid dissociating groups may be buried within the protein either in hydrophobic environments or in salt bridges; these groups may indirectly affect the isoelectric point. In a representative sample of 36 globular proteins, 95% of the ionizable groups were exposed to the solvent; 5% were buried in salt bridges (1). Also, the ability of small ions to bind

to a particular protein conformation is directly reflected in the isoelectric point.

It is expected then that the isoelectric point should be sensitive to conformational changes. These changes may involve variations in the proximity of one group to another. Potentially ionizable groups that are buried in hydrophobic environments or salt bridges in one conformation, may be exposed to solvent in another conformation. One conformation may bind small ions from the solvent more tightly than another.

A method of choice for measuring the isoelectric point of a protein is isoelectric focusing (2,3). Briefly, a protein is allowed to migrate under the influence of an electric field in a medium in which there is a gradient of pH. The protein then condenses at a place where the pH equals the isoelectric point of the protein. With the most prevalent method of isoelectric focusing, the pH gradient is established with the use of a large spectrum of amphoteric molecules with high buffering capacity usually referred to as carrier ampholytes. The carrier ampholytes commonly used are an ill-defined mixture of relatively high molecular weight species. One example is a

broad spectrum of polyamino-polycarboxylic acids synthesized by reacting different proportions of acrylic acid with a variety of polyethylene polyamines (4).

One important advantage of isoelectric focusing is that the measured shifts in isoelectric point may be unambiguously attributed to one isoform of the protein. Another advantage is that this method allows low protein concentrations to be used to measure isoelectric points; the limiting factor is the ability to detect the presence of the protein. It should be mentioned, however, that due to zero net charge at the isoelectric point, proteins may interact in unexpected ways because they no longer repel each other. If this appears to happen, protein concentrations may be lowered further.

Analytical Applications - Protein Conformation

Measurements of isoelectric points using isoelectric focusing with carrier ampholytes have been used to a limited extent to characterize protein conformational changes. For example, the modification of alpha-chymotrypsin by L-1-tosylamido-2-phenylethyl chloromethyl ketone (TPCK) results in a shift in

isoelectric point from 8.75 to 8.91 (5). The addition of TPCK to the enzyme is not expected to alter its charge. Therefore a conformational change resulting in a perturbed pK is the likely explanation. Theoretical considerations similar to those outlined above suggest that the perturbed pKa is that of an alpha amino group of an isoleucine residue at the end of the B chain.

Additionally, a conformational change in hemoglobin due to the Bohr effect was demonstrated by separating deoxyhemoglobin and oxyhemoglobin from a mixture of partially oxygenated material by isoelectric focusing also with carrier ampholytes. Oxyhemoglobin was found to have an isoelectric point of 6.95, and deoxyhemoglobin an isoelectric point of 7.15. Theoretical considerations suggest that a closer proximity of an aspartate residue increases the pKa of a histidine residue thereby increasing the isoelectric point for deoxyhemoglobin (6,7).

Problems with Established Methods

Although isoelectric focusing with carrier ampholytes has resolved a number of conformational states, the carrier

ampholyte system has several adverse characteristics. For one, there is the problem of the cathode drift (8). The pH gradient established with carrier ampholytes has a slow drift toward the negative electrode. This phenomenon is most pronounced in anti-convective matrices (e.g., polyacrylamide and agarose gels). It affects alkaline pH ranges substantially more than neutral or acid ranges. It is most deleterious with shallow pH gradients where the highest resolution is being sought. This drift is not well understood theoretically. Some investigators attribute this phenomenon to electroosmosis as a result of residual negative charges bound to the matrices (9). Others attribute the problem to more fundamental aspects of electrical and diffusional mass transports that may not be balanced (10).

Another difficulty with carrier ampholytes is their potential to form complexes with proteins. These ampholytes have been shown to bind to human growth hormone (11) and to bovine serum albumin (12,13). Additionally, carrier ampholytes are known to chelate metal ions (14). Moreover, the carrier ampholytes provide a low ionic strength environment for proteins. As a rule, proteins are least soluble at their isoelectric points.

The low ionic strength environment causes many proteins, in particular, globulins, to precipitate (15).

The immobilized pH gradient method, a less commonly used method for isoelectric focusing (16), employs a polyacrylamide gel with varying concentrations of buffering groups covalently bound to the gel matrix to generate the pH gradient. This method eliminates problems with instability in the pH gradient; it has been successful in a range of analytical and preparative applications. However, there are problems with this method also. For example, certain proteins have been shown to bind to the charged gel matrix thus preventing their migration to their isoelectric points (17). When used preparatively, proteins eluted from these gels are often chemically modified or contaminated as a result of having a residue of unconsumed reactants involved in gel polymerization (18).

IEF with Simple Buffers - Previous Attempts

Several efforts have been made to establish pH gradients without either carrier ampholytes or immobilized pH gradients.

One method employs a collection of well-defined, low molecular weight amphoteric and non amphoteric species to establish a pH gradient in a manner similar to that with carrier ampholytes (19). This method is suitable only for steep pH gradients and is still complicated by the cathode drift phenomenon.

Another approach involves establishing a pH gradient by imposing a temperature gradient on an otherwise constant buffer solution such as Tris-HCl (20). The effects of temperature on the pK's of the buffering species result in the pH gradient. Slopes of pH gradients vary from, for example, a pH difference of 0.028 per degree centigrade for Tris-HCl down to a pH difference of 0.003 per degree centigrade for phosphate. Complications arise here because isoelectric points of proteins also vary with temperature for the same reasons. Furthermore, there are serious difficulties involved in creating a stable thermal gradient in the presence of the joule heating associated with electrophoresis. Also, since a majority of common buffers provide the more shallow pH slopes with temperature, certain protein isoforms may have to be subjected to unsatisfactory temperatures for prolonged periods.

Still another approach has been taken to provide a stable pH gradient with simple buffers. This method involves establishing a buffer system for which each constitutive ion maintains a constant transport number (21). The transport of ions by electromigration and diffusion within an anti-convective matrix is then balanced by carefully metered flows of buffer solutions between electrode chambers. If ion transport is balanced, a theory predicts that a steady state will be obtained providing a stable pH gradient. This theory, however, ignores transport of protons and hydroxyl ions, which have a significant effect even at low concentrations because they have very high mobilities in electric fields. Also, discontinuities at the interfaces of the anti-convective matrix and the electrode chambers, has not been taken into account. For these reasons, it is believed, this approach has not as yet resulted in a useful system (22).

Alternatives to IEF

It is appropriate here to make a few comments about methods other than isoelectric focusing that may provide similar information about either shifts in pKa's or shifts in the

binding of small charged ligands, that may accompany conformational changes. Direct titration of bound or released protons is one such method (23). This type of measurement requires relatively high protein concentrations (e.g., 0.1 mM) for adequate sensitivity. Possibilities of protein-protein interactions and other effects due to anomalous activity coefficients have to be considered at these high protein concentrations.

To measure shifts in the binding of small charged ligands, one might consider using equilibrium dialysis methods (23). Here again, relatively high protein concentrations are necessary for adequate sensitivity. In addition, complications resulting from variations in protein partial specific volumes and solvent penetration, and effects due to Gibbs-Donnan equilibria, have to be considered. Moreover, weak binding may be very difficult to measure because of the low ratio of bound to free ligand. Spectroscopic and magnetic resonance methods may be more sensitive here if characteristic effects due to the bound ligand can be discerned, but these may be confusing as a result of multiple binding sites per protein molecule. ^{35}Cl NMR studies have been of some limited use to characterize

the binding of Cl ions to the active site zinc of LADH (24).

Another method, presently being developed, that is capable of measuring shifts in the binding of small charged ligands is equilibrium electrophoresis (25). This method, which is analogous to equilibrium sedimentation, involves an electrolyte solution containing the protein of interest and an applied electric field. A barrier that is impermeable only to the macromolecule is placed perpendicular to the electric field. This brings about an equilibrium concentration distribution where macromolecular electromigration is balanced by diffusion. The apparent charge of the macromolecule, including bound ligands, may then be deduced from this concentration distribution. At this time the advantages and difficulties of this method are not fully known.

Isoelectric focusing should be capable of detecting the weak binding of small charged ligands. Furthermore, by carrying out isoelectric focusing experiments in the presence and absence of a particular charged ligand, the shifts in isoelectric point due to ligand binding may be differentiated from those due to shifts in pKa's. This, however, would require an

isoelectric focusing system that provides a stable pH gradient in the presence of an adequate concentration of charged ligand. As a pratical matter, neither the carrier ampholyte method nor the immobilized pH gradient method allows a presence of adequate concentrations of small charged ligands in the focusing environment.

Membrane Isoelectric Focusing (MIEF)

The isoelectric focusing method that was developed as part of this work is described as follows. A shallow pH gradient is established in a thin granulated gel bed supported by a cation selective membrane of the type commonly used for electrodialysis (26) (a membrane permeable only to small cations). This membrane is positioned over a deep buffer-filled channel with a sloping bottom. An important feature of the experimental arrangement is that parallel components of the electric field (components parallel to the gel and membrane surfaces) may be considered fixed at any given position along the gel bed (independent of the variable buffer composition in the gel), but these components do vary from one position to another by increasing as the depth of the buffer

channel below decreases. This feature together with the cation selective property of the supporting membrane can account for the steady-state pH gradients obtained with this experimental arrangement. Specifically, if complicating factors such as diffusion, electroosmosis, and the transport of hydrogen and hydroxyl ions are neglected, and the cation selective membrane is considered to be absolutely impermeable to anions of the buffer, it is straightforward to show that the electric field will establish a steady-state along the gel bed where the anion flux (anions crossing unit cross-sectional area per unit time) is uniform. As the anion flux at any given position in the gel is proportional to both the concentration of anions and the parallel component of the electric field at that position, the steady-state anion concentration as a function of position along the gel will be inversely proportional to the parallel component of the electric field. To satisfy the condition of electroneutrality, the counter ion concentration will also be inversely proportional to the parallel component of the electric field. In effect, the experimental arrangement imposes an electric field gradient in the gel bed which then generates ion concentration gradients. These ion gradients, which are gradients of buffer components, generate the pH

gradient. As an example, a pH gradient may be obtained with a glycine/NaOH buffer system, where concentration gradients of glycine anions and sodium cations are established in a gel bed containing a uniform concentration of neutral glycine. A more detailed discussion of how this experimental arrangement establishes a steady-state pH gradient is presented in the Appendix.

Materials and Methods:

The Apparatus

A schematic cross-sectional diagram of the apparatus is shown in figure 1. The gel indicated was in the form of a thin rectangular slab of uniform thickness. Anode and cathode electrodes were parallel platinum wires. The apparatus, constructed out of acrylic plastic, was divided into three rectangular connecting chambers: anode, cathode, and gel. The anode and cathode chambers were separated from the gel chamber by dialysis membranes (Spectrapor, 8000 MWCO, Spectrum Medical Industries, Los Angeles, CA, USA). A wedge-shaped block of acrylic held under the central portion of the gel formed a wide channel with a sloping bottom. The channel was 34 cm wide, 7.5 cm long, and had a depth varying from 0.8 cm to 3 cm (depth increasing toward the cathode). The gel bed was supported by a composite membrane stretched and clamped on all sides over the gel chamber. The central portion of the composite consisted of (from the top) a dialysis membrane layer (same material as above), a polyester mesh layer (commonly used for screen printing, ISO 9001, monofilament, 43

divisions per cm, Saati, Como, Italy), a perfluorosulfonic acid cation selective membrane layer (Nafion 423 Du Pont, Wilmington, DE, USA), and a second dialysis membrane layer (same as above).

Figure 1. Schematic of the apparatus in cross-section with sloping buffer channel (1), cation-selective membrane (2), composite supporting membrane (3), gel bed (4), clamps for securing composite membrane (5,6), dialysis membranes (7,8), and anode and cathode electrodes (9,10).

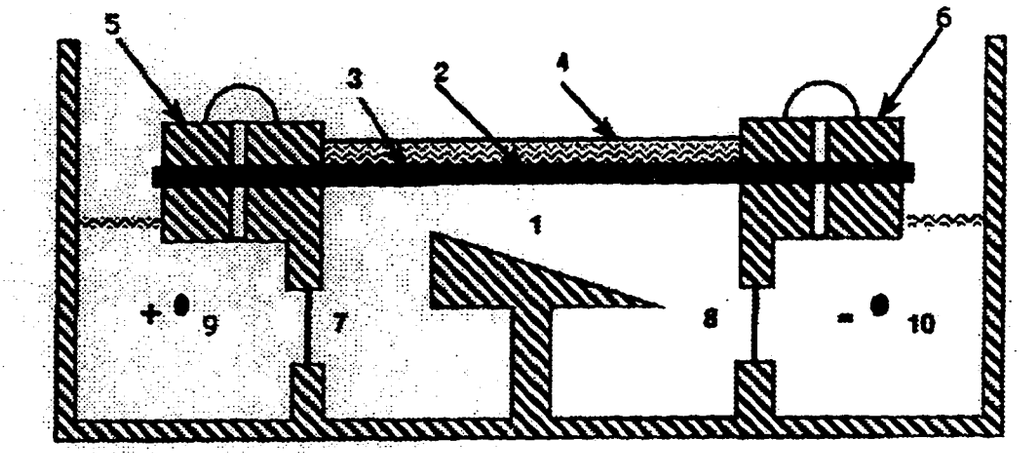

Fig. 1

The anode and cathode end portions of the composite consisted of the same layers minus the cation membrane. The uppermost dialysis membrane layer prevents proteins in the gel from contacting the cation selective membrane. The polyester mesh layer provides structural support, and the lower dialysis membrane layer facilitates the sealing of the composite over the gel chamber. Layers were spaced by thin films of starting buffer (see below); i.e., no binders were used. The central portion of the 34 cm wide composite measured 7.5 cm in length; the anode and cathode end portions each measured 2 cm in length. Cross-sectional dimensions of the apparatus (figure 1) were constant from side to side so that there was little transverse variation of the electric field.

Buffers and Gels

Anode, cathode, and gel chambers were filled with identical buffer solutions held at a constant composition and temperature (10° C) by rapid recirculation (greater than 500 ml per minute) through refrigerated buffer reservoirs (6 liters for a common reservoir for anode and cathode chambers

and 6 liters for a gel chamber reservoir). Buffer solutions in the recirculation systems were electrically insulated and kept away from metallic surfaces through the use of magnetically coupled chemical pumps and heat exchangers constructed with thin walled Teflon tubing. All buffer components were of reagent grade, and solutions were prepared with deionized water. The composite membrane layers were carefully assembled, and the composite membrane carefully sealed over the gel chamber so as to avoid trapping air bubbles between the layers or below the composite. The gel for each experiment, Sephadex G-75 SF (Pharmacia, Uppsala, Sweden), was swelled with starting buffer of the same composition as that in the buffer reservoirs, to a consistency of a thick slurry, poured over the composite supporting membrane, and formed into a rectangular slab having a uniform 2 mm thickness; the slab was formed by leveling the gel slurry with a straight-edge over 2mm thick spacers (rectangular gel beds occupied the full 11.5 cm length of the composite membrane, but gel widths for particular experiments varied in a range up to the full 34 cm width of the composite membrane). The liquid content of the gel need not be carefully adjusted, as the gel will equilibrate with the solution below the supporting membrane.

A constant voltage was applied to obtain an electric field strength in the gel bed (parallel to the gel surface in the direction from anode to cathode) varying from 3 V/cm to 10 V/cm over the cation membrane. Although not shown in figure 1, the apparatus included a loose fitting lid to limit evaporation from the gel surface.

Proteins and pH Measurement

Isoelectric focusing experiments are reported here for the following well-characterized proteins (lyophilized): bovine pancreatic ribonuclease A (Serva, Heidelberg, Germany); horse skeletal muscle myoglobin (no longer available from original source, equivalent, Sigma Chemical Co., St. Louis, MO, USA); bovine ß-lactoglobulin (Serva); chicken ovalbumin (Serva). For ribonuclease, ß-lactoglobulin, and ovalbumin, the gel was run without protein for 3 hours with the electric field strengths as above to insure that pH values were established in the gel that would prevent protein from migrating off the cation membrane; then protein solutions (approximately 3 mg protein in 0.5 ml buffer) were gently applied in the form of droplets

to a transverse strip of gel surface (approximately 6 to 8 cm^2) over the cation membrane located between 1.5 and 3.0 cm from its cathode edge. For myoglobin the protein was mixed with the gel slurry (approximately 0.2 mg/ml) that was subsequently formed into the gel bed. Ribonuclease was focused in two separate experiments with starting buffers consisting of a 6 mM glycine solution adjusted with NaOH to 6 mM Na, and a 12 mM glycine solution adjusted with NaOH to 12 mM Na. These were empirically determined to give an appropriate pH gradient. The protein solutions applied to the gel for each experiment were prepared with a 6 mM glycine solution adjusted with NaOH to 3 mM Na, and a 12 mM glycine solution adjusted with NaOH to 6 mM Na, for the 6 mM glycine and the 12 mM glycine starting buffers, respectively; the starting buffers have a pH too extreme for exposure to protein (the 3 hour pre-run of the gel also insured that protein would not be exposed to an extreme pH). ß-lactoglobulin was focused with a starting buffer consisting of a 10 mM MES (2-[N-morpholino]ethane sulfonic acid) solution adjusted with NaOH to 3 mM Na, and the protein solution applied to the gel was prepared with the same MES starting buffer. Similarly, ovalbumin was focused with a starting buffer consisting of a 7 mM acetic acid solution

adjusted with NaOH to 5 mM Na, and the protein solution applied to the gel was prepared with the same acetate starting buffer. Myoglobin was focused with a starting buffer consisting of a 9 mM imidazole solution adjusted with HCl to 3 mM Cl. The polarity of the electric field was reversed for the imidazole/HCl buffer so that the low field was at the anode edge of the cation membrane. No effort was made to characterize these proteins beyond the description given by the vendors.

The pH gradients were measured, as follows, after running gels under identical conditions but omitting protein: transverse gel sections (each approximately 1 cm of gel length in the anode to cathode direction) were harvested and thoroughly mixed; pH was then determined by immersing a flat surface combination pH electrode (476216, Corning Glass Works, Corning, NY, USA) into each gel sample. After focusing, protein patterns were detected as follows: strips of dry filter paper (Whatman 1) were inserted vertically into the gel bed along the direction of the electric field so that a single strip would record all focused protein bands in the gel. Protein is brought up into the paper as a result of capillary

flow of solvent. Strips were withdrawn before the solvent front reached the top of each strip. They were then fixed and stained with Coomassie Blue R 250 as previously described (27). Transverse sections of the gel bed (each approximately 0.7 cm of gel length in the anode to cathode direction) were then harvested at selected positions, protein eluted with buffer used to prepare original protein solutions, concentrated (Centricons, Amicon, Danvers, MA, USA) and applied to pre-cast polyacrylamide / carrier ampholyte gels (Precotes, pH range 3 - 10, Serva) that were run and stained with Coomassie Blue R 250 as recommended by the vendor.

Results

Ribonuclease

The pH gradient obtained with the 6 mM glycine buffer for focusing ribonuclease had a range of 8.4 to 9.2 as shown in figure 2. The pattern of focused ribonuclease observed with a Coomassie stained strip is shown in figure 3A. Two sharply defined intensely staining components are revealed, a broad component (higher pH) separated from a narrow component by a zone of low staining intensity. The presence of the low intensity zone suggests that there may have been a slow shift in isoelectric point of one or more of the proteins in the gel. The minor component at the anode edge of this and other strips is an artifact due to protein accumulation beyond the anode edge of the cation membrane that is often observed with these experiments. A major component with an isoelectric point of 8.9 and one or more minor components at lower isoelectric points, one known to be glycosylated, are commonly observed with carrier ampholyte focusing of ribonuclease A (27). Six gel sections were harvested between the positions indicated by arrows. Protein was eluted from these sections, and samples

applied to a pre-cast IEF gel, which is shown in figure 4. The sample applied to lane 3 clearly contained only the more acidic component; samples applied to lanes 6 and 7 contained only the more basic component.

Figure 2. pH gradients obtained with the following buffer systems: 6 mM glycine adjusted with NaOH to 6 mM Na; 9mM imidazole adjusted with HCl to 3 mM Cl; 10 mM MES adjusted with NaOH to 3 mM Na; 7mM acetic acid adjusted with NaOH to 5mM Na (harvested gel fractions for pH determinations were centered at positions indicated, measured from anode edge of cation membrane).

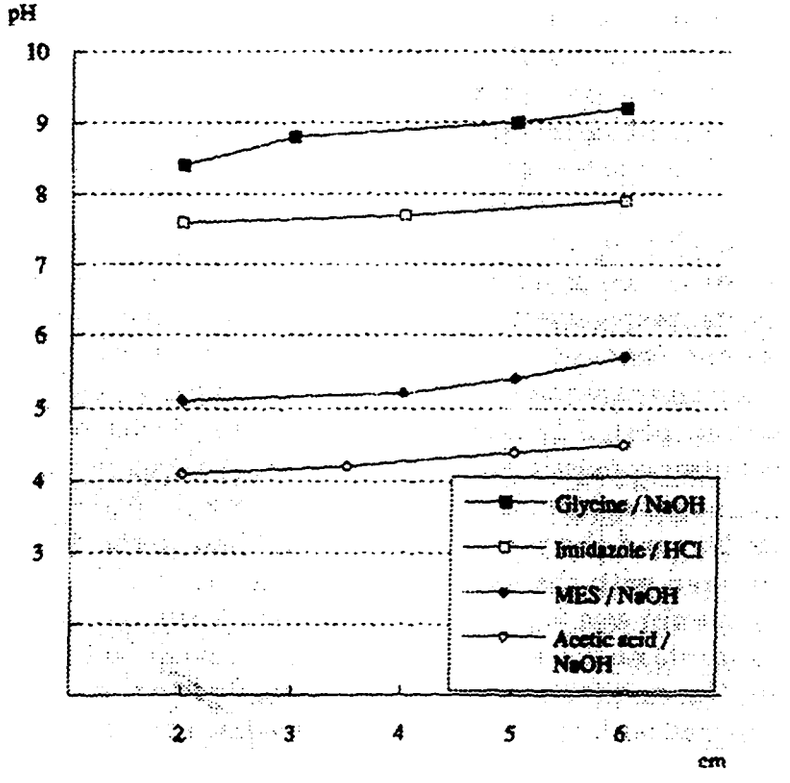

Fig. 2

Figure 3. Coomassie-stained strips. A. ribonuclease (6 mM glycine, arrows indicate positions 1 and 5 cm from anode edge of cation membrane, after 14 hours); B. ß-lactoglobulin (10 mM MES, arrows indicate positions 4 and 5 cm from anode edge of cation membrane, after 16 hours); C. ovalbumin (7 mM acetic acid, arrows indicate positions 4, 5, and 6 cm from anode edge of cation membrane, after 18 hours). Bottom edges of paper strips were cut with a slight curvature to accomodate a curvature of the gel bed due to increased pressure below the supporting membrane.

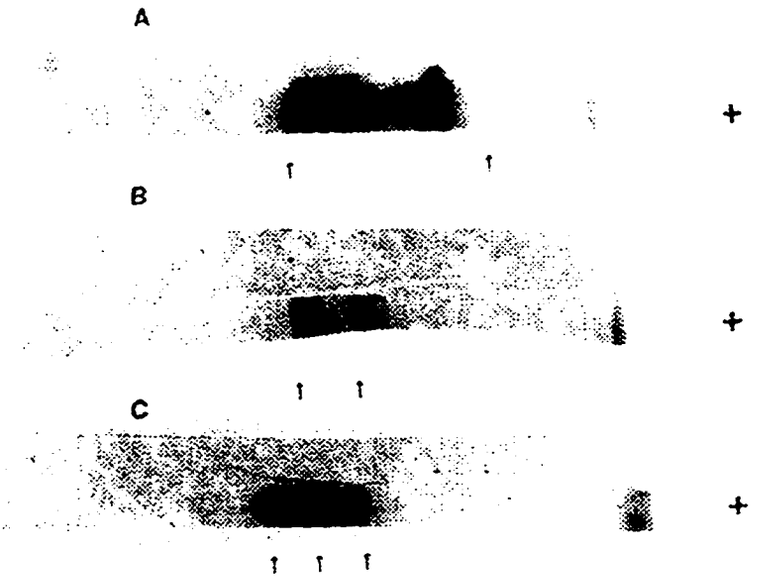

Fig. 3

Figure 4. Focused fractions of ribonuclease rerun on carrier ampholyte gel. Lane 1, starting proteins; lanes 2-7, six consecutive fractions harvested between positions indicated by arrows of Fig. 3 A (lane 2 most acid fraction).

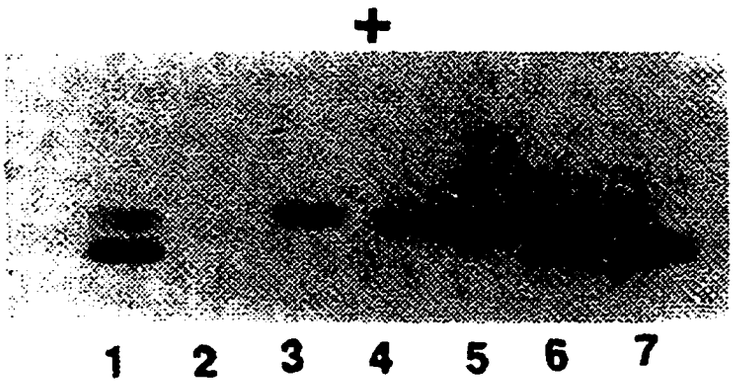

Fig. 4

Figure 5. Coomassie-stained strips for ribonuclease, 12 mM glycine, after 12 hours (A) and 18 hours (B).

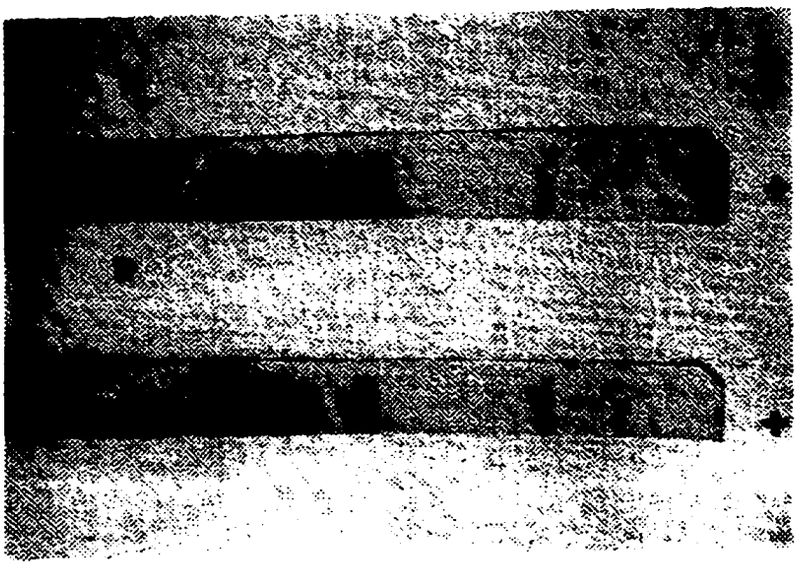

Fig. 5

Figure 6. Focused fractions of ß-lactoglobulin rerun on carrier ampholyte gel. Lane 1, starting protein (more intense top band due to protein precipitated in sample well); lane 2, fraction harvested at the basic position indicated by arrow in Fig. 3 B; lane 3, fraction harvested at the acidic position indicated by arrow in Fig. 3 B.

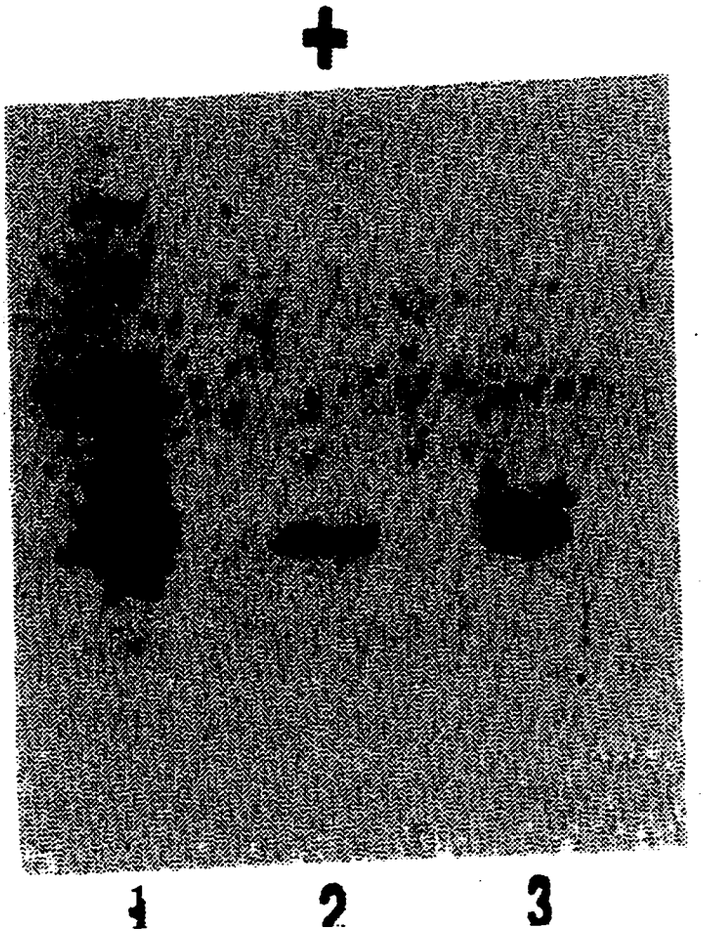

Fig. 6

Figure 7. Focused fractions of ovalbumin rerun on carrier ampholyte gel. Lanes 1 and 2, fraction harvested at most acidic position indicated by arrow in Fig. 3 C; lanes 3 and 4, fraction harvested at middle position indicated by arrow in Fig. 3 C; lanes 5 and 6, fraction harvested at most basic position indicated by arrow in Fig. 3 C; lane 7, starting protein.

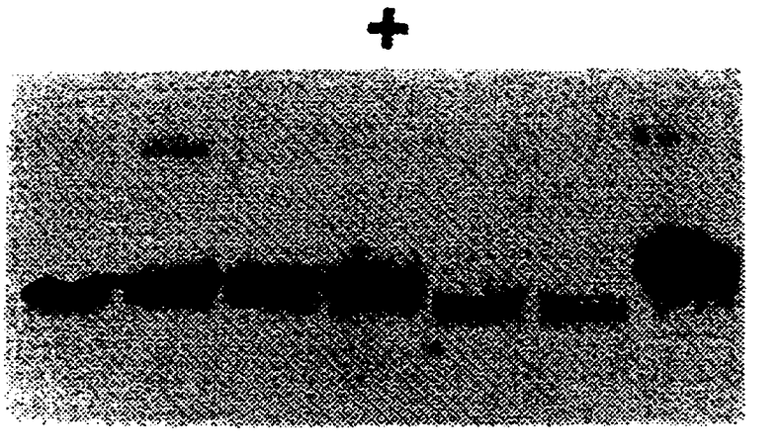

Fig. 7

Figure 8. Photographs of focused myoglobulin after 20 hours (A) and 40 hours (B).

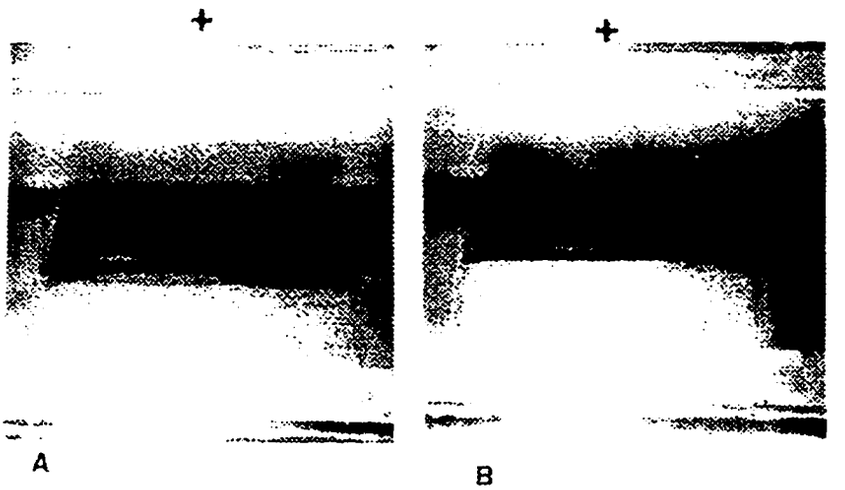

Fig. 8

These results confirm the separation of the components of ribonuclease. The stability of pH gradients in the alkaline range is illustrated with the focusing of ribonuclease with the 12 mM glycine buffer. Protein patterns observed after 12 and 18 hours are shown in figure 5. The patterns were substantially unchanged with a broad component at a higher pH spaced from a narrow component. These patterns, however, suggest the possibility of discrete transient components in the intervening space that may be due to deamidation, formation of dimers, or conformational changes. Comparison of the patterns in figures 3A and 5 illustrates the reproducibility of the protein patterns. Additionally, it should be noted that the protein pattern obtained with the 12 mM glycine buffer is shifted toward the cathode relative to the pattern obtained with 6 mM glycine. This corresponds to a shift of the pH gradient downward by approximately three tenths of a pH unit.

β-Lactoglobulin

The pH gradient obtained with the 10 mM MES buffer for focusing ß-lactoglobulin had a range of 5.1 to 5.7 as shown in figure 2. The resulting pattern of focused ß-lactoglobulin is shown in figure 3B, demonstrating two major components. Two gel sections were harvested at the positions indicated by arrows. Protein was eluted and samples applied to a pre-cast IEF gel; results are shown in figure 6. This protein, a dimer of identical subunits, occurs in primarily two genetic forms, A and B, with isoelectric points of 5.1 and 5.3, respectively, as determined with carrier ampholyte gels (27,28). The more basic gel section clearly contained only the B genetic form, as shown on the pre-cast gel, thus confirming a separation. It is unclear, however, why the A form had not been isolated in the more acidic gel section. This may result from a tendency of this protein to aggregate to multimeric forms containing both variants; the A form has the greater tendency to do so (29).

Ovalbumin

The pH gradient obtained with the 7 mM acetate buffer for focusing ovalbumin had a range of 4.1 to 4.5 as shown in figure 2. The resulting pattern of focused ovalbumin is shown in figure 3 C. Three gel sections were harvested at the positions indicated by arrows. Protein was eluted and samples applied to a pre-cast IEF gel. Results are shown in figure 7. The band patterns in the pre-cast gel are complex, as may be expected for IEF of ovalbumin which focuses into a large number of components between pH values of 4.2 and 5.2 as demonstrated with immobilized pH gradient gels (16). Nevertheless, the protein of each gel section yielded a distinctly different pattern, which confirms a separation of the starting material. The complexity of these patterns and the observation that many bands occur in overlapping pH ranges suggest that parts of these patterns may be artifacts due to protein-protein interactions or to the binding of carrier ampholytes to the protein.

Myoglobin

To illustrate the patterns of a focused protein more directly, myoglobin, a colored protein, was focused with the 9 mM imidazole buffer. The pH gradient obtained had a range of 7.6 to 7.9 as shown in figure 2. The gel was run for a total of 40 hours. Photographs of the gel as it appeared in the apparatus were taken after 20 and 40 hours and are shown in figures 8A and 8B. The patterns after 20 and 40 hours appear to be almost identical except for the disappearance of the most basic component (a sharp band located approximately halfway across the cation membrane) after 40 hours. This disappearance is accompanied by an increase in the intensity of the sharp band just above. These differences may be due to several factors which include shifts in the oxidation state of the heme, deamidation of an amino acid residue, or a conformational change. The broad protein bands observed here may be expected, since previous IEF studies of myoglobin with carrier ampholytes have demonstrated broad as well as sharp bands in a range of pH values from 6.8 to 7.8 (30). The width of the broad bands here (several centimeters) are expected to be

quite large, as the pH gradient is shallow. The fact that the protein pattern remained substantially constant over an extended interval confirms the stability of the pH gradient.

Discussion

The results presented above demonstrate that the membrane isoelectric focusing method (MIEF) introduced here is comparable to isoelectric focusing with carrier ampholytes. Although the pH gradients demonstrated are shallow, they are obtained in widely diverse pH ranges. Also, other experiments have shown that the pH gradient obtained with each buffer system may be shifted up or down by adjusting the composition of the starting buffer to higher or lower pH values. In addition, similarly shallow pH gradients have been obtained with other buffer systems: glycylglycine/NaOH, BICINE (N,N-Bis [2-hydroxyethyl] glycine)/NaOH, Hepes/NaOH, NaH_2PO_4/Na_2HPO_4, and Tris/HCl (polarity of the electric field is reversed for Tris/HCl). Thus useful pH gradients may be obtained over large portions of the pH range covered by carrier ampholytes. It should be noted that similar pH gradients have been obtained using other cation selective membranes (for example, the Ionics 61-AZL-386 membrane, Ionics, Watertown, MA, USA) with many of the buffer systems listed above. However, it has been observed that there are shifts in pH values of several tenths over the gradient range with changes to alternate membranes

using the same buffer system. It has also been observed that buffer ion concentrations vary substantially with changes to alternate membranes. These effects may be attributed to membrane polarization effects discussed at length elsewhere (31). The Nafion membranes are preferable, since they do not need to be stored in a wet state to retain their ion selective properties. To obtain an appropriate pH gradient for focusing a specific protein with a known isoelectric point, a buffer system was selected having a pK generally within one pH unit of the isoelectric point of the protein. Buffer composition was then adjusted in a trial and error approach to the desired pH gradient. The pH of the appropriate buffer was generally less than one pH unit above the pH range of the desired gradient, and concentrations of buffering species used were generally in the 5 to 20 mM range. For a given buffer composition, pH gradients obtained in separate experiments usually varied up or down by no more than one or two tenths of a pH unit. Maintaining the ratios of buffer components, but varying concentrations over the 5 to 20 mM range, resulted in shifts of the pH gradient in many cases of no more than five tenths of a pH unit. This is illustrated with the focusing of ribonuclease where the 12 mM glycine pattern is shifted toward

the cathode relative to the 6 mM glycine pattern by an amount corresponding to approximately three tenths of a pH unit.

Resolution obtained with MIEF is comparable to resolution with carrier ampholytes. For example, the MES/NaOH buffer system used for ß-lactoglobulin has demonstrated the potential to clearly resolve protein components that differ in isoelectric point by as little as 0.05 pH units. This follows from consideration of the width of the basic component of ß-lactoglobulin which is less than 0.5 cm as observed with a Coomassie stained strip (figure 3B), and the slope of 0.1 pH units per cm for the associated pH gradient (figure 2). Similarly, the imidazole/HCl system used for myoglobin has clearly resolved components that differ in isoelectric point by as little as 0.06 pH units. This follows from consideration of the spacing of 0.7 cm (peak to peak) between the most basic component of myoglobin and the adjacent component (figure 7A), and the slope of 0.08 pH units per cm for the pH gradient. This may be compared with a theoretical limit for resolving myoglobin components with carrier ampholytes that has been given as 0.02 pH units of difference in isoelectric point (32).

An interesting phenomenon related to resolution that is being explored further involves the concentration distribution of a focused protein component. From the theory of isoelectric focusing (33), the concentration distribution for an individual protein species is gaussian and may be given by the equation

$$C(x) = C(0) \exp (-p E x^2 / 2D)$$

where C(x) is protein concentration as a function of position x; C(0) is the peak protein concentration; p is the slope of the pH dependent protein mobility versus position curve; E is the electric field strength, and D is the diffusion coefficient for the protein. For ribonuclease under the given experimental conditions, the theory predicts a focused band width of less than 1 mm (taken between concentrations of 1/2e on either side of the peak). The experimentally determined distributions for the main focused band of ribonuclease, figures 3 and 5, lowest pH band, have widths of the order of 1 cm, which is substantially broader than the theoretical values even when allowances are made for band spreading

associated with the measurement process. These broad distributions may be a consequence of transitions linking two or more conformational states. Extensive theoretical models (34) for isoelectric focusing of proteins that undergo conformational changes or changes of states of aggregation suggest that these proteins, when focused, have concentration distributions that are complex. For example, proteins assumed to undergo pH dependent conformational changes, such that they have multiple isoelectric points, can have equilibrium (focused) concentration distribution patterns with multiple peaks, each corresponding to the isoelectric point of a particular conformation. To investigate this phenomenon further, more precise methods are being developed to measure the steady-state protein distributions and pH gradients; these methods include measuring spectral absorption characteristics directly in the gel bed. Also, efforts are being made to improve the resolution of MIEF by increasing electric field strengths and adjusting other parameters.

MIEF allows isoelectric focusing to be used without many of the difficulties associated with carrier ampholytes. For example, pH gradients here are stable; carrier ampholyte gels

are subject to a cathode drift (displacement of focused proteins toward the cathode) that limits resolution and is most significant for alkaline pH ranges. The stability of the pH gradient with MIEF was demonstrated with the essentially constant patterns of focused ribonuclease in the alkaline range and focused myoglobin in the neutral range. Other experiments have shown that patterns of focused ß-lactoglobulin and ovalbumin in the acid range, were similarly constant over extended time interval. Another difficulty is eliminated, as focusing experiments should be more reproducible with the simple buffer method; they do not depend upon poorly defined carrier ampholytes that may vary from batch to batch. The reproducibility of focused protein patterns with MIEF is illustrated with the two independent experiments for ribonuclease (compare figures 3A and 5). Other experiments have shown that the focused protein patterns for myoglobin, ß-lactoglobulin, ovalbumin, and other proteins are similarly reproducible. Additionally, the ionic strength of the focusing environment provided here is substantially higher than that provided by carrier ampholytes; this allows the focusing of many proteins that are insoluble in carrier ampholyte gels. Furthermore, when IEF is used preparatively,

protein is easily eluted from the granulated gel and there is no possibility of contamination by carrier ampholytes. Many of the difficulties of the immobilized pH gradient gels are also eliminated. There is no potential for a protein to bind to or otherwise interact with a charged gel matrix, and proteins cannot be modified by or contaminated with unconsumed reactants involved in gel polymerization. Finally, a significant advantage of this method over both the carrier ampholyte and immobilized pH gradient methods is that it provides a well defined microenvironment for focusing. This is important for the study of physico-chemical properties of proteins related to isoelectric point. For example, as mentioned above, transitions linking two or more conformational states of a protein may be investigated. More specifically, this method may be used to study shifts in protein conformation due to either ligand binding or covalent modification that may be correlated with shifts in isoelectric point derived from molecular models (35).

Appendix: Theory of MIEF

Although the experimental arrangement appears relatively simple, it is difficult to consider theoretically because complicating factors common to all electrophoretic systems (diffusion, electroosmosis, etc.) must be taken into account in the presence of the cation selective membrane. Nevertheless, straightforward arguments can account for the steady-state pH gradients obtained, at least qualitatively, provided that simplifying assumptions are made. These arguments are useful in that they serve as a theoretical framework for further development and application of the method. They involve the determination of the electric field distribution in the gel bed and buffer channel, and the ion transport engendered by this electric field distribution. Moreover, these arguments take into account the constraints that the cation selective membrane imposes on the transport of ions: cations may be transported through the membrane, but anions may not. The arguments are illustrated with a glycine/NaOH buffer system.

The discussion that follows assumes a basic knowledge of electric fields in electrically conducting media (36). The electric field distribution in the gel bed and buffer channel may be determined by solving Laplace's equation (36)

$$\nabla \cdot \sigma \nabla V = 0 \qquad 1.1$$

where σ is electrical conductivity as a function of position, and V is the electrical potential (∇ is the gradient operator); the electric field E is given by $-\nabla V$. The equation is solved for the appropriate boundary values on the surfaces of the gel bed and buffer channel (V specified on the anode and cathode faces of the buffer channel and gel, and the normal component of E set to zero on the remaining bounding surfaces). It is useful to consider that at each position in the gel bed the electric field may be resolved into two components: E_p parallel to the gel (and membrane) surface, and E_n normal (perpendicular) to the gel (and membrane) surface. It follows from solutions to Laplace's equation that if the gel bed is assumed to be thin relative to the depths of the buffer channel, and the cation selective membrane is

considered to be an infinitely thin ion selective barrier, substantial shifts of conductivities in the gel bed will cause only small perturbations in the overall electric field distribution. Shifts of conductivity in the gel bed may result from changes of buffer composition in the gel. Also, remember that the conductivities at all positions in the buffer channel are uniform as a result of the rapid recirculation of buffer through the external reservoir. Specifically, substantial shifts of conductivities in the gel will cause only small shifts in the parallel components of the electric field E_p in the gel. Therefore, as an approximation, the parallel component E_p may be considered fixed at each position in the gel. This component E_p, however, will vary substantially from one position to another in the gel bed, increasing as the depth of the buffer channel below each position decreases.

These concepts are illustrated in figure 9, with electric field distributions for two cases. The first case (panel B) illustrates a conductivity distribution in the gel bed that is uniform and equal to the conductivity in the buffer channel (this illustrates the starting conditions). The second case (panel C) illustrates a conductivity as a function of position

in the gel bed that is inversely proportional to the approximately fixed parallel component of the electric field E_p as a function of position in the gel bed. The reasons for considering the latter conductivity distribution will become apparent from the discussion below. (This conductivity distribution is unique because it would give rise to electric field components in the gel equal to the fixed parallel components E_p even if the gel were supported by a flat insulating surface instead of the cation selective membrane over the buffer channel.

Figure 9. A. Schematic of the electric field distribution shown in cross-section with gel bed (1), buffer channel (2), cation-selective membrane (3), a set of equipotential surfaces (4), and an area magnified in (B) and (C) (5). The electric field is orthogonal to the equipotential surfaces; the magnitude of the electric field, which decreases toward the cathode, is suggested by the spacing between equipotential surfaces. B. Magnification of the gel bed and a representative equipotential surface, where the conductivity in the gel bed is uniform. Components of the electric field E_p and E_n are shown. Angles in this panel and (C) are exaggerated to illustrate the concepts. C. Magnification of the gel bed and a representative equipotential surface where the conductivity in the gel bed is inversely proportional to the parrallel component of the electric field E_p. The component of the electric field E_p is shown; the component E_n is zero.

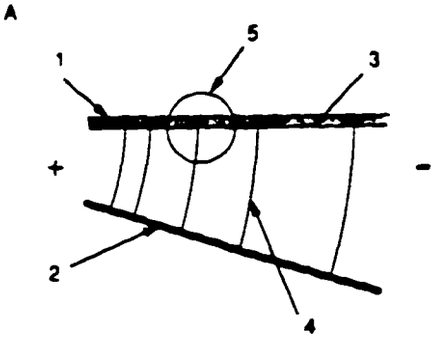

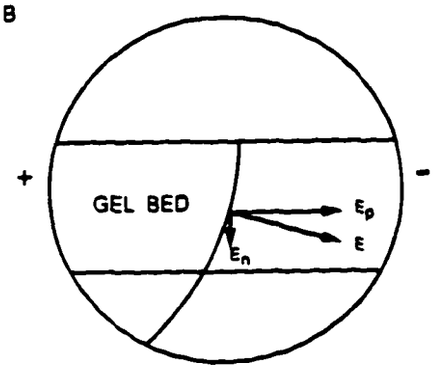

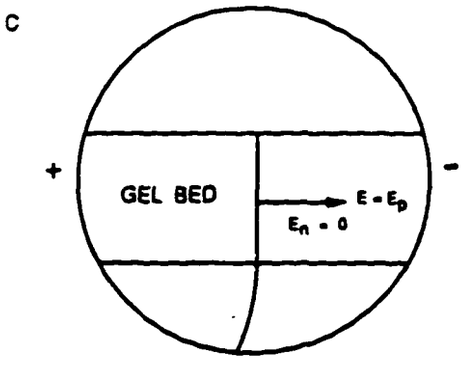

The normal components E_n are zero everywhere in the gel bed for this conductivity distribution.) It is apparent from figure 9 that there is only a small perturbation in the electric field distribution when conductivities in the gel bed shift substantially, as in going from the situation in panel B to the situation in panel C. It is straightforward to observe that the parallel components E_p in the gel bed, which are insensitive to small shifts in the electric field distribution, remain approximately constant as the conductivity in the gel is varied.

To simplify considerations of edge effects and transport processes, it is useful to make additional assumptions. First, the buffer compositions in the gel bed at the anode and cathode edges of the cation selective membrane may be held at fixed values (starting buffer values). Additionally, all transport processes in the gel bed other than those directly due to the electric field (diffusion, electroosmosis, etc.) may be neglected, and effects due to the transport of hydrogen and hydroxyl ions also may be neglected. It will then be shown, as follows, that a steady-state concentration gradient

of glycine anions may be maintained in the gel bed, where the concentration is inversely proportional to $E_p(x)$ (x is the position in the gel bed measured from the cathode edge of the cation membrane).

In order to have a steady-state glycine anion concentration gradient in the gel bed, it is necessary that the transport per unit time of glycine anions into any segment of the gel be equal to the transport per unit time out of that segment. This may be stated more explicitly in terms of the flux of glycine anions, F_{gly}, in the gel bed (ions crossing unit cross-sectional area of the gel bed per unit time) which may be given by

$$F_{gly}(x) = \mu_{gly}\alpha_{gly}(x)\,C_{gly}(x)\,E_p(x) \qquad 1.2$$

where μ_{gly} is the mobility of glycine anions, $\alpha_{gly}(x)$ is the degree of dissociation of glycine, $C_{gly}(x)$ is the total concentration of glycine (the glycine anion concentration is given by $\alpha_{gly}(x)C_{gly}(x)$), and $E_p(x)$ as described above is the electric field component parallel to the gel (and membrane)

surface, which is considered fixed at each position x. Since the cation selective membrane is impermeable to anions, the transport of glycine anions through the membrane, due to the normal component of the electric field E_n, may be neglected. Also, the gel bed has a constant cross-sectional area. It then follows that for a steady state it is necessary that the flux of glycine anions in the gel bed F_{gly} be constant; that is, for all positions x along the cation membrane

$$\frac{dF_{gly}(x)}{dx} = 0 \qquad 1.3$$

Since the buffer composition and E_p are held fixed at x = 0 (this is assumed above), the flux of glycine anions at x = 0 is constant and given by

$$F_{gly}(0) = \mu_{gly}\alpha_{gly}(0)\,C_{gly}(0)\,E_p(0) \qquad 1.4$$

It follows from equation 1.3 that for a steady state the flux of glycine anions at positions x in the gel bed may be given by

$$F_{gly}(x) = \mu_{gly}\alpha_{gly}(0)\,C_{gly}(0)\,E_p(0) \qquad 1.5$$

From equations 1.2 and 1.5 a concentration gradient of glycine anions that may be maintained by $E_p(x)$ is given by

$$\alpha_{gly}(x)\,C_{gly}(x) = \frac{\alpha_{gly}(0)\,C_{gly}(0)\,E_p(0)}{E_p(x)} \qquad 1.6$$

Since $E_p(x)$ may be considered fixed at all positions x, it is straightforward to show that if glycine anion concentrations do not initially conform to equation 1.6 (for example, the starting conditions, where glycine anion concentrations are uniform throughout the gel bed, do not conform to equation 1.6), the electric field and the resulting flux of glycine anions will adjust these concentrations until they conform to

equation 1.6. Once the steady state is reached, the electric field will oppose any tendency of the glycine anion concentrations to drift away from the steady-state values.

When considering the sodium counter ion, the normal component of electric field E_n cannot in general be neglected, as the cation membrane is permeable to sodium ions. However, as will be shown shortly, E_n goes to zero over the cation membrane for a sodium ion concentration gradient that satisfies the condition of electroneutrality with the glycine anion gradient given by equation 1.6. Since transport processes other than those due directly to the electric field may be neglected, the flux of sodium ions through the cation membrane for this sodium ion concentration gradient may be neglected. It then follows from arguments similar to those leading from equations 1.2 through 6, that this sodium ion concentration gradient will be consistent with the steady state. As discussed above (figure 8C), $E_n(x)$ goes to zero over the cation selective membrane when the conductivity in the gel bed is inversely proportional to the fixed parallel component of the electric field. It follows from equation 1.6 and the condition for electroneutrality that the glycine anion and sodium ion

concentrations are inversely proportional to $E_p(x)$. Since the conductivity is approximately proportional to the total ion concentration, the conductivity $\sigma(x)$ in the gel bed may be considered to be inversely proportional to $E_p(x)$, and it follows that $E_n(x)$ goes to zero over the cation membrane. (E_n, however, need not tend to zero near the anode edge of the cation membrane. A significant E_n may be required to accomodate discontinuities in conductivity and ion concentrations at the anode edge where the low concentrations of the ion gradients at the shallow end (high electric field end) of the sloping buffer channel meet the starting buffer ion concentrations as assumed above; in particular this adjusts the sodium ion flux in the gel bed at the anode edge of the cation membrane.) As with the glycine anion concentrations, it is straightforward to show that if the sodium ion concentrations at positions x do not initially conform to the steady-state values, the electric field will adjust these concentrations until they conform to steady-state values. Here the electric field will include significant normal components $E_n(x)$ that engender a sufficient flux of sodium ions through the cation selective membrane (either into or out of the gel) so that the sodium ion concentrations

satisfy, at all times, the condition of electroneutrality with the glycine anion concentrations. Again, these normal components $E_n(x)$ and the associated flux of sodium ions through the cation selective membrane approach zero as the steady state is approached. It should be noted that measurements of gel conductivities (not presented here) for the steady state confirm that the glycine anion and sodium ion concentrations increase with decreasing $E_p(x)$, albeit in a way somewhat more complex than that given by a simple inverse proportionality.

Neglecting all transport processes other than those due directly to the electric field and neglecting transport of hydroxyl ions, the concentrations of neutral glycine (acid form of the amino group) may be considered constant, and given by

$$[1-\alpha_{gly}(x)]C_{gly}(x) = [1-\alpha_{gly}(0)]C_{gly}(0) \qquad 1.7$$

With the Henderson-Hasselbalch equation

$$pH = pK + \log\frac{[base]}{[acid]} \qquad 1.8$$

the resulting pH gradient in principle may be given by

$$pH(x) = pK + \log\frac{\alpha_{gly}(0)E_p(0)}{[1-\alpha_{gly}(0)]E_p(x)} \qquad 1.9$$

Additionally, it is instructive to note that the hydroxyl ion concentration gradient resulting from equation 1.9 is consistent with the steady state; that is, it may be shown that

$$\frac{dF_{OH}(x)}{dx} = 0 \qquad 1.10$$

where $F_{OH}(x)$ is the flux of hydroxyl ions.

Arguments similar to those presented above may be given to account for the pH gradients obtained with the imidazole/HCl, MES/NaOH, and acetic acid/NaOH buffer systems. For the MES/NaOH, and acetic acid/NaOH systems, where there are significant hydrogen ion concentrations, other transport processes in addition to those due directly to the electric field need to be considered to give a more complete account of the steady-state pH gradient. This is so because the condition for a steady state,

$$\frac{dF_H(x)}{dx} = 0 \qquad 1.11$$

where $F_H(x)$ is the flux of hydrogen ions, is inconsistent with $E_p(x)$ and the hydrogen ion concentration gradients specified by pH(x). The additional transport processes that need to be considered include diffusion of sodium and hydrogen ions through the cation membrane.

To conclude, it is important to emphasize that the above arguments represent an oversimplification. Although these

arguments outline the basic mechanisms, a more complete description, which is presently being developed, must take into account many other factors associated with transport processes and artificial membranes. These factors are discussed extensively elsewhere (26). Additional factors being considered include coupled diffusion in gradients of electrochemical potential, electroosmosis, and the actual conductivities and permselectivities of the cation and other membranes relative to the gel matrix and the free buffer. It is particularly important to consider a phenomenon known as membrane polarization (31), which involves the production of either hydrogen or hydroxyl ions at the interface of a solution phase and an ion selective membrane. This phenomenon is due to an inadequate flux of the permeating ion to the membrane surface that results from a discontinuity in the transport number of the permeating ion at the interface. Arguments involving this phenomenon can account for the fact that the pH gradients observed experimentally (for example, the actual pH gradients obtained with glycine buffers) are generally lower than might be expected from the compositions of the starting buffers.

Part 2. Studies with Alcohol Dehydrogenase and Ligand Complexes.

Introduction

LADH - Isozymes and Structure

Alcohol dehydrogenase from horse liver (LADH) is one of the most extensively characterized proteins known. This enzyme catalyzes the reversible oxidation of many primary, secondary, branched, and cyclic alcohols with nicotinamide adenine dinucleotide (NAD^+) as coenzyme. The physiological substrates for LADH, however, are unclear; one function of this enzyme may be to metabolize alcohols, including ethanol, that are produced in the intestinal tract as a result of bacterial action. There are several extensive reviews in the literature (37,38,39). A schematic diagram of this enzyme is illustrated in figure 10. The enzyme is a dimer (monomers are enzymatically inactive) composed of identical or almost identical subunits; each single chain subunit has a molecular weight of 40,000 daltons, 80,000 daltons for the dimer. There

are two types of subunits, E and S, which give rise to three main isoforms resulting from combinations of these subunits, EE, ES, and SS.

Figure 10. Schematic of the LADH dimer showing substrate and coenzyme binding pockets (Reprinted with permission, ref. 57)

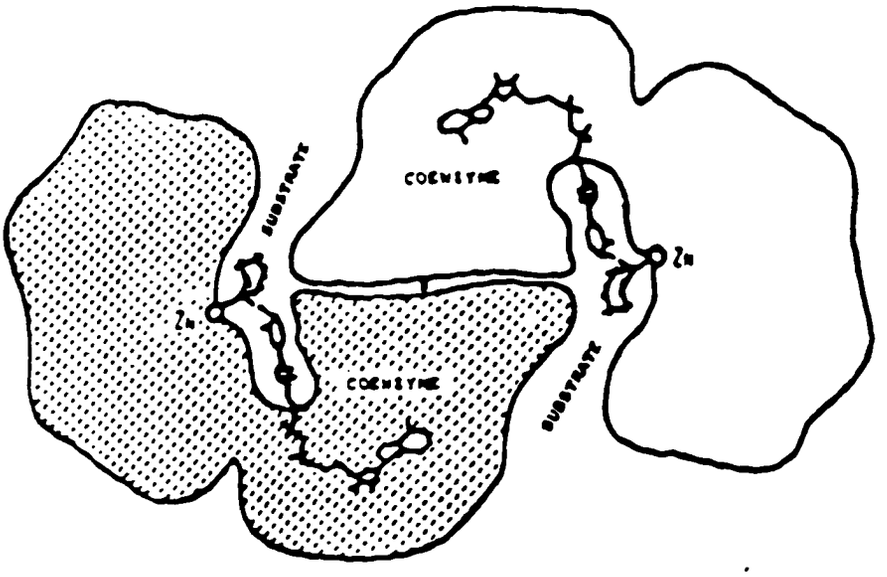

The S subunit differs from E at six amino acid positions; the S subunit has three more units of positive charge at physiological pH than does the E subunit. The E subunit is so designated because the corresponding homodimer is primarily active toward ethanol; the S subunit is so designated because of primary activity toward steroids. The ES and SS isoforms retain at least a residual activity toward ethanol; the EE isoform is substantially inactive toward steroids. As measured in a carrier ampholyte / sucrose gradient system, an isoelectric point of 9.3 has been found for the ES isoform; the SS isoform was found to have an isoelectric point greater than 10 (40). The EE isoform has been resolved by ampholyte focusing into four separate peaks with isoelectric points reported as 8.08, 8.28, 8.51, and 8.70 (40). The reasons for having this distribution of peaks is not clear; isoforms corresponding to these peaks have been shown to slowly interconvert.

Each subunit of the enzyme consists of a coenzyme binding domain with 143 amino acids and a catalytic domain with 231 amino acids and two zinc ions, only one of which is involved

in catalysis (41,42). The two domains are joined at a narrow neck and are separated by a deep active site cleft. The molecule is 28% helix and 34% pleated sheet. Two molecules of NAD^+ bind, each independently of the other, per dimer at the two active sites (43). Each NAD^+ molecule binds in an extended conformation with the adenine moiety bound in a hydrophobic pocket at one end of the coenzyme binding domain. The pocket is bounded by six strands of parallel pleated sheet linked by four helices. N-10 of adenine is hydrogen bonded to the side chain of Asp 273; N-7 is hydrogen bonded to the guanidinium group of Arg 271, which forms a salt bridge with Asp 273. The adenosine ribose is hydrogen bonded to one of the carboxyl oxygens of an aspartate residue (Asp 223) through the O-2' hydroxyl. This linkage appears to be very important for proper coenzyme binding, as it is conserved in a number of NAD^+ binding dehydrogenases. For example, in lactic dehydrogenase this linkage is through Asp 53, and in glyceraldehyde phosphate dehydrogenase through Asp 32 (44). The secondary structure in this binding pocket is also similar in these dehydrogenases. In LADH, the other hydroxyl of the adenosine ribose is hydrogen bonded to Lys 228. Pyrophosphate is hydrogen bonded to Arg 47, which provides balancing positive

charge. The nicotinamide ribose moiety is bound by two hydrogen bonds to main chain carboxyl oxygens of isoleucine and glycine residues. Nicotinamide fits into a second hydrophobic pocket, placing the C-4 carbon atom 4.5 angstroms from the catalytic zinc atom. Parts of both subunits line deep hydrophobic pockets for substrate at the bottom of which are the catalytic zinc atoms, each liganded to two cysteine residues and one histidine residue. The second zinc atom of each catalytic domain is liganded to four cysteine residues and it appears to play a role only in maintaining the structural stability of the dimer (41).

Binding of Coenzyme

The binding of coenzyme brings about a conformational change in the enzyme that consists of a rotation of each catalytic domain of 7.5 degrees relative to the dimer as a whole together with a small displacement of a four residue loop in the coenzyme binding domain. The rotation of the catalytic domain occurs about a hinge region of hydrophobic residues between helices that comprise the link to the coenzyme domain (42). A result of this conformational change is a narrowing of

the access to the active site. The reaction mechanism with alcohol as substrate may be summarized as follows: the binding of coenzyme is followed by the binding of alcohol to zinc, which displaces a water molecule. The alcohol is deprotonated and hydride is transferred from the alkoxide ion to NAD^+; the result is NADH and zinc bound aldehyde. A water molecule then displaces the aldehyde, and the last and rate limiting step is the dissociation of NADH.

The equilibrium binding of NAD^+ and NADH to the enzyme is pH dependent. Dissociation constants for NAD^+ are 351.0 μM at pH 6, 30.1 μM at pH 8, and 5.5 μM at pH 10; the binding is tighter with increasing pH. Equilibrium dissociation constants for NADH are 0.21 μM at pH 6; 0.46 μM at pH 8, and 5.0 μM at pH 10. Binding is weaker with increasing pH, but overall, NADH is bound more tightly than NAD^+ (45). These results may be accounted for in a simple way by considering electrostatic interactions. NAD^+ binding is weaker than that for NADH because of the electrostatic repulsion between the positively charged nicotinamide ring of NAD^+ and the positively charged zinc; this interaction is absent with NADH. The fact that the binding of NAD^+ becomes tighter with increasing pH may be

attributed to the ionization of a zinc bound water. Conversely, NADH binding becomes weaker with increasing pH, and this can be correlated with decreasing positive charge at the pyrophosphate binding site, e.g., with the titration of Arg 47.

A more extensive analysis of NAD^+ binding, which takes into account measurements of enthalpy changes upon binding and proton release/uptake as a result of perturbed pK's of ionizable groups upon binding (46), suggests that binding is controlled by a single ionizable group with a pK of approximately 9.2 in the free enzyme and a perturbed pK of 7.6 in the binary complex. Calculations of intrinsic (pH independent) enthalpy for binding of NAD^+ result in values close to zero. This indicates that the binding is driven by a substantial positive entropy change. The binding of ADP ribose has been found to be exothermic (46). Hence, the binding of the nicotinamide moiety should be endothermic to cancel the exothermic component of the ADP ribose moiety of the coenzyme. It has been suggested that the interaction of the nicotinamide moiety with the protein involves a conformational change in the protein that is endothermic. X-ray analysis reveals a

conformational change in the coenzyme binding domain that occurs with coenzyme binding (42): amino acid residues 294 through 297 are displaced to accomodate the positioning of the nicotinamide ring. The binding of NADH, which also has been found to have a zero intrinsic enthalpy change (47), is associated with a very similar conformational change in the protein (42). This conformational change does not occur with ADP ribose. NADH, however, affects the controlling ionizable group in an opposite way to that of NAD^+; it perturbs its pK to a value above 10, i.e., proton uptake upon binding (45).

Additionally, it has been found that the association rates for both NAD^+ and NADH binding decrease with increasing pH, even though the equilibrium dissociation constants decrease with increasing pH for NAD^+ but increase for increasing pH for NADH. These association rates may be correlated with an ionizable group on the protein with a pK of 9.2 (45). This finding indicates that the simple explanation involving electrostatic interactions between coenzyme and the LADH binding site, as described above, is insufficient. These results cannot be explained by electrostatic interactions influenced by ionization of zinc bound water and protonation

of residues at the pyrophosphate binding site with increasing pH. To account for this it has been hypothesized that access to the coenzyme binding site is controlled by a conformational change in the protein that is correlated to an ionizable group with a pK of 9.2 (45,46). That is, the ionization of a group on the protein with a pK of 9.2 causes a conformational change that interferes with the binding of the coenzyme. Several candidates have been suggested for this ionizable group. These include a water molecule coordinated to the active site zinc, Cys 46, which is also coordinated to the active site zinc, His 51, which has its imidazole ring close to the nicotinamide ring of coenzyme, Tyr 286, which has been proposed to account for a pH dependent fluorescence transition governed by an ionization with a pK close to 9.2, and Lys 228, which is hydrogen bonded to adenosine ribose of coenzyme (48,49,50,51). There are no compelling arguments in favor of any one of these candidates. It should be emphasized that the controlling ionizable group need not be part of the coenzyme binding site; in principle, a conformational change can be triggered by an ionizable group anywhere in the protein.

Inhibitors

There are many molecules that are known to be inhibitors of LADH. Most of these belong to one of two groups: one competitively inhibits binding of substrate and the other binding of coenzyme. Those that inhibit coenzyme may be further divided into three categories, each binding to a separate area of the coenzyme binding site: the adenosine pocket, the pyrophosphate subsite, and the nicotinamide binding subsite near the catalytic zinc. Those that bind in the adenosine pocket include aromatic molecules having a negatively charged group attached to the ring system. Among these are anilinonaphthalene sulfonate (ANS), 2,6-toluidinonaphthalene sulfonate (TNS), triiodothyroacetate, and salicylate (52,53). By fluorescence methods, salicylate and its derivative iodosalicylate have been shown to bind in a strictly competitive way with ANS, i.e., all three bind at the same site (53). X-ray crystal studies of iodosalicylate-LADH complexes show that this molecule binds in a manner very similar to the binding of the adenosine part of the coenzyme (53). The phenyl ring binds to the same region as does the hydrophobic adenine, and the hydroxyl group is hydrogen bonded

to Asp 223, the same residue that bonds to O-2' of adenosine ribose. Additionally, the carboxyl group is close enough to Arg 271 to form a salt bridge.

X-ray studies have also shown that another coenzyme competitive inhibitor, the heavy metal anion $Pt(CN)_4^{2-}$, binds at the same site as the pyrophosphate of coenzyme, close to Arg 47 and Arg 369 (54). Small anions such as perchlorate, chloride, thiosulfate, and sulfate, have been shown to competitively inhibit coenzyme binding; it is presumed that these anions also bind at the same site as pyrophosphate. Coenzyme fragments such as adenosine, ADP-ribose, and AMP have also been shown to competitively inhibit the binding of complete coenzyme (55).

Metal chelating agents such as 2,2-bipyridine and 1,10-phenanthroline have been shown to bind to the catalytic zinc close to the nicotinamide binding subsite. These agents bind independently of ADP-ribose and other smaller coenzyme fragments, but competitively with NAD^+ and NADH (56); they are partially competitive toward ethanol. Heterocyclic nitrogen bases such as imidazole, an ethanol competitive inhibitor,

have been shown to bind to the catalytic zinc displacing a water molecule. Ternary complexes with imidazole and coenzyme have been isolated (57). Other substrate competitive inhibitors include isobutyramide and dimethylsulfoxide (58,59). Several long chain fatty acids (60) and pyrazole (61) form ternary complexes with LADH and NAD^+ but not with NADH. Pyrazole is very tightly bound in the ternary complex, having a dissociation constant of 0.22 μM (61). NAD^+ is also more tightly bound in this complex, with a dissociation constant of 0.1 μM (61). The binding of pyrazole in this ternary complex may be correlated with a further downward shift in pK of the ionizable group, that has been suggested to control coenzyme binding, from 7.6 to a value of 6 or below. Formation of this ternary complex is exothermic, but this may be accounted for almost entirely by the binding of pyrazole; the enthalpy change in forming the binary pyrazole / LADH complex is very close to that for the formation of the ternary complex (46). One of the nitrogen atoms of pyrazole is bound to the catalytic zinc; the other nitrogen atom is approximately 2 angstroms from the C-4 atom of the nicotinamide ring of coenzyme in the ternary complex (62). 4-alkyl-substituted pyrazole derivatives are bound more tightly than pyrazole.

This is true only for the 4 position. Substitutions at positions N-1, C-3, or C-5 abolish inhibition. As the 4-substituted alkyl chain increases from methyl to pentyl, binding becomes tighter. This may be correlated with hydrophobic features of the substrate binding pocket (63).

Theory of Isoelectric Point

Introduction

Electrostatic interactions play key roles in biochemistry involving, for example, enzyme catalysis, ligand binding, voltage gating of membrane channels, and protein folding. pH is a parameter that plays a central role in influencing these electrostatic interactions. It is not a coincidence that the pH of blood is carefully regulated so that it remains close to 7.4. pH affects biological function by controlling the charges on macromolecules, mainly proteins. The charge characteristics of a protein are determined largely by the pK's of titratable groups. It is therefore important that any theoretical study of protein structure as it relates to biological function include calculations of the pK's of titratable groups.

Difficulties with the determination of pK's of titratable groups center on the fact that the pK's of these groups are altered from values that they would have if the titratable groups were alone in a solvent (water) environment. The pK's are shifted by the lower dielectric constant of the protein

interior, by interactions with fixed (non-titratable) charges in the protein environment, and by interaction with other titratable groups.

An important question in doing pK calculations is: what is the dielectric constant in the interior of the protein? Estimates of between 2 and 4 have been made from dessicated protein powders (64). However, pK calculations, as discussed below, suggest that the dielectric constant is of the order of 20. It has been hypothesized that this higher dielectric constant is appropriate because it reflects the flexibility of the protein structure such that dipolar charge distributions can change their orientations in response to an electric field. It has been found in a limited number of calculations with small proteins that pK's calculated with a dielectric constant of 20 agree with experimentally determined pK's better than pK's calculated with dielectric constants of 2 to 4 (65).

The present study aims to compare pK's determined theoretically using dielectric constants of both 4 and 20 with experimentally determined pK's for a large protein and one of its complexes with ligands to try to determine which

dielectric constant is appropriate for the protein interior. Specifically, the protein for this study is LADH.

The theoretical and experimental pK's are compared indirectly by comparing calculated and measured isoelectric points for the protein and a protein complex. The isoelectric point is a parameter that is directly dependent upon the pK's of the macromolecule.

The Null Model

The simplest way of relating the isoelectric point to the pK's for a protein is with the null model. The null model assumes that the pK's of ionizable groups as part of the protein molecule remain unchanged from values that these groups have in solvent, i.e., water. These pK values are for side chains of amino acids in peptides having no other charged groups. The total positive charge P due to ionizable groups at a given pH may be given by (66)

$$P = \sum_{i=1}^{n} \frac{1}{1 + 10^{pH - pK_i}} \qquad 2.1$$

Similarly, the total negative charge N may be given by (66)

$$N = \sum_{i=1}^{n} -\frac{1}{1+10^{pK_i - pH}} \qquad 2.2$$

Permanent charges may be included, P_o the total fixed (non-titratable) positive charge, and N_o the total fixed negative charge of the protein molecule. With the given pK's the equation

$$P(pH) + P_o = N(pH) + N_o \qquad 2.3$$

may be solved for the pH at which the molecule is isoelectric, that is, the isoelectric point pI.

Shifted pK's

More refined calculations of isoelectric point need to take into account the shifts of the pK's of the ionizable groups that occur when a group is moved from solvent to the protein environment. It should be noted that substantial pK shifts for

a large number of residues have negligible effects on the isoelectric point. For example, if the isoelectric point is 8.8 from the null model, a pK shift of 4.3 to 5.8 for a GLU residue has negligible effect on the isoelectric point; however, if a LYS residue has a pK shift from 10.5 to 9.3, this would significantly lower the isoelectric point. An important consequence of this is that the isoelectric point is sensitive to only a subset of the titratable residues.

The shifts in pK's may be attributed to changes in free energy ΔG in going from solvent to protein. Specifically, pK_i^{pro}, the pK of a titratable group i in the protein environment without interactions with other titratable groups may be given by

$$pK_i^{pro} = pK_i^0 - \gamma(i)\Delta\Delta G_i^{env}/2.3kT \qquad 2.4$$

where pK_i^0 is the solvent pK of the group, $\gamma(i)$ is -1 or 1 for an acidic or basic group respectively, and $\Delta\Delta G_i^{env}$ is the change of the energy of ionizing the group in the protein environment relative to ionizing in solvent, again in the

absence of interactions with other titrating groups. $\Delta\Delta G_i^{env}$ may be given as

$$\Delta\Delta G_i^{env} = -\gamma(i)\,[\Delta G_i^{env}(A) - \Delta G_i^{env}(AH)] \qquad 2.5$$

where $\Delta G_i^{env}(A)$ is the difference in free energy in moving the unprotonated state A of the group from the solvent to the protein environment, and $\Delta G_i^{env}(AH)$ is the corresponding difference in free energy for the protonated state of the group.

The free energy changes giving rise to the pK shift for a titratable group may be divided into three components. The first is the desolvation energy, the energy change in moving the titratable group from a polar solvent having a high dielectric constant (e.g., water has a dielectric constant of 80) to a position that is partially or totally immersed in the environment of the protein which has a low dielectric constant. The second is the fixed charge interaction energy, the energy change due to the interaction of the titratable group with the fixed charge distribution in the protein. The

third is the titratable group interaction energy, the energy increment due to the interaction of the titratable group with all other titratable groups in the protein.

Energies affecting pK shifts are predominantly electrostatic (67). For the calculations presented here other contributions to the free energy such as contributions due to entropy (entropies of conformation and organization of water) and van der Waals forces will be neglected. Two approaches toward calculating pK shifts have been pursued. One method calculates energies with a screened Coulomb potential (SCP) (68). Energies are calculated with Coulomb's law; electric fields are screened by a distance dependent dielectric permittivity that is determined empirically. A second method calculates energies with a finite difference numerical integration of the linearized Poisson-Boltzmann equation for the electrical potential (FDPB) (67). The latter method takes into account the detailed shape of the protein molecule and its relation to the position of titratable groups. Suites of computer programs have been developed to carry out these calculations with both of the above approaches.

Screened Coulomb Potential (SCP)

The SCP method calculates desolvation energies for a titratable group with a generalization of an integral form of the Born equation for calculating free energy changes in moving an ion from a vacuum to a radially inhomogeneous solvent with permittivity $\epsilon(r)$ (69). With SCP an equation relating energy to electric field distribution is used to calculate free energy changes in moving a charge distribution from one solvent s with permittivity $\epsilon(r)$ to another solvent s' with permittivity $\epsilon'(r)$. Similar distance dependent permittivities have been used to account for dissociation constants of bifunctional organic acids and bases of varying distances between functional groups (70). The distance dependent permittivity takes into account the restricted orientational mobility of solvent (water) molecules (orientation of electric dipoles) surrounding the functional groups (68) as well as potential charge transfer reactions (68).

This is accomplished in terms of the dielectric energy densities

$$u(r) = \frac{1}{2}\epsilon(r)E^2; \quad u(r) = \frac{1}{2}\epsilon'(r)E'^2 \qquad 2.6$$

E and E' are the respective electric field distributions. The free energy change ΔG^{sol} in moving a charge distribution from one solvent to another (from water to the interior of a protein) may then be given by

$$\Delta G^{sol} = \frac{1}{8\pi}\left(\int \epsilon'(r)E'^2 dv - \int \epsilon(r)E^2 dv \right) \qquad 2.7$$

The integration is taken over all volume outside of the charge distributions. The electric field E outside of a spherically symmetric ion of charge q may be given by

$$E = \frac{q}{\epsilon(r)r^2} \qquad 2.8$$

The electric field of a typical charge distribution (the net charge of a titratable group is not centered at a single point) may be given by a sum of the electric field distributions for a set of spherically symmetric ions. To

account for effects of ionic strength a Debye screening factor exp(κr) (68) is included. In addition, to account for the fact that a titratable group may not be totally buried within the protein, a factor is included that is the ratio of surface area of the titratable group that remains exposed to solvent when the group is in its correct position in the protein, to the total surface area of the titratable group in the solvent. This accessible molecular surface is defined with a 1.4 Å probe sphere (71).

The fixed charge interaction energy ΔG^{fix} for a titratable group i may be given by

$$\Delta G_i^{fix} = q_i \Phi(r_i) \qquad 2.9$$

where q_i is the charge of the titratable group i, and $\Phi(r_i)$ is the screened Coulomb potential given by

$$\Phi(r_i) = \sum_j q_j / \epsilon(r_{ij}) r_{ij} \qquad 2.10$$

The q_j's are the fixed charges in the protein; $\epsilon(r_{ij})$ is the distance dependent permittivity, and r_{ij} is the distance between the titratable group i and a charge q_j.

The pK shifts attributable to the interaction energies between titratable groups are calculated according to the Tanford-Roxby approximation (72) which assumes that the average charge of a particular titratable group depends upon the average charges of all other titratable groups. This method begins with an initial guess for the average charges for all of the titratable groups. These initial guesses may be made by assuming that the pK of each titratable group is equal to pK_i^{sol}, the pK that the group i would have in solvent. With the pH specified the initial guess for the average charge for each group may be given by

$$\log \frac{f_i}{1-f_i} = pK_i^{sol} - pH \qquad 2.11$$

where f_i is the fractional degree of protonation; the average charge is then $f_i q$, where q is the charge of protonation. The pK's may then be adjusted by the equation

$$pK_i^{fin} = pK_i^{pro} - \sum_{j=1, j\neq i}^{N} Y(i) f_i q \Delta G^{ij}/(2.3kT) \qquad 2.12$$

pK_i^{fin} is the adjusted pK; pK^{pro} is as above, the pK of a titratable group in the protein environment without interaction with other titratable groups. The ΔG^{ij} are calculated with the screened Coulomb potential as above; r_{ij} is the distance between the titratable groups i and j. A new set of f_i may then be calculated with the adjusted pK^{fin} instead of the pK_i^{pro}, and a new set of pK_i^{fin} may be determined. This process is iterated until a self-consistent set of pK_i^{fin}'s are determined.

Finite Difference Poisson-Boltzmann Equation (FDPB)

The FDPB method (67,73) calculates the desolvation energies as well as all other interaction energies of titratable groups by mapping dielectric permittivity, ionic strength, and charge distribution onto a three dimensional grid. The protein-solvent interface is determined with a 1.4 Å molecular probe

(71). A finite difference algorithm is then used to integrate the linearized Poisson-Boltzmann equation (73)

$$\nabla[\epsilon(r)\nabla\phi(r)] - \kappa^2(r)\epsilon(r)\phi(r) = -4\pi\rho(r) \qquad 2.13$$

where ϕ is the electrostatic potential; ρ is the charge distribution with each charge in the form of a point located at the center of an atom; $\epsilon(r)$ is the dielectric constant as a function of position r (ϵ may assume the value of 80 in the solvent, water; ϵ may be, for example, 4 in the protein interior); $\kappa(r)$ is the Debye screening constant (67) as a function of position (the Debye screening constant is the inverse of the Debye length, a function of ionic strength).

Desolvation energies of titratable groups, free energy changes in moving titratable groups from a solvent environment to a position in the protein-solvent environment, are calculated by first solving the Poisson-Boltzmann equation for the potential energy for the titratable group in a solvent of given dielectric constant and ionic strength. The Poisson-Boltzmann equation is then solved for the potential energy for the

titratable group in position in the protein-solvent environment with dielectric constants given for both protein and solvent; an ionic strength is specified for solvent. The desolvation energies are the differences between the results of these two separate calculations. Interaction energies of titratable groups with the fixed charge distribution in the protein are calculated similarly with the Poisson-Boltzmann equation for which the charge distribution consists only of the fixed charges.

The pH dependent pK shifts of titratable groups due to interaction energies with other titratable groups may be calculated with the Tanford-Roxby approximation and an iterative, self-consistent method essentially the same as with SCP. The interactive free energy changes ΔG^{ij}, however, are calculated with the Poisson-Boltzmann equation. Alternatively, a hybrid statistical mechanical Tanford-Roxby approach (73) may be taken. Since charge-charge interactions in proteins fall off rapidly with distance, a cutoff distance of 7 Å is set. This value has been determined to give calculated results that are closest to experimentally measured results. For all titratable groups within 7 Å of a given titratable group a

statistical mechanical approach is taken to determine contributions to the pK shifts; for titratable groups more than 7 Å from a given titratable group the Tanford-Roxby approach is taken.

pK shifts may be obtained from a purely statistical mechanical treatment by taking an average over the 2^N states of the protein that arise with N titratable groups. A given state of the protein, n, where n = 1 to 2^N, may be specified in terms of a vector with N components $\delta_n(i)$, i = 1 to N, for which $\delta_n(i)$ is 0 when the group i is neutral and 1 when it is charged. A reference state may be taken for which all titratable groups are neutral. The free energy of the state n, ΔG^n may be given by

$$\Delta G^n = \sum_{i=1}^{N} [\delta_n(i)\gamma(i)[2.3kT(pH - pK_i^{pro})]$$

$$+ \delta_n(i) \sum_{1 \le j < i} \delta_n(j) \Delta G^{ij}] \qquad 2.14$$

$\gamma(i)$ = -1 for an acidic group or 1 for a basic group; pK_i^{pro} is the pK for the titratable group i in the protein in the

absence of interaction with other titratable groups; ΔG^{ij} is the pairwise charge-charge interaction energy between titratable groups. The ΔG^{ij} are calculated with the Poisson-Boltzmann equation. The fractional charge f_i for group i may be obtained from the statistical mechanical average

$$f_i = \sum_{n=1}^{2^N} \delta_n(i)\gamma(i)\exp(-\Delta G^n/kT)Z \qquad 2.15$$

$$Z = \sum_{n=1}^{2^N} \exp(-\Delta G^n/kT) \qquad 2.16$$

where Z is the partition function. The pK's may then be obtained from the f_i with equation 2.11 as above. If N is large, the extent of the calculations become prohibitive; therefore, the hybrid statistical mechanical Tanford-Roxby approach is a useful compromise.

The statistical mechanical Tanford-Roxby method is outlined as follows. Initially, the Tanford-Roxby iterative procedure alone is used to obtain a set of fractional charges for the N titratable groups of the protein. Then a particular titratable

group s is considered. Those groups within the cutoff distance of 7 Å from group s are designated as 1 to j-1; those outside of the cutoff distance are designated j to N. For those groups outside of the cutoff distance the fractional charges determined with the initial Tanford-Roxby procedure are held fixed. The groups within the cutoff distance are then treated with the statistical approach. The ΔG^n for the states of the protein are then given by

$$\Delta G^n = \sum_{i=1}^{j-1} [\delta_n(i)\gamma_n(i)[2.3kT(pH - pK_i^{pro})] + \delta_n(i)\sum_{k=j}^{N} f_k \Delta G^{ik} + \sum_{1\le m<i} \delta_n(m)\Delta G^{im}] \qquad 2.17$$

The first term on the right in this equation is the free energy of charging the groups within the cutoff distance. The second term represents the interaction of the charge on group i with the charges on the groups outside of the cutoff distance as determined by the initial Tanford-Roxby procedure. The third term represents the interaction of group i with other groups within the cutoff distance. The fractional charge f_s of group s may then be calculated with equations 2.15 and 2.16 as above; the sum is now over 2^{j-1} states. This procedure

is carried out for all groups s from 1 to N of the protein; it is then iterated until a self-consistent set of fractional charges are obtained. The total charge of the protein is simply the sum of the fractional charge set plus the fixed net charge of the protein. A titration curve for the protein may be obtained by repeating the above calculations for a full range of pH values.

Comparison: SCP - FDPB

From protein structures known from x-ray crystallography a limited number of pK calculations have been carried out with both the SCP and FDPB approaches. When comparing calculated pK values with values obtained experimentally (measurements were made primarily with NMR techniques; errors are estimated to be ±0.2 (65)), it appears that the SCP method is marginally better than the more detailed FDPB method. Calculated values are closest to experiment with a dielectric constant of 20 in the protein interior (65). Neither method is substantially better than the null model, i.e., assuming that pK's are not

shifted by the protein environment from values that they have in solvent.

pK values were previously calculated with SCP and FDPB for ribonuclease A, ribonuclease T_1, and trypsin inhibitor from bovine pancreas, and hen eggwhite lysozyme, and compared with values obtained experimentally (65) (E. Mehler, personal communication). For 16 residues of ribonuclease A pK values calculated with SCP have a root mean square deviation (rmsd) of 0.67 when compared with experimental values. Errors in pK values range from 0.06 for HIS 105 (calculated pK 6.64, experimental 6.7) to 0.79 for ASP 53 (calculated pK 4.69, experimental 3.9). Comparing FDPB calculated pK values with experimental values, a rmsd of 0.75 is obtained. Errors in pK values range from 0.1 for GLU 49 (calculated pK 4.6, experimental 4.7) to 1.7 for HIS 12 (calculated pK 4.5, experimental 6.2). The null model has an rmsd of 0.86.

For 4 residues of ribonuclease T_1 pK values calculated with SCP have a rmsd of 0.60 when compared with experimental values. Errors in pK values range from 0.3 for HIS 40 (calculated pK 7.58, experimental 7.9) to 0.8 for HIS 27

(calculated pK 6.5, experimental 7.3). Comparing FDPB calculated pK values with experimental values, an rmsd of 1.1 is obtained, Errors in pK range from 0.4 for HIS 40 (calculated pK 7.5, experimental 7.9) to 1.8 for GLU 58 (calculated pK 2.5, experimental 4.3). The null model has an rmsd of 0.60.

For 10 residues of trypsin inhibitor pK values calculated with SCP have a rmsd of 0.32 when compared with experimental values. Errors range from 0.07 for LYS 15 (calculated pK 10.50, experimental 10.43) to 0.53 for CTERM (calculated pK 3.58, experimental 3.05). Comparing FDPB calculated pK values with experiment, a rmsd of 0.4 is obtained. Errors range from 0 for GLU 7 (calculated pK 3.7) to 1 for NTERM (calculated pK 7.1, experimental 8.1). The null model has an rmsd of 0.6.

For 18 residues of hen eggwhite lysozyme pK values calculated with SCP have a rmsd of 0.75 when compared with experiment. Errors in pK values range from 0.04 for ASP 119 (calculated pK 2.54, experimental 2.5) to 1.8 for ASP 48 (calculated pK 2.46, experimental 4.3). Comparing FDPB calculated pK values (19 residues) with experiment, a rmsd of 0.67 is obtained. Errors

range from 0.1 for LYS 33 (calculated pK 10.5, experimental 10.4) to 1.7 for GLU 35 (calculated pK 4.4, experimental 6.1). The null model has a rmsd of 1.0.

Calculations with SCP and FDPB for most groups that have substantial pK shifts (of order 1.5) away from solvent values, as measured experimentally, result in substantial shifts in the right direction (65) (E. Mehler, personal communication). For example, for lysozyme FDPB calculations give pK values of 3.1 for GLU 7 (experimental pK 2.6, null 4.4), 4.4 for GLU 35 (experimental pK 6.1, null 4.4), 11.0 for TYR 53 (experimental pK 12.1, null 10.0), and 2.1 for ASP 66 (experimental pK 2.0, null 4.0). For ribonuclease A FDPB calculations give 2.5 for GLU 2 (experimental pK 2.8, null 4.4) and 1.9 for ASP 14 (experimental pK < 2.0, null 4.0). SCP calculations give similarly shifted results. These results indicate that both theoretical approaches are able to take into account factors in the protein environment, i.e., desolvation effects, interactions with fixed charges in the protein (including hydrogen bonds), and interactions with other titratable groups, that contribute to substantial pK shifts.

It should also be mentioned that substantial shifts in calculated pK's have been obtained for which experimentally measured pK's indicate only slight pK shifts. For example, an FDPB calculation for ribonuclease A (65) has resulted in a pK shift to 4.5 for HIS 12 (experimental 6.2, null 6.3), and a pK shift to 2.0 for ASP 83 (experimental 3.5, null 4.0). SCP calculations for ribonuclease A (E. Mehler, personal communication) resulted in a pK shift to 7.4 for HIS 48 (experimental 6.0, null 6.3), and a pK shift to 5.8 for GLU 49 (experimental 4.7, null 4.4). Factors that contribute to these false pK shifts may include inaccuracies in atomic coordinates from x-ray crystallography including those for crystal waters. Also, the solution conformation of a particular residue may be different from the crystal conformation. For FDPB calculations the effective dielectric constant at the position of a particular residue may be substantially different from the value used throughout the protein. For SCP calculations the distance dependent dielectric constant used throughout the protein may be inappropriate for a particular residue.

A significant advantage of the SCP method over the FDPB method is that it is simpler and hence requires substantially less

computer processing time. Also, the SCP method has been marginally better in calculating pK's than the FDPB method in a limited number of calculations that have been performed. However, the FDPB method has several advantages over SCP. First, although SCP calculations need not use the Tanford-Roxby iterative procedure to obtain fractional charges and pK's, computer algorithms that are presently available use this approach. The Tanford-Roxby approximation may, however, lead to incorrect results particularly if there are strongly interacting titratable groups that have solvent pK's that are close in value (74). Computer algorithms for the FDPB calculations as described above use a hybrid statistical mechanical Tanford-Roxby approach. The statistical mechanical treatment is applied to groups that are within 7 Å of each other, groups that are most likely to interact strongly. This eliminates a source for potentially incorrect results. Additionally, a significant advantage of the FDPB approach is that it takes into account the detailed shape of the protein solvent boundary. Clefts and channels in the protein solvent boundary can substantially magnify electrostatic fields, which, in turn, can substantially affect pK values (67). SCP approaches are generally insensitive to these effects; the

screened coulomb potentials are independent of the position of a particular residue in the protein relative to the surface. In addition to magnification of electrostatic fields in clefts and channels, similar effects project out into the solvent and can have a substantial impact on association rates of charged molecules. Applications of FDPB to Cu, Zn-superoxide dismutase have successfully accounted for observed rate constants for the diffusion of superoxide to the active site, as well as the dependence of the rate constants on ionic strength (67). SCP models failed to give results that agree with experiment (67).

To summarize, from the limited number of pK calculations that have been done it may be concluded that neither of the two approaches, SCP or FDPB, is significantly better than the other. However, the available computer algorithms for SCP employ the Tanford-Roxby method that may give incorrect results under certain circumstances; this tends to favor the FDPB approach for which available computer algorithms employ a hybrid statistical mechanical Tanford-Roxby method, thus eliminating a potential source of error. Additionally, the FDPB approach is favored by the fact that it is sensitive to the shape of the protein-solvent boundary and the position of

a titratable group with respect to this boundary; the SCP approach is insensitive to effects associated with the shape of this boundary. The present work is concerned with determining isoelectric points from calculated pK's for the macromolecule LADH and one or more of its complexes with ligands. The FDPB approach was selected primarily because LADH and its complexes may differ from one another by changes in conformation; these changes in protein conformation are likely to involve changes in shape of the protein-solvent boundary. Moreover, this molecule has deep clefts and pockets for substrate and coenzyme. The SCP approach would not be sensitive to the electric field magnifying effects of this geometry.

FDPB Calculations - Methods

pK calculations according to the null model were carried out as outlined above using a readily available computer algorithm (66). pK calculations according to the FDPB method were carried out as the result of a collaboration with A. Windemuth and A. Yang using the suite of computer programs of A. Yang, et al (73); these programs employ the hybrid statistical

mechanical Tanford-Roxby method as outlined above. The protein is treated as a low dielectric cavity embedded in an aqueous solvent medium. Dielectric constants of 4 and 20 for the protein interior were used in separate calculations to determine which agrees better with experimentally measured isoelectric points. The dielectric constant for the solvent was set at 80 for water; the ionic strength was set at 0.015 M to agree with experimental conditions. Atomic coordinates for protein structures were obtained from the Protein Data Bank (PDB) at Brookhaven (75). pK calculations were carried out for the following structures: apo-LADH (LADH withoug ligands), PDB designation 8ADH; LADH complexed with NAD^+ and p-bromobenzyl alcohol (substrate analog) (hereinafter referred to as LADH / NAD^+), PDB designation 1HLD; LADH complexed with ADP-ribose and 2-methyl-2,4-pentanediol (substrate analog) (hereinafter referred to as LADH / ADP-ribose), PDB designation 5ADH. Hydrogen atoms were placed in the protein structure with HBUILD of the CHARMM suite of programs (76). Charges were placed at the centers of atoms; charges were derived from the DISCOVER (77) and CHARMM parameter sets (76). The protein-solvent boundary was defined by the solvent accessible surface area using a 1.4 Å probe (71). The protein

structure is mapped onto a lattice of 65 X 65 X 65 cubic cells from 0.7 cell per Å in initial runs up to 3 cells per Å in final runs. Solvent pK's used were ASP 3.9, GLU 4.3, HIS 6.5, CYS 8.3, LYS 10.5, TYR 10.0, ARG 12.5, C-terminus 3.6, N-terminus 8.0.

FDPB - Titration Curves

Titration curves calculated with FDPB for apo-LADH, LADH / ADP-ribose, and LADH / NAD^+, are shown in figure 11.

Figure 11. FDPB calculated titration curves for the following structures: A, apo-LADH ϵ = 4; B, apo-LADH ϵ = 20; C, LADH / ADP-ribose ϵ = 4; D, LADH / ADP-ribose ϵ = 20; E, LADH / NAD^- ϵ = 4; F, LADH / NAD^- ϵ = 20.

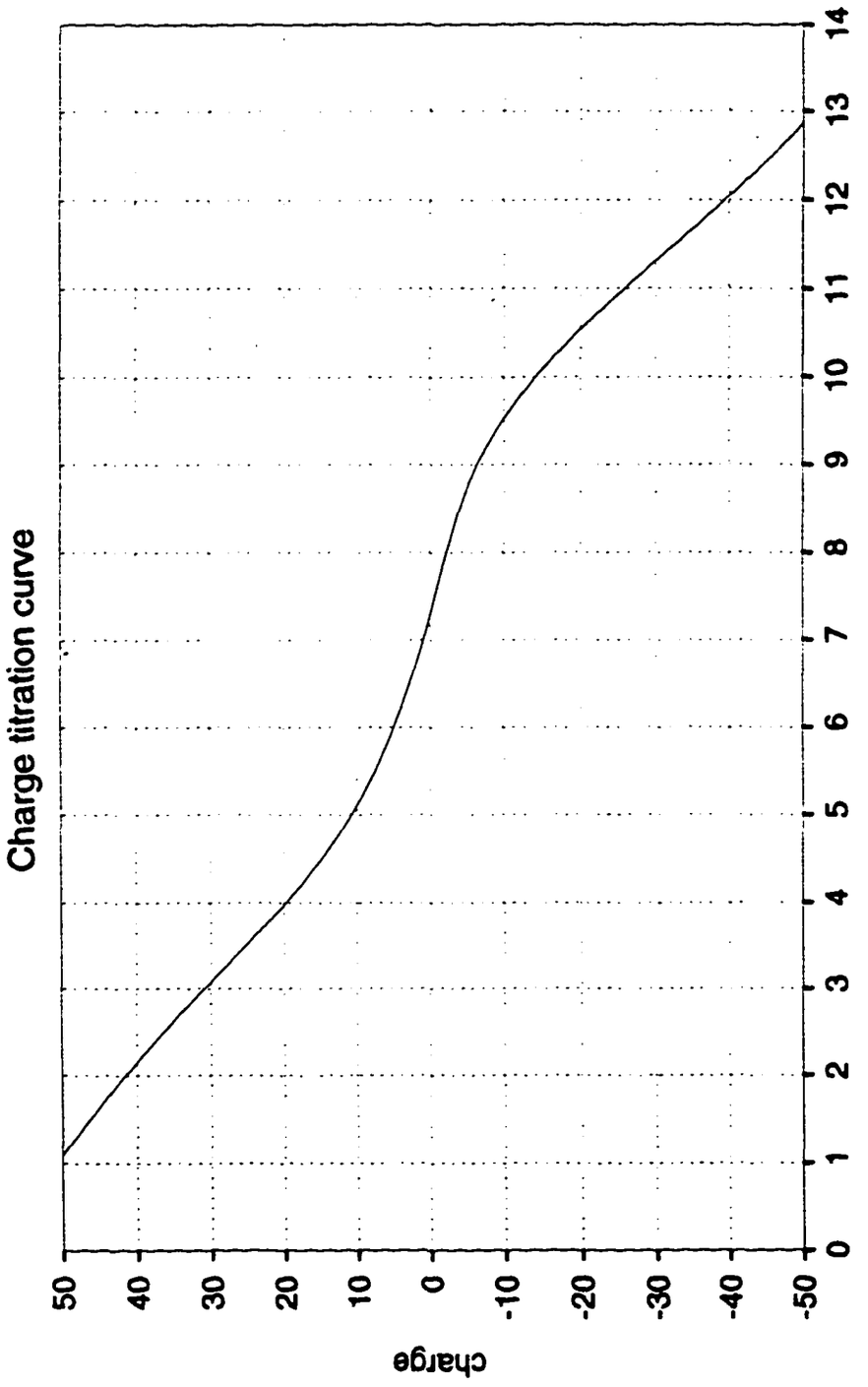

Fig. 11 A

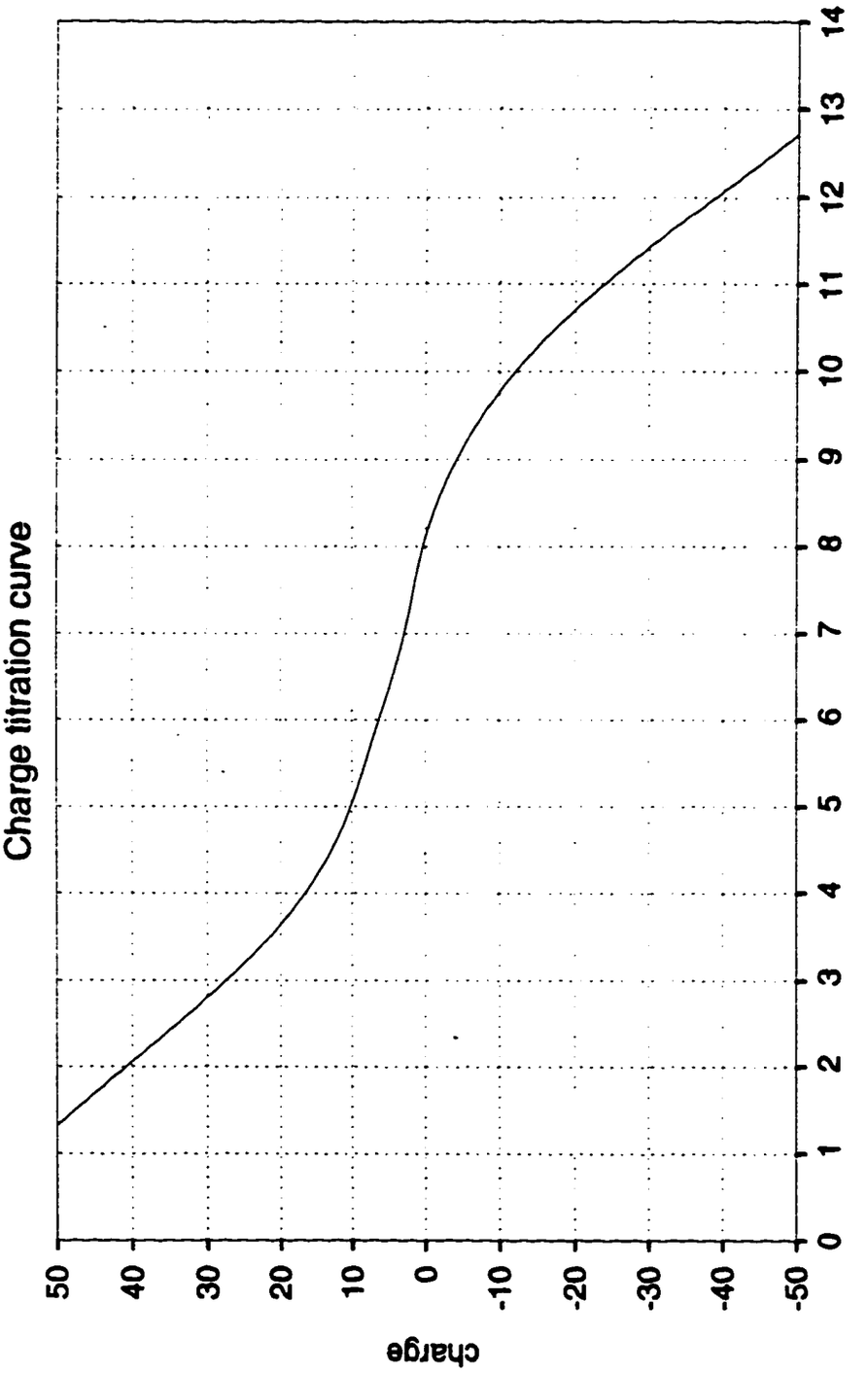

Fig. 11 B

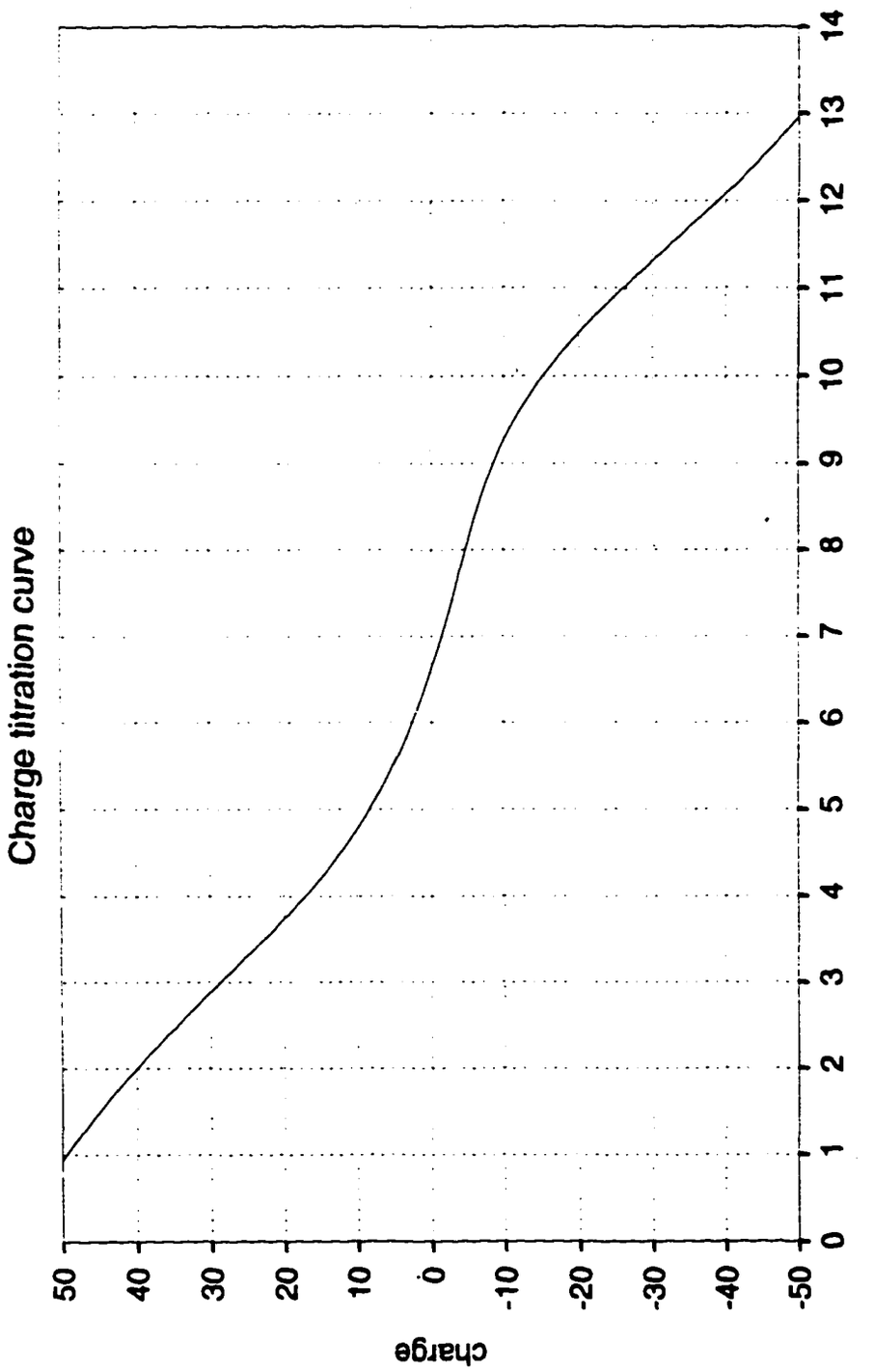

Fig. 11 C

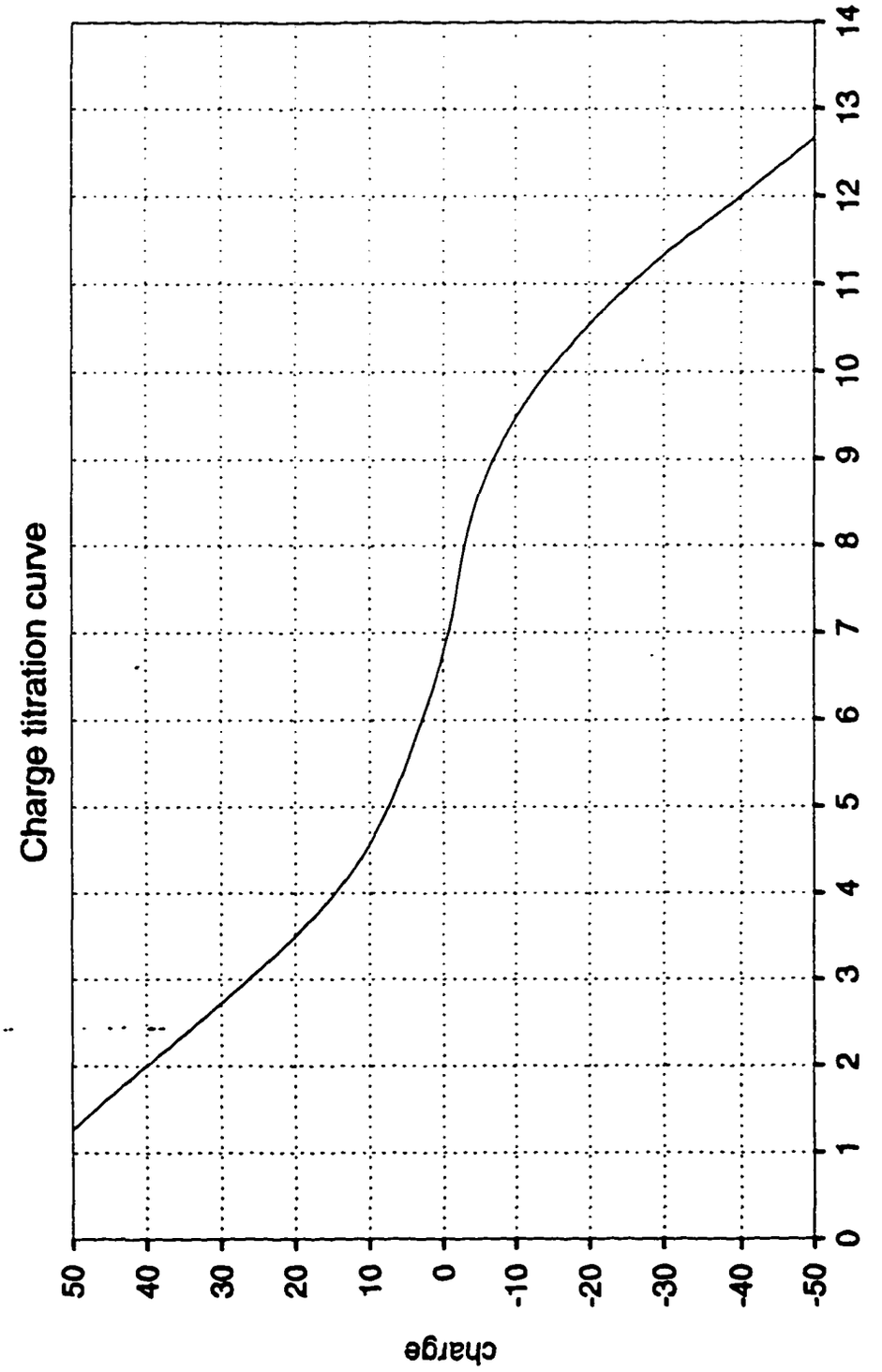

Fig. 11 D

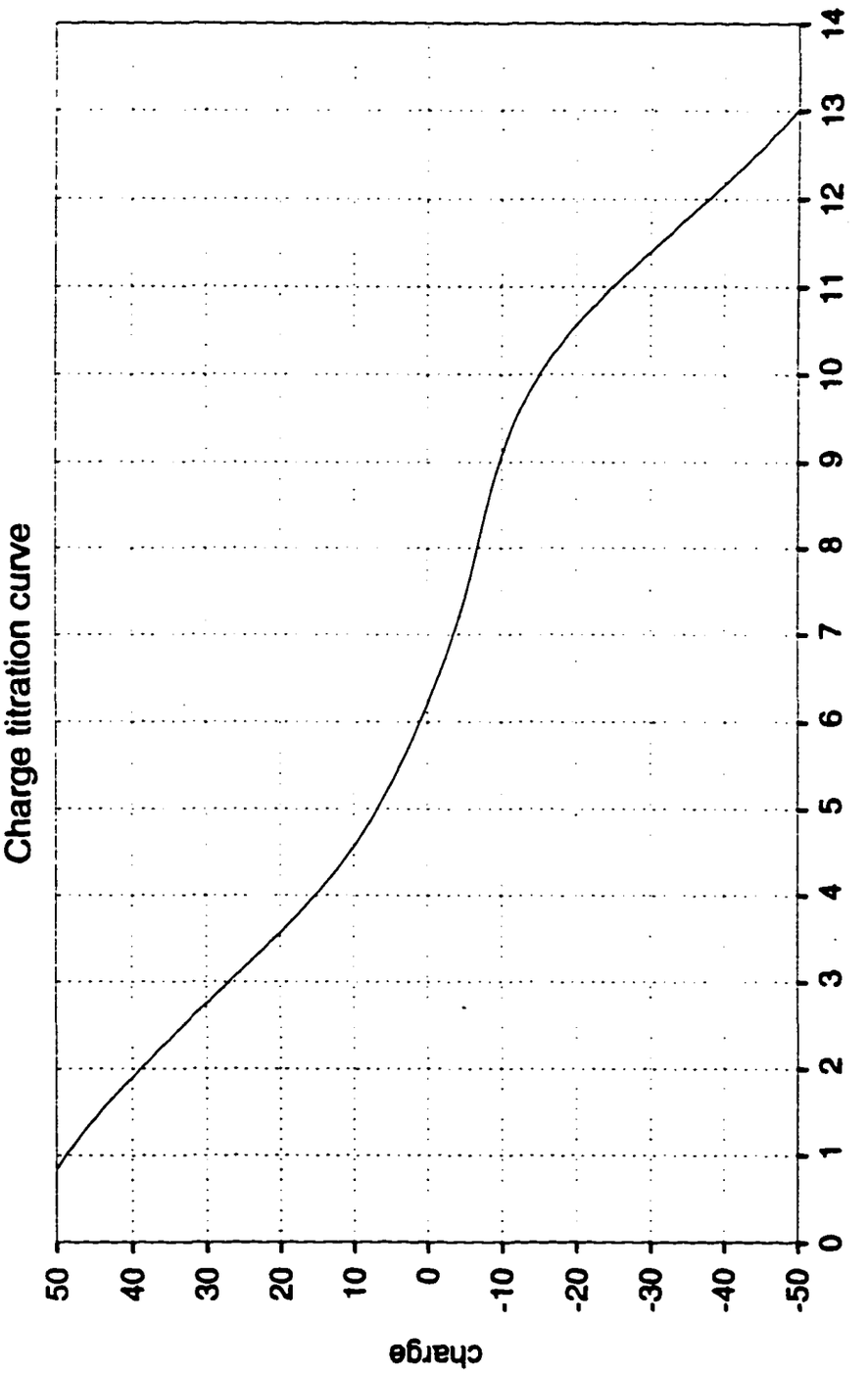

Fig. 11 E

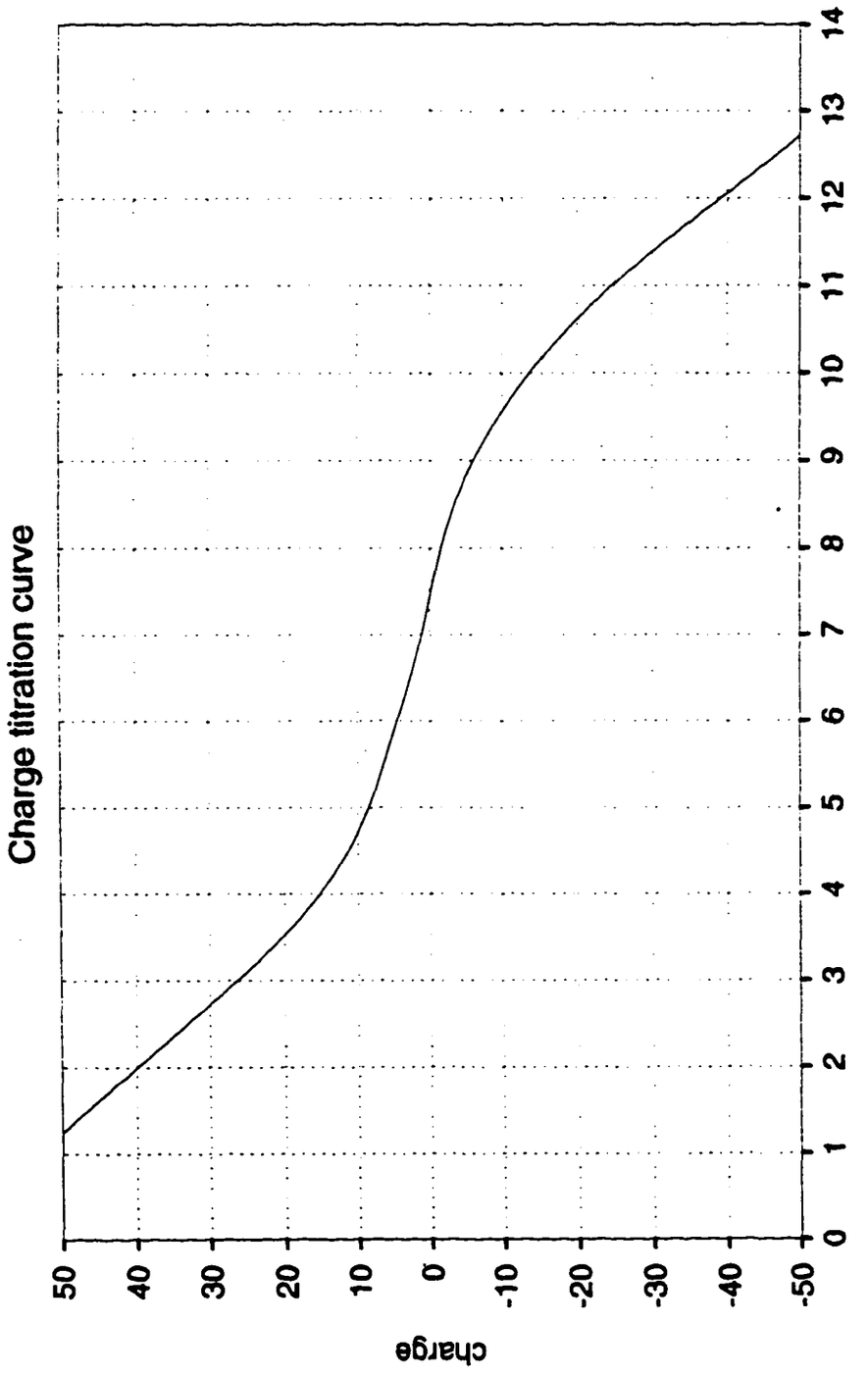

Fig. 11 F

There are two curves for each structure, one for a protein dielectric constant $\epsilon = 4$, and one for $\epsilon = 20$. The calculated isoelectric points are as follows: apo-LADH $\epsilon = 4$ pI = 7.27, $\epsilon = 20$ pI = 8.11; LADH / ADP-ribose $\epsilon = 4$ pI = 6.60, $\epsilon = 20$ pI = 6.77; LADH / NAD^+ $\epsilon = 4$ pI = 6.2, $\epsilon = 20$ pI = 7.42. Calculations according to the null model result in a pI of 8.86 for apo-ADH.

All of the titration curves have slopes in the range of 3 to 5 charges per pH unit in a range of one pH unit on either side of the calculated isoelectric points. The null model gives slopes of 20 charges per pH unit in the range of the calculated isoelectric point. The substantial differences between the null model slopes and FDPB slopes may be accounted for since CYS and to a lesser extent TYR residues (solvent pK's of 8.3 and 10.0) have their calculated pK's shifted substantially upward by the protein environment; at the higher pK's these groups have negligible change in charge with change in pH in the range of the isoelectric point. In all of the structures for which the dielectric constant $\epsilon = 4$, the pK's of all CYS and TYR residues have their pK's shifted above 14

due to the high desolvation energies associated with bringing the charged form of these residues into the protein where x-ray crystal structures indicate that they are substantially buried. (It should be remembered that pK values are functions of pH; for titratable residues cited here and below the given pK's are values calculated at pH 7. These values are good indicators for substantial shifts in titration curves for individual residues compared to their solvent titration curves. It must be emphasized that the titration curves for individual residues in the protein environment have shapes that may be different from those of solvent titration curves due to the pH dependence of the pK; precise average charges cannot be readily inferred from these pK's as they are from solvent pK's. However, precise values for average charges of particular residues as a function of pH have been calculated by the computer algorithms.) For the calculations for which ϵ = 20, CYS and TYR residues are also shifted to higher pK's, however, these pK's are lower compared with ϵ = 4 values since desolvation energies are smaller with the higher dielectric constant. For apo-LADH, CYS residues with pK's shifted upward but to values below 10.5 are CYS 240, shifted to 9.1, and CYS 9, 132, and 281 shifted to 10.3; all other CYS and TYR

residues have pK's shifted to values above 10.5. Similarly, LADH / ADP-ribose has CYS 9 shifted to 9.9, CYS 240 shifted to 10.1, and CYS 195 shifted to 10.3; all other CYS and TYR residues are shifted to values above 10.5. For LADH / NAD^+, CYS 195 and CYS 240 are shifted to 9.3, CYS 9 is shifted to 9.7, and all other CYS and TYR residues are shifted to values above 10.5.

FDPB - Isoelectric Points

As stated above the calculated isoelectric points for the apo-LADH structure are 7.27 for $\epsilon = 4$ and 8.11 for $\epsilon = 20$. This difference in pI can be accounted for by the differences in pK's for several residues due largely to differences in desolvation energies with changes in protein dielectric constant. A summary of residues with significant pK shifts affecting isoelectric points of LADH and its complexes is given in table 1.

Table 1. Summary of Residue pK's.

	LADH ϵ=4 pI=7.3	LADH ϵ=20 pI=8.1	LADH/ ADPr ϵ=4 pI=6.6	LADH/ ADPr ϵ=20 pI=6.8	LADH/ NAD^+ ϵ=4 pI=6.2	LADH/ NAD^+ ϵ=20 pI=7.4
ARG 47	10.7	14.1	14.1	14.1	14.1	14.1
LYS 113	7.3	9.5	6.5	9.3	7.1	8.7
LYS 228	9.5	12.5	14.1	14.1	14.1	14.1
GLU 267	4.9	0.0	8.5	3.1	0.0	0.0
LYS 323	5.7	9.9	5.7	10.1	4.7	9.7
ARG 369	14.1	14.1	14.1	14.1	5.5	14.1

Specifically, LYS 113, which is part of a lobe in the catalytic domain that binds the non-catalytic zinc, is shifted from 9.5 at $\epsilon \approx 20$ to 7.3 at $\epsilon \approx 4$; LYS 323 at one end of a hydrophobic core in the catalytic domain is similarly shifted from 9.9 to 5.7. Differences in pI for LADH / ADP-ribose may

be similarly attributed to shifts in pK's of the same LYS residues. LYS 113 is shifted from 6.5 at ϵ = 4 to 9.3 at ϵ = 20; LYS 323 is shifted from 5.7 to 10.1. In addition, GLU 267, which is part of a β-sheet that forms a hydrophobic core in the coenzyme binding domain, is shifted from 3.1 at ϵ = 20 to 8.5 at ϵ = 4 as a result of greater desolvation energies as well as greater interaction energies with the pyrophosphate of ADP-ribose at the lower dielectric constant. The difference in pI for LADH / NAD^+ in going from ϵ = 20 to ϵ = 4 may be accounted for mainly by LYS 323 going from 9.7 at ϵ = 20 to 4.7 at ϵ = 4, as a result of larger desolvation energies at ϵ = 4, and ARG 369, part of a β-sheet in the catalytic domain surrounding the active site zinc (38), going from over 14 at ϵ = 20 to 5.5 at ϵ = 4, also as a result of larger desolvation energies at ϵ = 4. ARG 369 has a strong charge-charge interaction with GLU 68, which is 5 Å from the catalytic zinc. It also has a weaker charge-charge interaction with pyrophosphate of NAD^+; both interactions should raise the pK. However, at ϵ = 4 the desolvation energy is much greater than the sum of these charge-charge interaction energies.

FDPB - Isoelectric Point Shifts

The differences in isoelectric point ΔpI between the apo-LADH and LADH / ADP-ribose structures at $\epsilon = 20$ and $\epsilon = 4$ are 1.34 and 0.67 respectively. At $\epsilon = 20$ there are no significant pK shifts contributing to ΔpI. The change in isoelectric point may be attributed to the addition of negative charge from ADP-ribose. At $\epsilon = 4$ the isoelectric point is also shifted by the addition of negative charge due to ADP-ribose. In addition, a small shift in LYS 113 going from 7.3 in LADH to 6.5 in LADH / ADP-ribose results in a small loss of positive charge. However, a shift of GLU 267 from 4.9 in LADH to 8.5 in LADH / ADP-ribose contributes a larger loss of negative charge. This is due to greater desolvation of this residue in the complex, as well as an added interaction with pyrophosphate. It is of interest to note that ARG 47 is shifted from 10.7 in LADH to over 14 in LADH / ADP-ribose as a result of the interaction with the negative charges of the pyrophosphate of the ligand. Also, LYS 228 is shifted from 9.5 to over 14 as a result of hydrogen bonding to a hydroxyl group of the adenosine ribose. These shifts, however, result in negligible changes in charge. The net result is that at $\epsilon = 4$ the charge difference between apo-LADH and LADH / ADP-ribose is less than the charge

difference at $\epsilon = 20$; this accounts for the smaller shift in isoelectric point at $\epsilon = 4$ relative to the shift at $\epsilon = 20$.

The differences in isoelectric point between LADH and LADH / NAD^+ behave in an opposite way with respect to dielectric constant, i.e., at the lower dielectric constant there is a greater isoelectric point shift. Specifically, at $\epsilon = 20$ ΔpI is 0.69, and at $\epsilon = 4$ ΔpI is 1.07. At $\epsilon = 20$ there are no residues that contribute substantially to ΔpI; the isoelectric point shift of LADH / NAD^+ relative to apo-LADH is due largely to the addition of the negative charge of the ligands. At $\epsilon = 4$, ARG 369 is shifted from over 14 in apo-LADH to 5.5 in LADH / NAD^+ and this may be attributed to increased desolvation in the LADH / NAD^+ complex. This pK shift accounts for the larger change in isoelectric point at $\epsilon = 4$ relative to $\epsilon = 20$. It is of interest to speculate as to whether ARG 369 is related to the ionizable group governing the pH dependent effects of coenzyme binding and associated proton release. Again, it is of interest to note that ARG 47 is shifted from 10.7 in apo-LADH to over 14 in LADH / NAD^+, and this may be attributed to interaction with the pyrophosphates of the NAD^+ ligands; the contribution to ΔpI is negligible. LYS 228 is also shifted

from 9.5 to over 14 by the interaction with the adenosine ribose; again, the contribution to ΔpI is negligible.

LADH - IEF and MIEF Experiments

The isoelectric focusing method (MIEF) developed as part of this work was employed to focus LADH, the LADH complex with NAD^+ and pyrazole, and the LADH complex with salicylate. These experiments were performed in an attempt to answer the following three questions:

One, are the complex patterns obtained when LADH is focused with carrier ampholytes a result of interactions with carrier ampholytes and/or a result of protein-protein interactions that arise in a low ionic strength environment? Proteins are more likely to interact with other large molecules if surface charges are not shielded by counter ions of the solvent. The MIEF system eliminates the high molecular weight carrier ampholytes and provides a substantially higher ionic strength environment for focusing.

Two, is there evidence for pH-dependent conformational changes for LADH or its complexes with ligands? A pH-dependent conformational change has been proposed to account for the pH

dependence of coenzyme association rates. If LADH or any of its complexes should individually have more than one isoelectric point, this would be strong evidence that the protein undergoes a pH-dependent conformational change. According to the theory of titration curves, a single conformation of a protein should have only one isoelectric point (78).

Three, how do the isoelectric points and shifts in isoelectric point with complex formation, as measured experimentally, compare with calculated values for this protein and its complexes? Specifically, which values of dielectric constant for the protein interior, 4 or 20, give calculated isoelectric point results that agree better with experiment?

Materials and Methods

The methods used were essentially the same as described in Part 1. The ion-selective membrane used for these experiments was Nafion 450. Sephadex G 150 superfine was used for the gel matrix. LADH (EE isoform) was obtained from Boehringer as the 10% ethanol suspension (20 mM phosphate buffer pH 7). Protein

was extensively dialyzed against the MIEF starting buffer for each electrofocusing run and applied to a gel with an established pH gradient. Enzymatic activity of LADH was detected in gels and paper strips with an activity stain (phenozine methosulfate / thiazolyl blue / ethanol / NAD^+) (79) . The activity of recovered LADH samples was measured by monitoring spectrophotometrically the reduction of NAD^+ with ethanol as substrate according to the method of Dalziel (80). No effort was made to maximize recovery of proteins from gel samples. pH measurements were obtained by making one to one dilutions of harvested gel samples with deionized water followed by immersion of a pH electrode into the sample. Buffer composition was determined by comparing gel sample conductivity measurements with conductivity measurements of samples of known composition, and taking into account the pH measurements. NAD^+ and salicylate concentrations were determined spectrophotometrically by measuring absorbance at 259 nm and 300 nm respectively using molar extinction coefficients of 18,000 and 4234 respectively (buffers used have negligible absorbance at these wavelengths). Pyrazole concentrations were determined by titration of LADH in an activity assay according to Dalziel (80). Focusing times for

MIEF runs were determined empirically; protein bands were considered focused when continued application of the electric field resulted in a protein band displacement of less than 0.5 mm per hour. This movement was determined by sampling the gel with vertically inserted filter paper strips, as previously described, after consecutive time intervals. Sampling positions varied between 0.5 and 1 cm across the gel (in a direction perpendicular to that of the electric field). It has been found that these consecutive gel samplings do not substantially perturb the focusing process.

Error Analysis

Errors in pH values assigned to focused protein bands were estimated by summing determinate errors: errors in pH measurement (± 0.02 pH units), errors in positions for gel sample harvesting and band location (± 0.15 cm x pH gradient slope), errors due to pH gradient drift (± 0.005 pH units), and errors due to electroosmosis (± 0.005 pH units). Errors in assigned pH values due to pH gradient drift were estimated as follows. An upper limit to the displacement velocity of an apparently focused protein band (velocity due to pH shifts

away from isoelectric values) was determined by measuring the maximum distance that a protein band is displaced over a fixed time interval after focusing (less than 0.5 mm per hour). With the assumption that a pH gradient drift may be characterized by a linear variation of pH values with time at each gel position, it follows that the measured pH will differ from the isoelectric pH for an apparently focused protein by a maximum of twice an average pH shift away from the isoelectric pH. This average pH shift may be related to the measured displacement velocity as follows. The displacement velocity may first be related to the average net charge through the following electrophoretic mobility equation (81)

$$v = q E / f$$

where v is the displacement velocity; E is the imposed electric field strength; q is the net protein charge; and f is a frictional coefficient for the protein molecule. A frictional coefficient, f, for LADH of 6.2×10^{-8} g sec^{-1}, may be derived from a measured diffusion coefficient of 6.5×10^{-7}

cm^2 sec^{-1} (82). The average net charge may then be related to the average pH shift through the slope of the titration curve for LADH near the isoelectric point. A value of 4 proton charges per pH unit as obtained with the FDPB calculations was used.

Errors due to electroosmosis were determined in a similar manner. The difference between the measured pH and the isoelectric pH is correlated with a pH shift and associated net charge that, together with the imposed electric field, gives a displacement velocity equal in magnitude to the velocity of electroosmotic flow as measured by the displacement of cyanocobalamine (vitamin B_{12}), an uncharged, low molecular weight, colored molecule that moves along with the hydrodynamic flow in the gel bed engendered by electroosmosis (83).

Results - IEF with Carrier Ampholytes

LADH focused on a conventional carrier ampholyte gel is shown in figure 12 A. There is an intensely staining band at pH 7.9 and at least four closely spaced bands of varying intensity

between pH 7.2 and 7.9. There are, in addition, two weak spaced-apart bands above pH 7.9. As shown in figure 12 B, all of these bands have been shown to be enzymatically active. The isoelectric point of the most intense band is substantially lower than that previously reported for carrier ampholyte focusing of the EE isoform of LADH, i.e., 8.7 for the main component (40). The isoelectric point discrepancy between present and previous experiments might be due to carrier ampholyte effects: previous isoelectric focusing experiments were done with ampholytes containing mostly amino and carboxyl groups (Ampholine); the present experiments were done with ampholytes containing residues of phosphonic acid and sulfonic acid (Servalyt).

Figure 12. LADH focused on carrier ampholyte gel pH 3-10, A. stained with Coomassie blue R 250. Lane 1, LADH (EE isoform); lane 2, marker proteins (protein applied near anode). B. focused LADH (EE isoform) stained for activity.

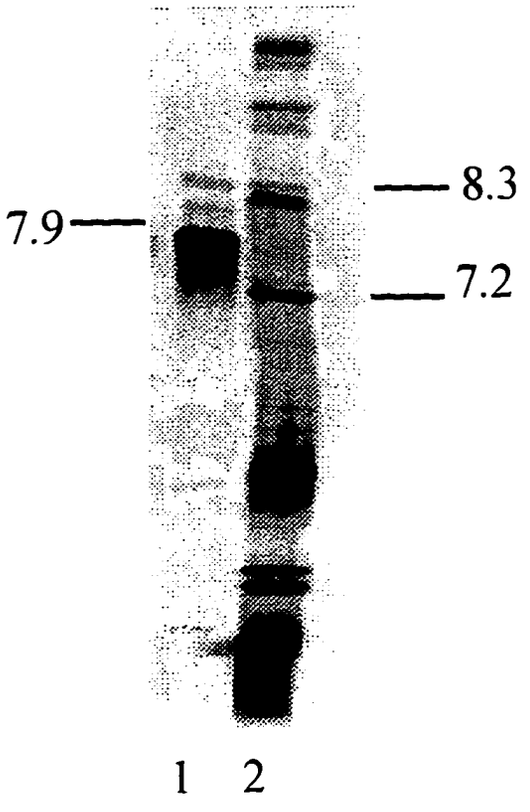

Fig. 12 A

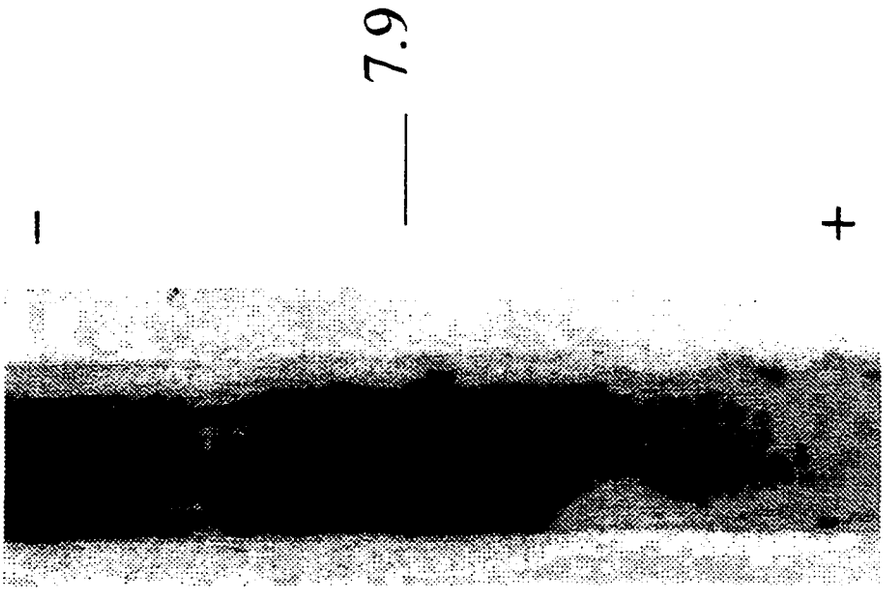

Fig.12 B

Results - MIEF - LADH

Results of an MIEF run with a sample concentration of approximately 1 mg protein per ml gel in the sample application zone, are shown in figure 13. Protein bands were located by the filter paper strip method after 18 hours. The paper strip shows a complex banding pattern. Five consecutive gel fractions were harvested, protein eluted, and the recovered protein samples were re-focused on a carrier ampholyte gel in corresponding consecutive lanes 2 through 6, as shown in figure 14. The banding patterns of fractions in lanes 2, 3, 5, and 6 appear mutually similar and similar to the original LADH sample in lanes 1 and 8 with the exception that the two weak higher pH bands of the original sample are absent; these bands are also absent for the fraction in lane 4. The fraction in lane 4 has a weak band where the other fractions have a most intense band. Additionally, this fraction has at least two lower-pH bands that are substantially more intense than corresponding bands for other fractions. The differences in the banding pattern for the

fraction in lane 4 relative to the patterns for other fractions appears to confirm that the MIEF run has brought about a separation of heterogeneous protein components.

Figure 13. LADH (1 mg per ml gel) focused with MIEF (18 hours), glycine/NaOH buffer. Filter paper strip stained with Coomassie blue R 250.

Fig. 13

Figure 14. LADH samples harvested from MIEF run as in figure 12, and refocused on carrier ampholyte gel pH range 3-10. Lanes 1 and 8, LADH; lanes 2 through 6, consecutive gel fractions (lane 2 most acidic); lane 9, marker proteins.

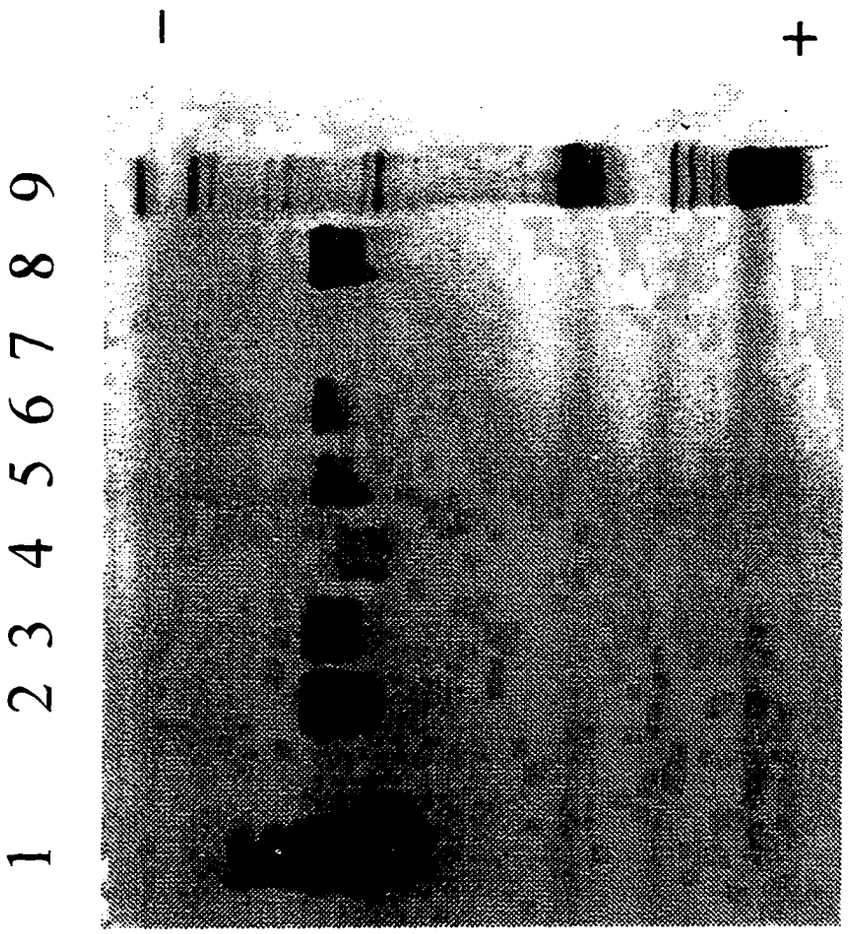

Fig. 14

Figure 15. LADH (1 mg per ml) focused with MIEF (40 hours), glycine/NaOH buffer. Filter paper strip stained with Coomassie blue R 250.

Fig. 15

Figure 16. LADH (1 mg per ml) focused with MIEF (40 hours), glycine/NaOH buffer. Filter paper strip stained for activity with phenozine methosulfate/thiazolyl blue/ethanol/NAD.

Fig. 16

Figure 17 A. LADH (0.1 mg per ml) focused with MIEF (18 hours), glycine/NaOH buffer. Filter paper strip stained with Coomassie blue R 250. Isoelectric point 8.88 ± 0.14.

Figure 17 B. LADH (0.1 mg per ml) focused with MIEF (18 hours), glycine/NaOH buffer. Enzymatically active LADH (micrograms) as a function of gel position (measured with the assay according to Dalziel (a)).

Figure 17 C. LADH (0.1 mg per ml) focused with MIEF (18 hours), glycine/NaOH buffer. pH as a function of gel position.

Figure 17 D. LADH (0.1 mg per ml) focused with MIEF (18 hours), glycine/NaOH buffer. Electric field strength (volts per centimeter) as a function of gel position.

Figure 17 E. LADH (0.1 mg per ml) focused with MIEF (18 hours), glycine/NaOH buffer. Sodium ion concentration (mM) as a function of gel position.

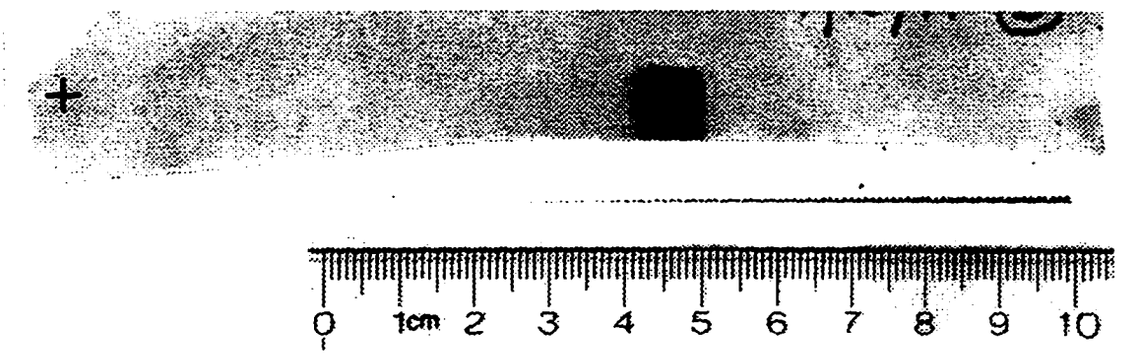

17 A

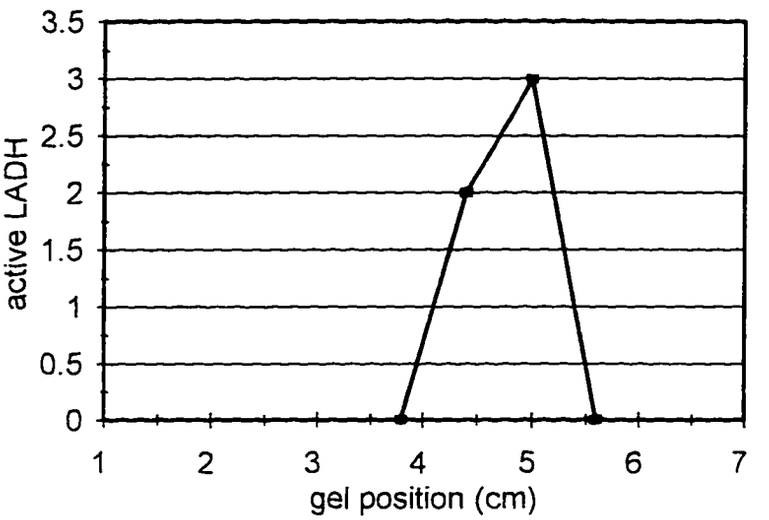

17 B

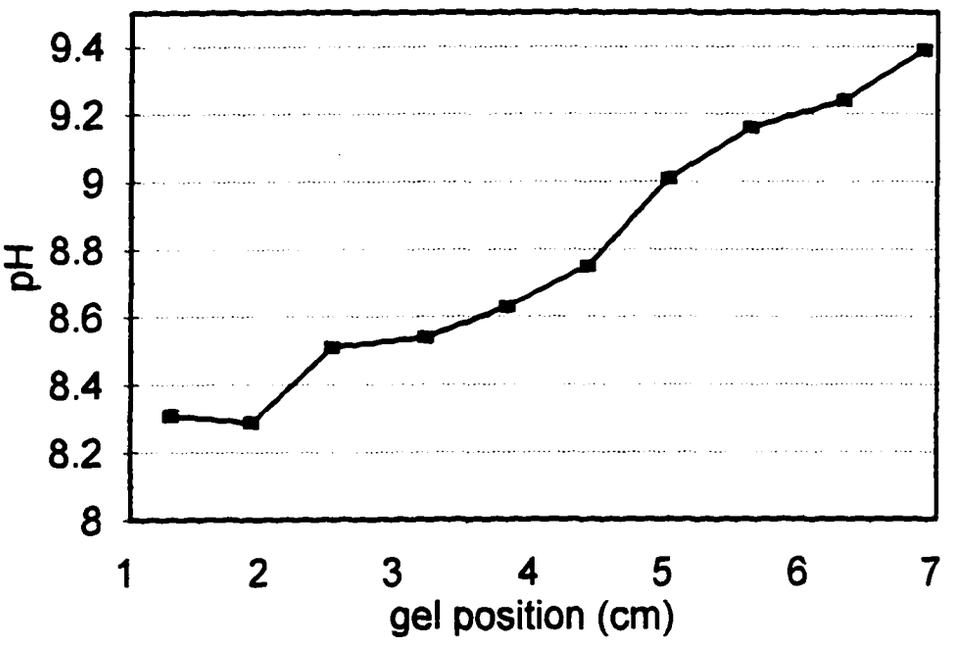

Fig. 17 C

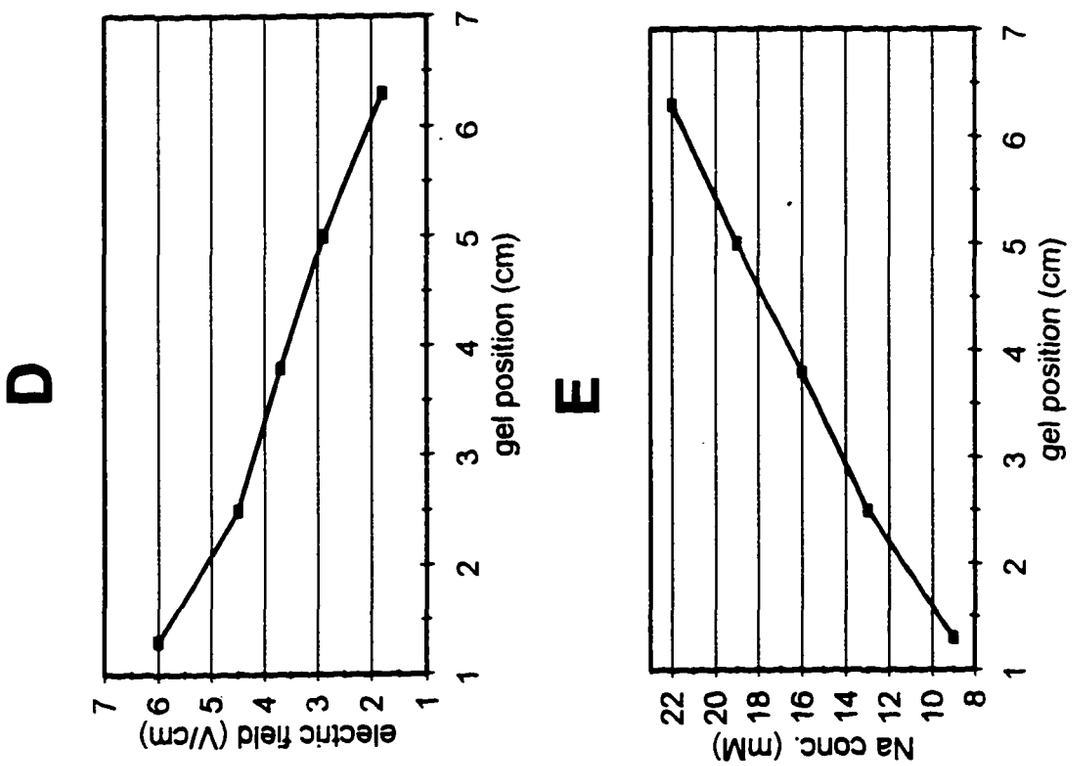

Fig. 17

Figure 18 A. LADH (0.1 mg per ml) focused with MIEF (18 hours), glycine/NaOH buffer; 50 μM NAD and 1 mM pyrazole in focusing gel. Filter paper strip stained with Coomassie blue R 250.

Figure 18 B. LADH (0.1 mg per ml) focused with MIEF (18 hours), glycine/NaOH buffer; 50 μM NAD and 1 mM of pyrazole in focusing gel. pH as a function of gel position.

Figure 18 C. LADH (0.1 mg per ml) focused with MIEF (18 hours), glycine/NaOH buffer; 50 μM NAD and 1 mM pyrazole in focusing gel. Electric field strength (volts per centimeter) as a function of gel position.

Figure 18 D. LADH (0.1 mg per ml) focused with MIEF (18 hours), glycine/NaOH buffer; with 50 μM NAD and 1 mM pyrazole in focusing gel. Sodium ion concentration (mM) as a function of gel position.

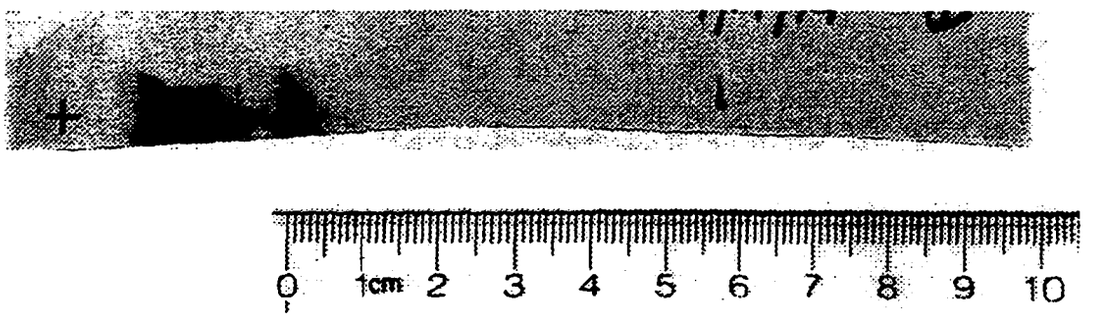

Fig. 18 A

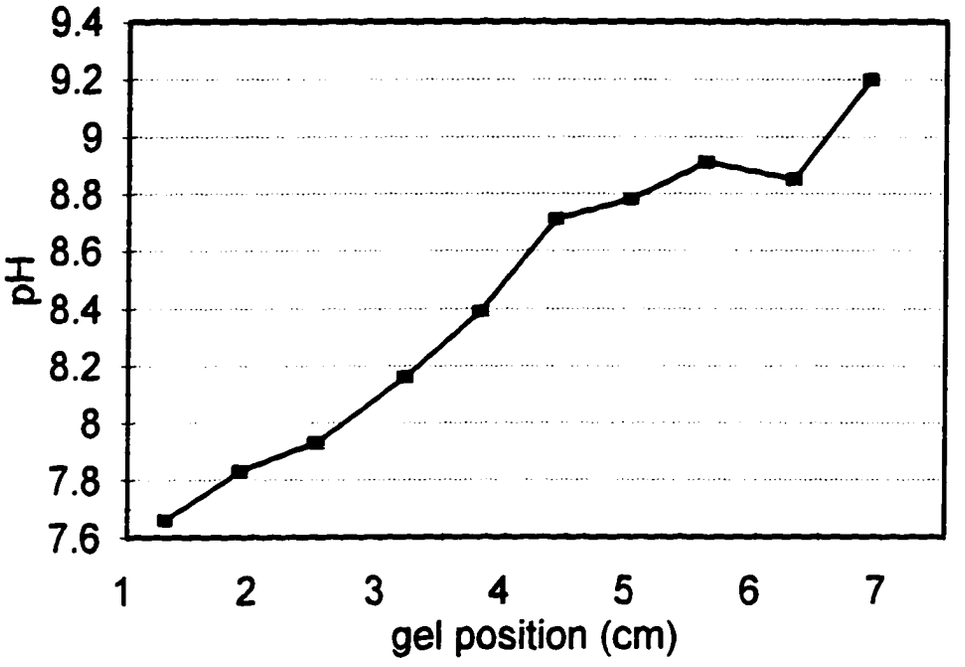

Fig. 18 B

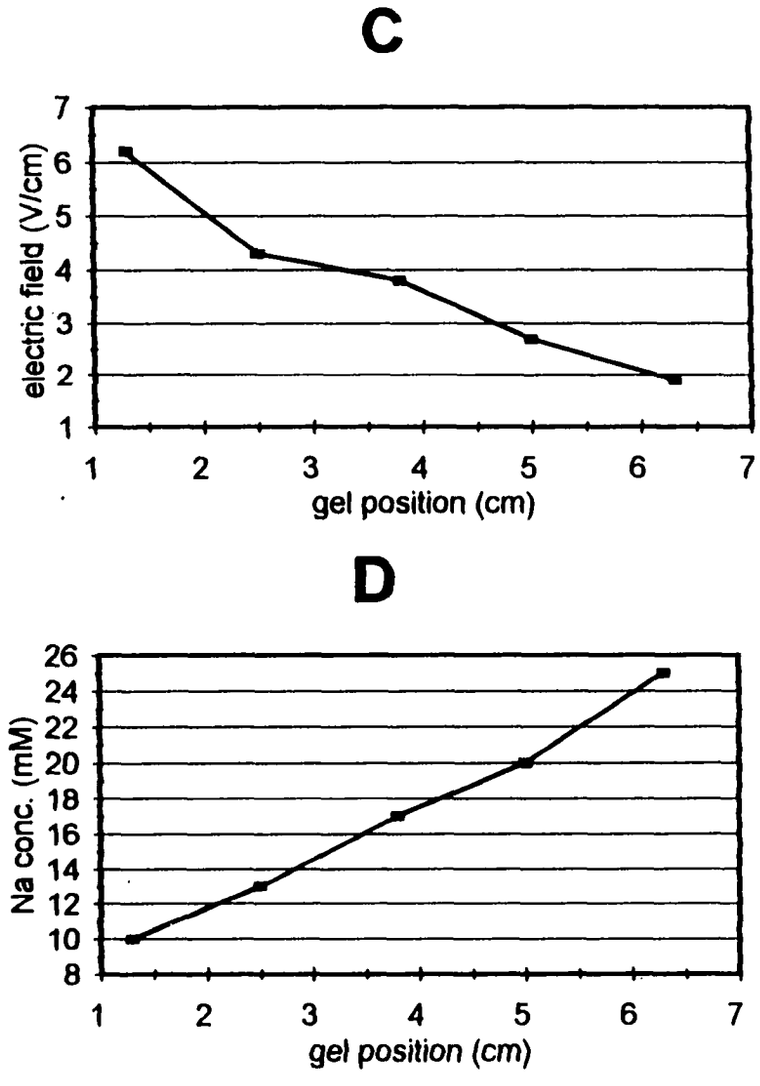

Fig. 18

Figure 19 A. LADH (0.1 mg per ml) focused with MIEF (18 hours), bicine/NaOH buffer; 40 μM NAD and 0.5 mM pyrazole in focusing gel. Filter paper strip stained with Coomassie blue R 250. Isoelectric point 7.61 ± 0.13.

Figure 19 B. LADH (0.1 mg per ml) focused with MIEF (18 hours), bicine/NaOH buffer; 40 μM NAD and 0.5 mM pyrazole in focusing gel. pH as a function of gel position.

Figure 19 C. LADH (0.1 mg per ml) focused with MIEF (18 hours), bicine/NaOH buffer; 40 μM NAD and 0.5 mM pyrazole in focusing gel. Electric field strength (volts per centimeter) as a function of gel position.

Figure 19 D. LADH (0.1 mg per ml) focused with MIEF (18 hours), bicine/NaOH buffer; 40 μM NAD and 0.5 mM pyrazole in focusing gel. Sodium ion concentration (mM) as a function of gel position.

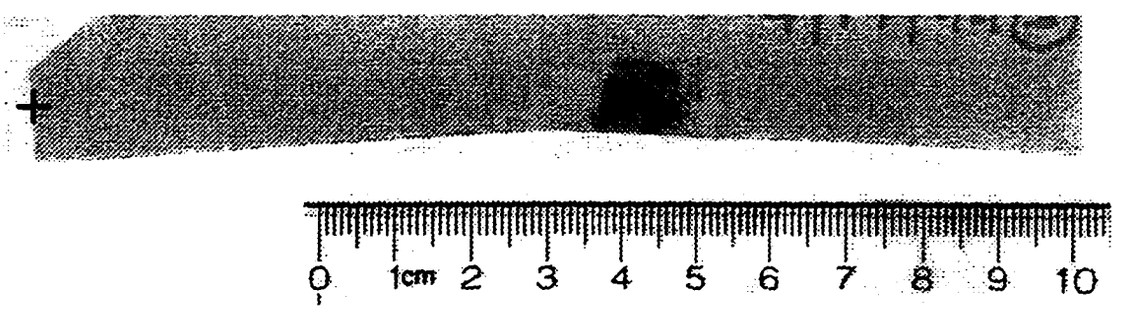

Fig. 19 A

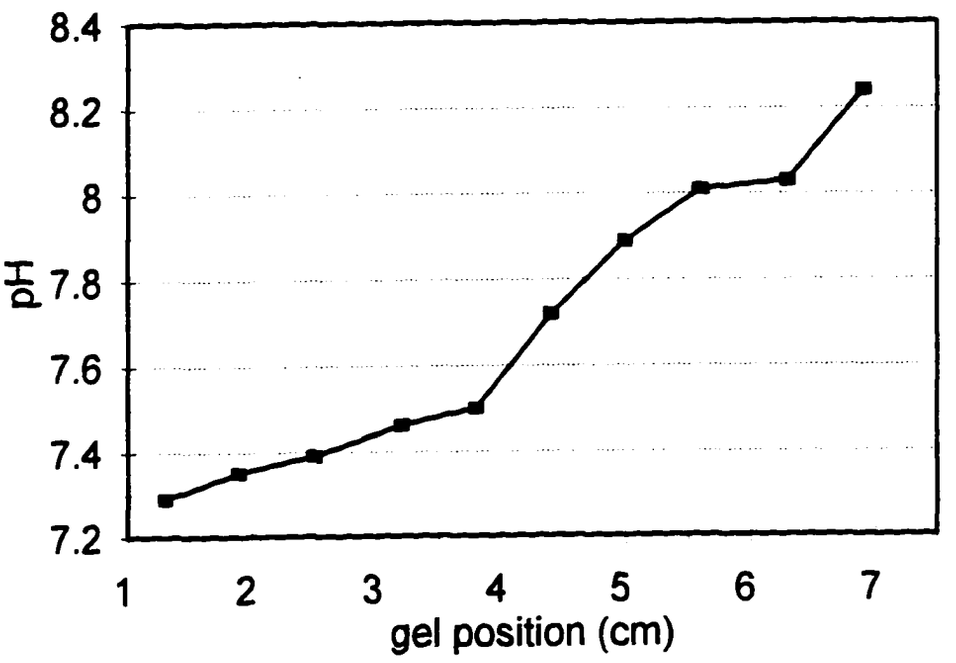

Fig. 19 B

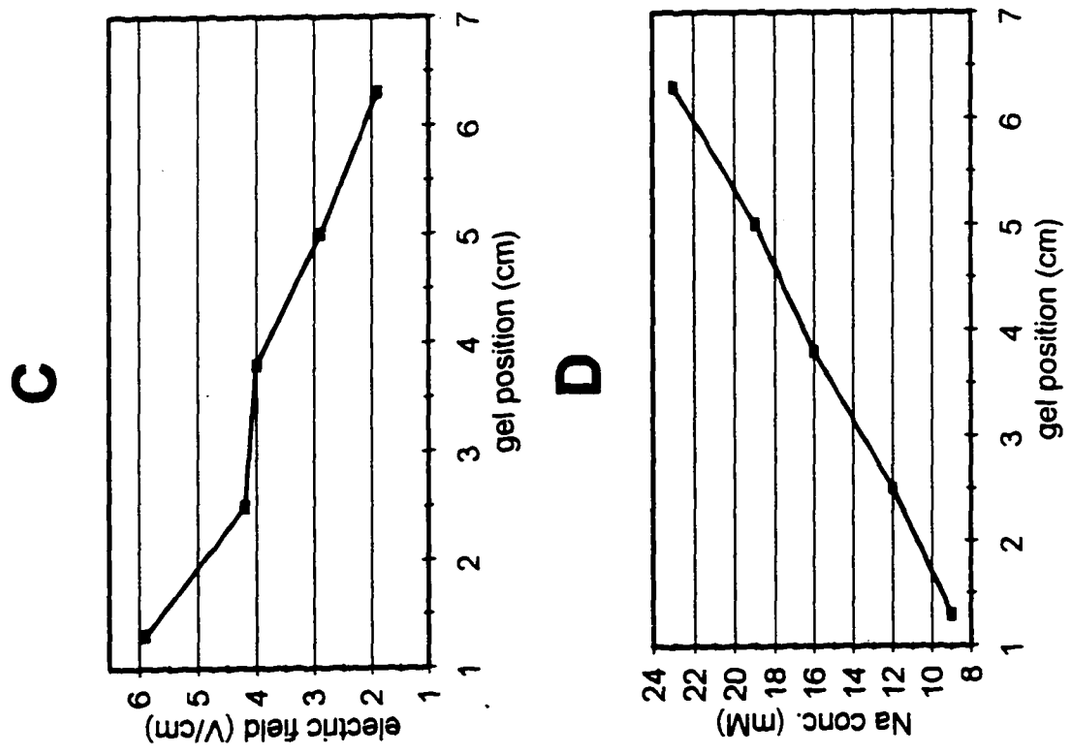

Fig. 19

Figure 20. LADH (0.1 mg per ml) focused with MIEF (18 hours); bicine/NaOH buffer, pH range 8.0 to 9.0; 100 μM NAD in focusing gel; Filter paper strip stained with Coomassie blue R 250.

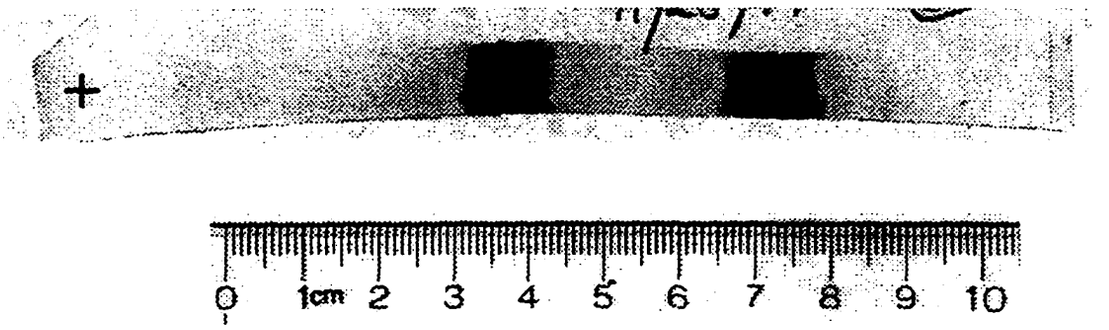

Fig. 20

Results of an extended MIEF run for 40 hours is shown in figure 15. Paper strips show that the complex banding pattern collapses to that of a single component with an isoelectric point of 8.9. This component is shown to be enzymatically active with the phenozine / thiazolyl blue stain as shown in figure 16. Substantially lower concentrations of LADH (approximately 0.1 mg protein per ml gel in the sample application zone) were applied to an MIEF gel; results are shown in figure 17. This and subsequent figures include the Coomassie stained filter paper strip showing the location of protein bands, results of LADH enzymatic activity assays of gel samples, the measured pH gradient, the imposed electric field, and sodium concentrations, which, together with pH values, specify buffer composition in each gel sample. These data provide a more complete description of the experiments for which quantitative results are given. The results given in figure 17 show that a single focused band with an isoelectric point of 8.88 appears in the same time and under the same conditions that had given a complex pattern with higher concentrations of LADH.

Results - MIEF - LADH / NAD^+

The LADH / NAD^+ / pyrazole complex was examined with an MIEF run under the same conditions as above for LADH alone, except for the inclusion of NAD^+ and pyrazole in the protein sample applied, in the gel, and in the starting buffer so as to have saturating levels of both NAD^+ and pyrazole in focusing gel. For this and subsequent experiments concentrations of 0.1 mg of protein per ml of gel were used at the sample load positions. As shown in figure 18, protein migrates off the ion-selective membrane at the anode edge. The conclusion is that the isoelectric point of the complex is below the range of the pH gradient established with the glycine / NaOH buffer. This MIEF run was repeated with a bicine buffer establishing a pH gradient in a lower range. Again, saturating levels of NAD^+ and pyrazole were included in the protein sample, in the gel and in the bicine starting buffer. Results are shown in figure 19. The LADH / NAD^+ / pyrazole complex focused at a pH value of 7.61.

Attempts to focus the LADH / NAD^+ binary complex had anomalous results. Including NAD^+ in the protein sample, the gel, and

the starting buffer so as to have close to saturating levels in the focusing gel, caused the protein to focus as complex banding patterns close to the positions of protein sample application to the gel, over the pH range of 8.0 to 9.0. This occurred even if protein was applied at two widely separated positions in the same gel. Results of an MIEF run in which protein is applied at two distinct positions is shown in figure 20.

Results - MIEF - LADH / Salicylate

Finally, the binding of salicylate to LADH was examined with MIEF runs using glycine and bicine buffers. A run with glycine was performed with salicylate in the protein sample, gel, and starting buffer; salicylate levels in the focusing gel were sufficient for greater than 80% occupancy. The dissociation constant for salicylate has been found to be close to 1.25 mM over the pH range from 7 to 10 (53). Protein was applied to the gel at the cathode edge. Results are shown in figure 21. There is no substantial shift in isoelectric point when

compared with runs without salicylate. Similarly, an MIEF run was performed with bicine which establishes a pH gradient in a lower range than that established with glycine. Again, this MIEF run incorporated salicylate sufficient for greater than 80% occupancy. Protein, however, was applied at the anode edge of the focusing gel, i.e., protein approached the isoelectric point from low pH values. Results of this run are shown in figure 22. Clearly, there is a substantial downward shift of isoelectric point under these conditions.

Figure 21 A. LADH (0.1 mg per ml) focused with MIEF (18 hours), glycine/NaOH buffer; 5.6 mM salicylate in focusing gel. Filter paper strip stained with Coomassie blue R 250. Isoelectric point 8.95 ± 0.09.

Figure 21 B. LADH (0.1 mg per ml) focused with MIEF (18 hours), glycine/NaOH buffer; 5.6 mM salicylate in focusing gel. Enzymatically active LADH (micrograms) as a function of gel position (measured with the assay according to Dalziel (a), corrected for salicylate).

Figure 21 C. LADH (0.1 mg per ml) focused with MIEF (18 hours), glycine/NaOH buffer; 5.6 mM salicylate in focusing gel. pH as a function of gel position.

Figure 21 D. LADH (0.1 mg per ml) focused with MIEF (18 hours), glycine/NaOH buffer; 5.6 mM salicylate in focusing gel. Electric field strength (volts per centimeter) as a function of gel position.

Figure 21 E. LADH (0.1 mg per ml) focused with MIEF (18 hours), glycine/NaOH buffer; 5.6 mM salicylate in focusing gel. Sodium ion concentration (mM) as a function of gel position.

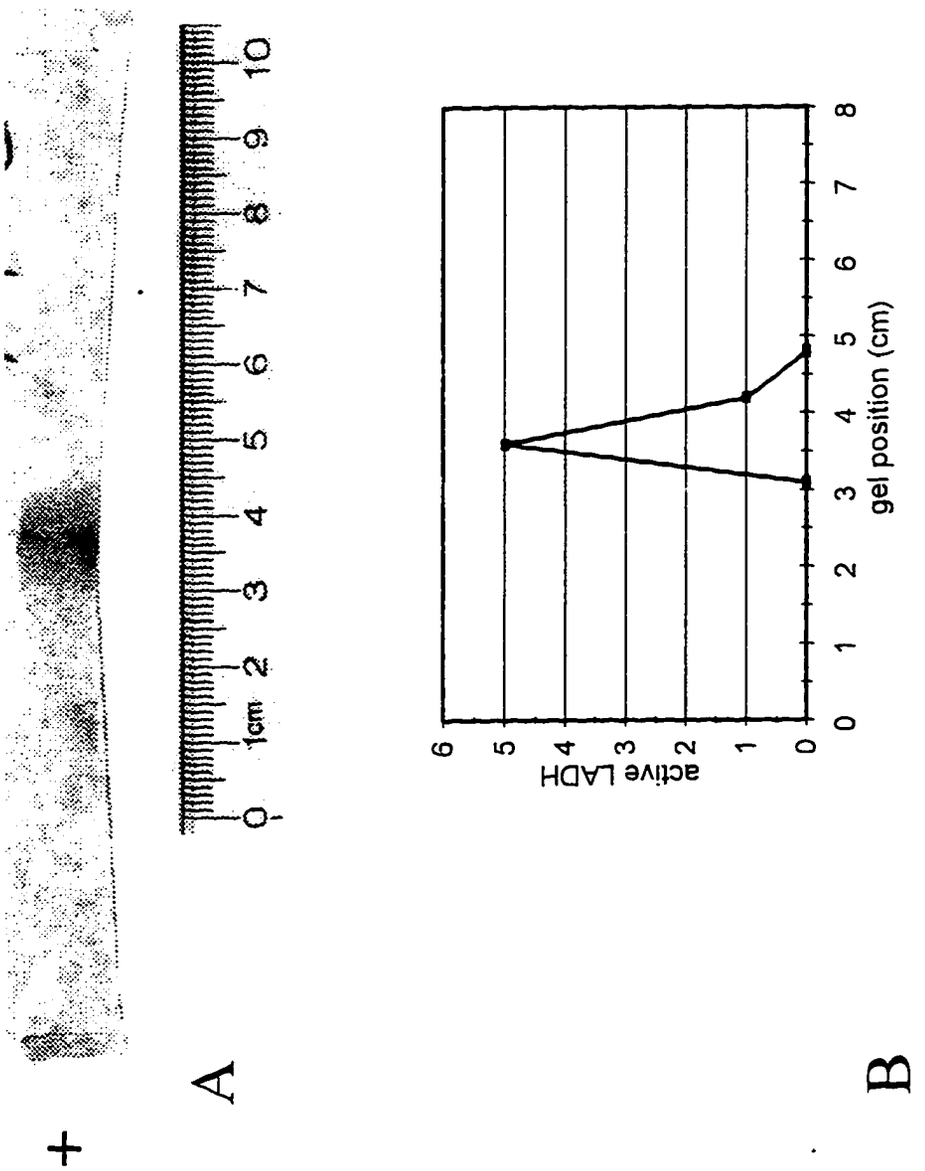

Fig. 21

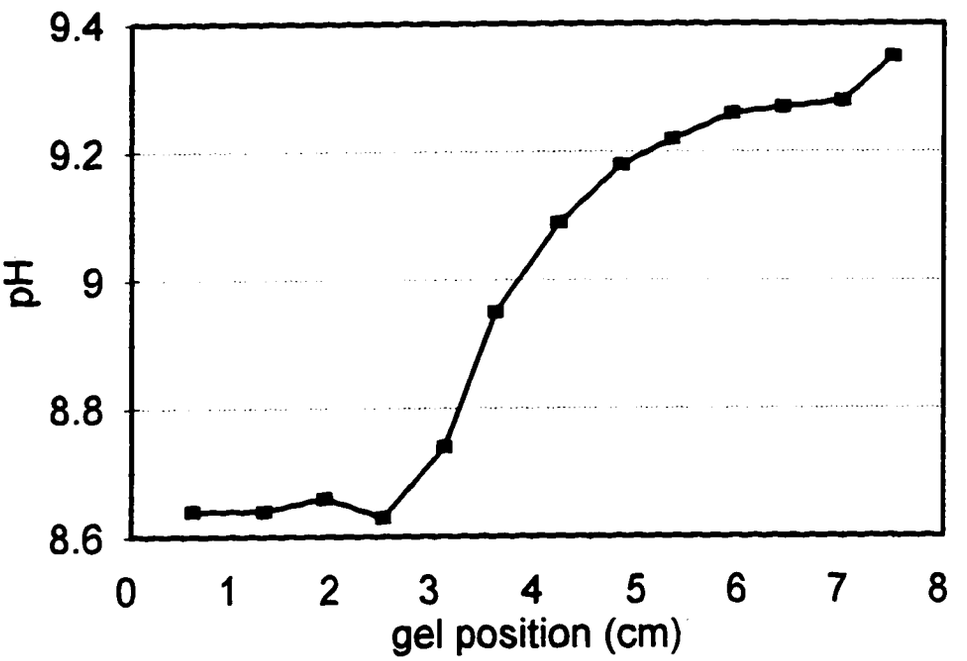

Fig. 21 C

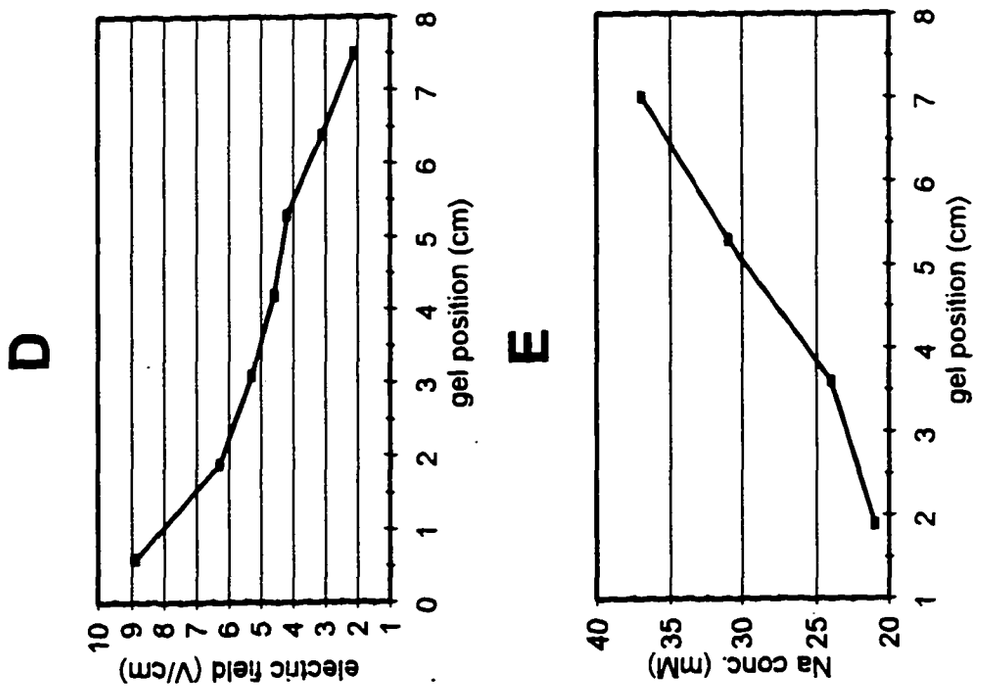

Fig. 21

Figure 22 A. LADH (0.1 mg per ml) focused with MIEF (18 hours), bicine/NaOH buffer; 5.2 mM salicylate in focusing gel; protein applied at anode edge. Filter paper strip stained with Coomassie blue R 250. Isoelectric point 8.09 ± 0.13.

Figure 22 B. LADH (0.1 mg per ml) focused with MIEF (18 hours), bicine/NaOH buffer; 5.2 mM salicylate in focusing gel; protein applied at anode edge. Enzymatically active LADH (micrograms) as a function of gel position (measured with the assay according to Dalziel (a), corrected for salicylate).

Figure 22 C. LADH (0.1 mg per ml) focused with MIEF (18 hours), bicine/NaOH buffer; 5.2 mM salicylate in focusing gel; protein applied at anode edge. pH as a function of gel position.

Figure 22 D. LADH (0.1 mg per ml) focused with MIEF (18 hours), bicine/NaOH buffer; 5.2 mM salicylate in focusing gel; protein applied at anode edge. Electric field strength (volts per centimeter) as a function of gel position.

Figure 22 E. LADH (0.1 mg per ml) focused with MIEF (18 hours), bicine/NaOH buffer; 5.2 mM salicylate in focusing gel; protein applied at anode edge. Sodium ion concentration (mM) as a function of gel position.

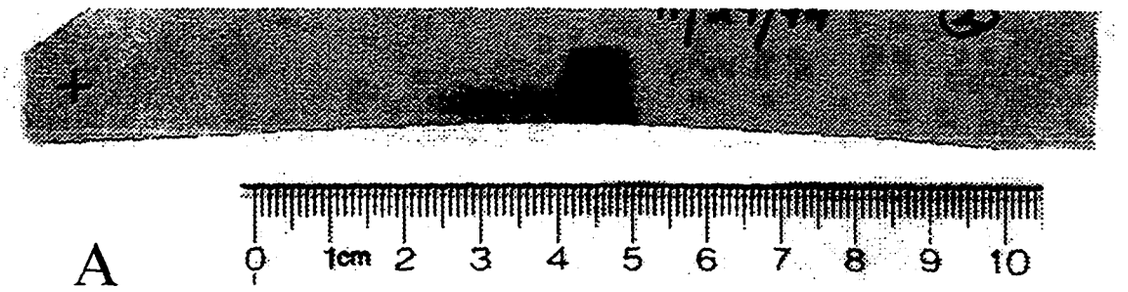

A

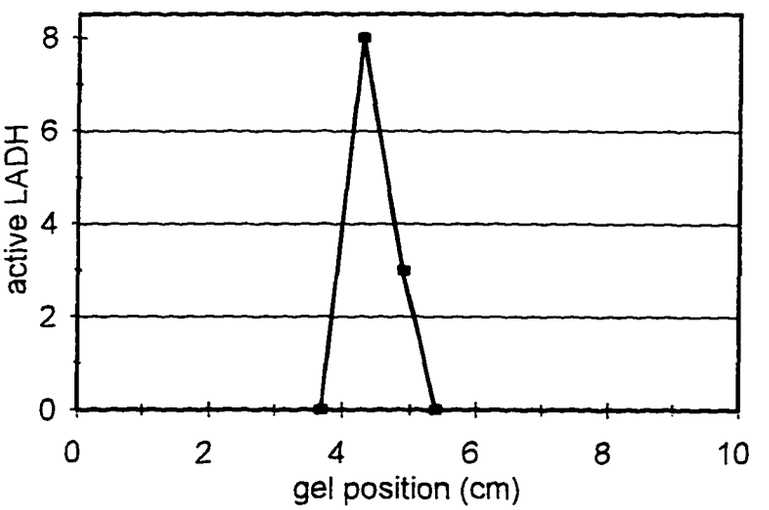

B

Fig. 22

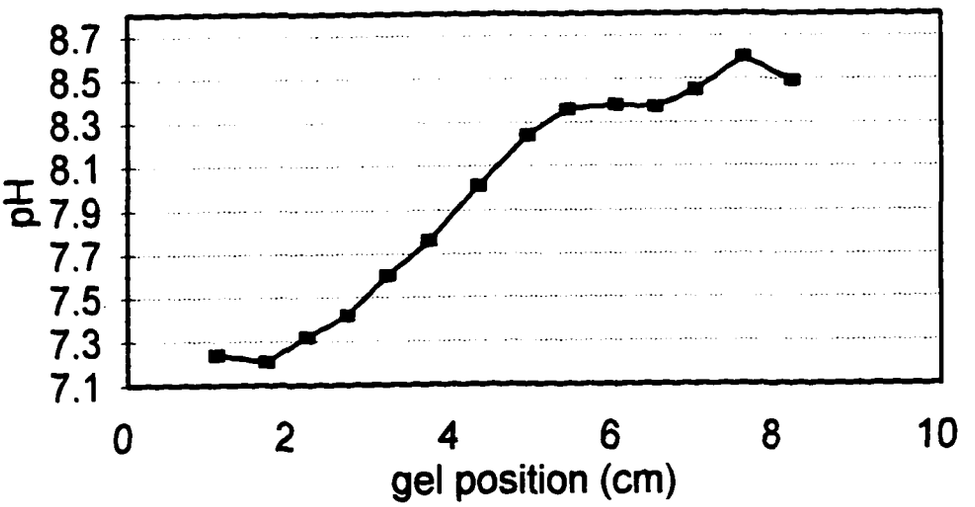

Fig. 22 C

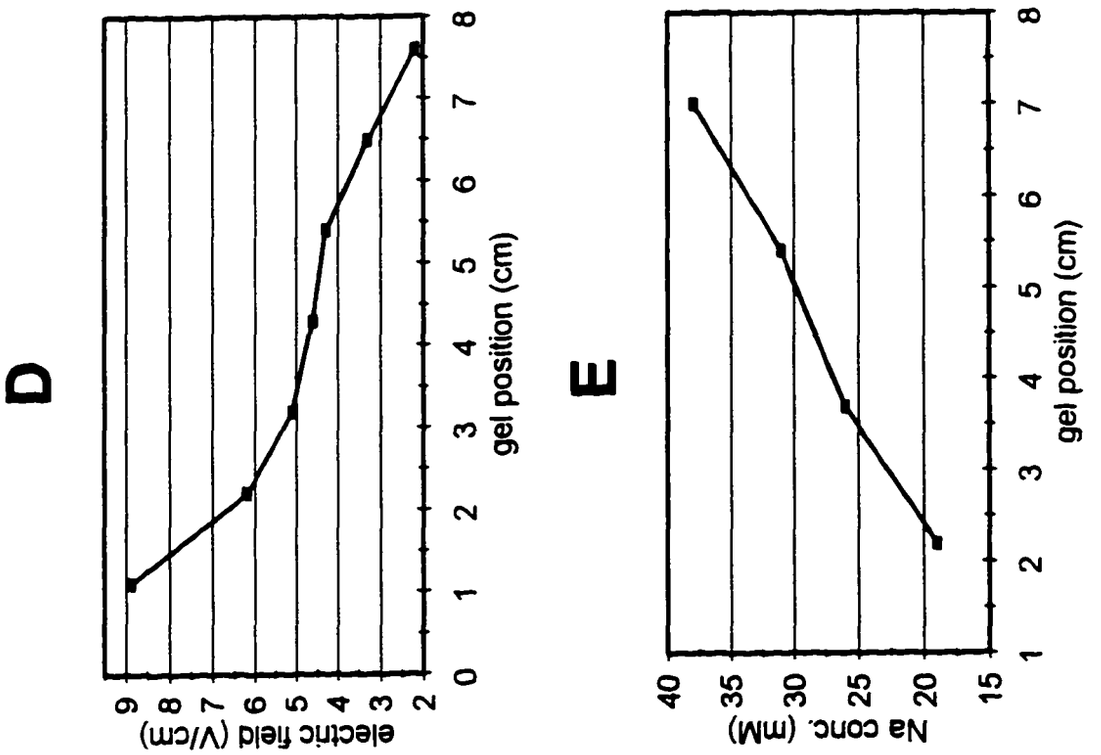

Fig. 22

Figure 23 A. LADH (0.1 mg per ml) focused with MIEF (18 hours), bicine/NaOH buffer; protein applied at anode edge. Filter paper strip stained with Coomassie blue R 250. Isoelectric point 8.96 ± 0.06.

Figure 23 B. LADH (0.1 mg per ml) focused with MIEF (18 hours), bicine/NaOH buffer; protein applied at anode edge. Enzymatically active LADH (micrograms) as a function of gel position (measured with the assay according to Dalziel (a)).

Figure 23 C. LADH (0.1 mg per ml) focused with MIEF (18 hours), bicine/NaOH buffer; protein applied at anode edge. pH as a function of gel position.

Figure 23 D. LADH (0.1 mg per ml) focused with MIEF (18 hours), bicine/NaOH buffer; protein applied at anode edge. Electric field strength (volts per centimeter) as a function of gel position.

Figure 23 E. LADH (0.1 mg per ml) focused with MIEF (18 hours), bicine/NaOH buffer; protein applied at anode edge. Sodium ion concentration (mM) as a function of gel position.

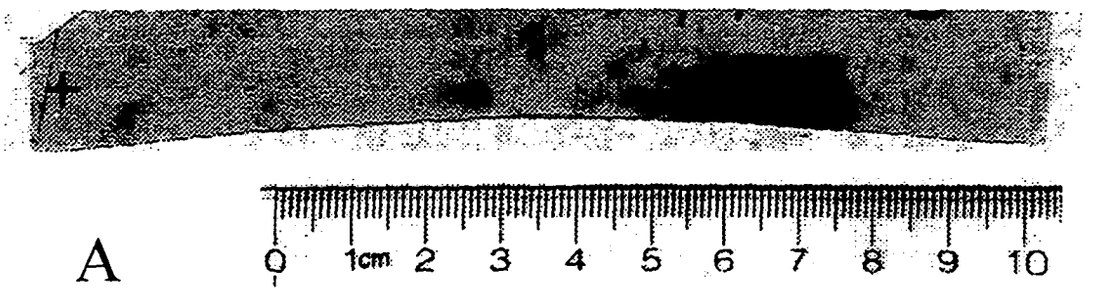

A

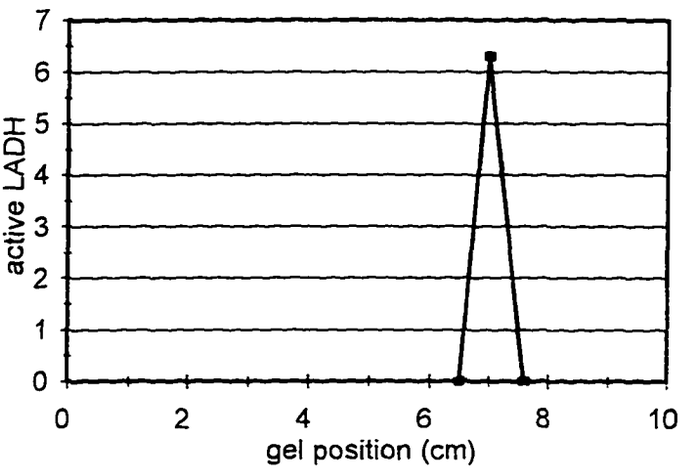

B

Fig. 23

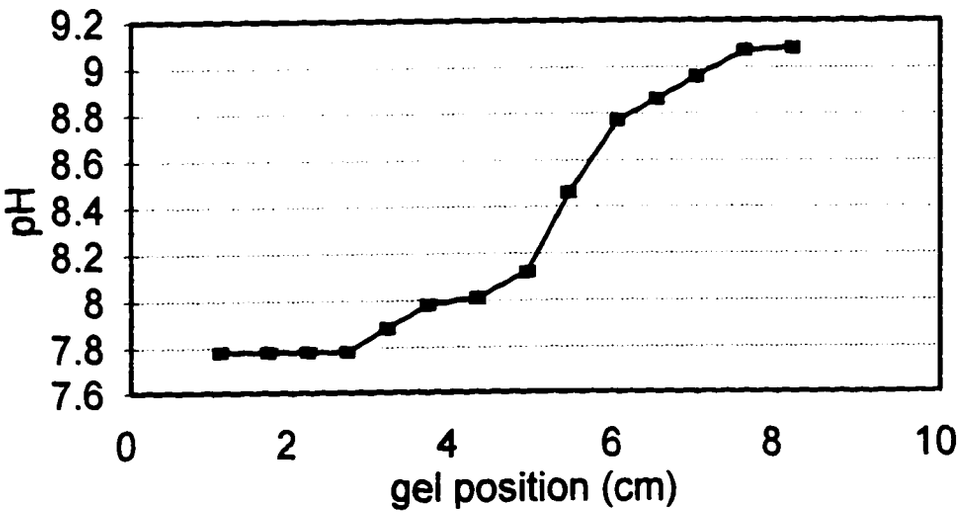

Fig. 23 C

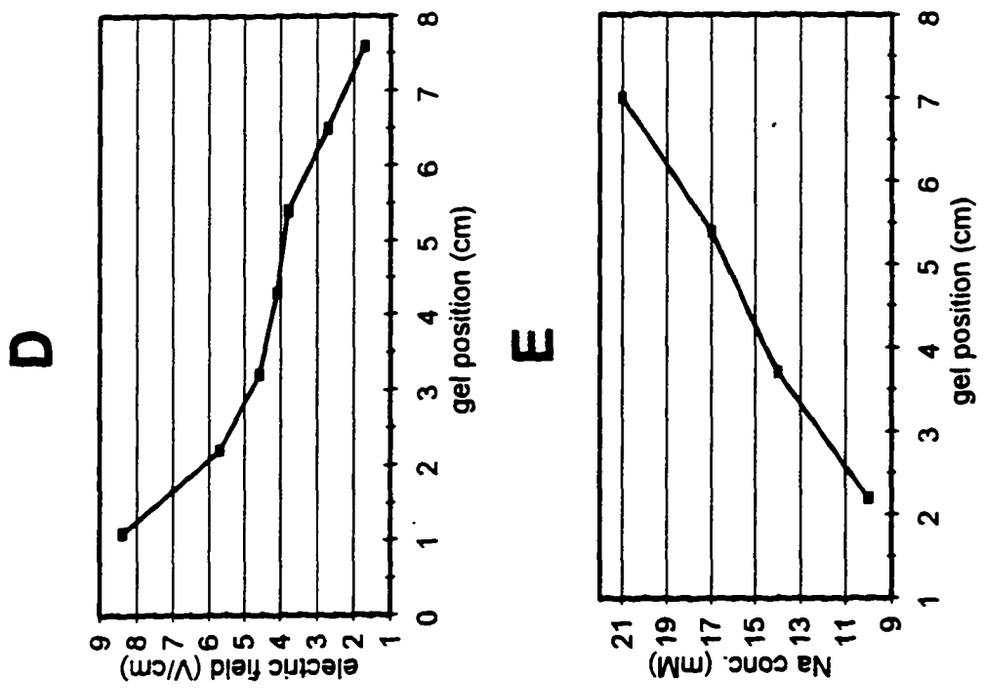

Fig. 23

It is informative to examine the effects due to LADH sample application at a pH below the isoelectric point in a focusing gel with bicine, but in the absence of salicylate. Therefore, an additional MIEF run with bicine was performed under the same conditions as above (protein applied at anode edge of gel) except that salicylate was omitted. Results are shown in figure 23. In the absence of salicylate LADH focuses at a pH close to that at which it focuses in the glycine runs as above, with and without salicylate.

Discussion

Comparison - MIEF vs. Carrier Ampholytes

The experiments presented in this section demonstrate the usefulness of MIEF as an analytical tool. This is evident at the outset of these experiments. MIEF of the EE isoform of LADH affords a comparison of isoelectric focusing in systems with and without ampholytes. As discussed previously, focused bands in carrier ampholyte systems may not be true protein isoforms. Several of these bands may be due to protein complexed with certain ampholyte components. Comparing the banding patterns in carrier ampholyte and MIEF gels as shown in figures 11 and 12, it is seen that they are similar in that there are a number of closely spaced bands focusing over an interval of several tenths of a pH unit. They differ in that two weakly staining discrete higher pH bands on the carrier ampholyte gel are absent in the MIEF gel, but these bands may correspond to isoforms with isoelectric points above the range of the MIEF pH gradient. A significant difference between the MIEF and carrier ampholyte results is that the isoelectric points of the major bands in the MIEF gel (8.9 and above) are

substantially higher than those in the carrier ampholyte gel (7.9 and below). The isoelectric points in the carrier ampholyte gel, as reported, here are also substantially lower than those reported previously for carrier ampholyte focusing of LADH (8.7 and below) (40). The differences in isoelectric point between the present and previous carrier ampholyte experiments may be due to differences in the ampholytes used in these experiments. The present experiments were done with ampholytes containing residues of phosphonic acid and sulfonic acid (Servalyt); previous experiments were done with ampholytes containing only amino and carboxyl groups (Ampholine). It may be that LADH has a significant affinity for phosphonic and/or sulfonic acid groups, causing the binding of ampholytes; this may then lower isoelectric points.

The results of refocusing with carrier ampholytes of fractions from the MIEF gel shown in figure 14, are not consistent with the simple focusing of isoforms at their respective isoelectric points in the MIEF gel. Four of five consecutive fractions focused with MIEF are quite similar when refocused and do not suggest that they contain different protein components. The middle fraction, however, appears to be

substantially different when refocused. Although this fraction contains the same bands as in the other fractions, the relative intensities are substantially altered. This suggests that components focused in the MIEF gel are either isoforms that interconvert at rates that are slow relative to focusing times, or aggregates of isoforms with association / dissociation kinetics that are slow relative to focusing times, or perhaps a combination of these alternatives. Previous carrier ampholyte isoelectric focusing experiments (40) have suggested that the EE isoform of LADH has minor isoforms that interconvert.

Extended focusing of the EE isoform of LADH in the MIEF system, figure 14, demonstrates that what is initially a complex banding pattern collapses over time into one component. Again, this may be explained by slow interconversion of isoforms and/or slow association / dissociation kinetics of aggregate formation. As shown in figure 17, time-limited focusing of low concentrations of protein with MIEF results in a single component, i.e., the complex banding pattern as in figure 13 does not appear. Since protein - protein interactions are concentration dependent,

these results suggest that the complex banding pattern obtained with MIEF for high concentrations of protein is a consequence of aggregate formation. There is evidence from light scattering studies that LADH does undergo some form of aggregate formation (79).

To summarize, the complex banding patterns for LADH obtained with carrier ampholyte focusing in this work are not consistent with previous ampholyte focusing results (40). Moreover, focusing with MIEF either for extended time intervals or with low protein concentrations results in a single protein component. These findings strongly suggest that results obtained with carrier ampholytes are due to artifacts related to ampholyte binding to the protein or to protein-protein interactions that are more probable in the low ionic strength environment of the ampholyte gels.

Experimental pI's Compared to Theory

One of the questions that this study has attempted to answer is: how do results from present theoretical methods for calculating individual residue pK's and isoelectric points

compare with experimental values? In an effort to obtain an answer to this question MIEF measurements of isoelectric point were made for LADH and one of its ligand complexes; these results were then compared to values obtained with FDPB calculations. Specifically, MIEF was employed to measure isoelectric points for LADH and the LADH / NAD^+ / pyrazole complex. The FDPB method was employed to calculate pK's and isoelectric points for the structure of LADH as recorded in the Protein Data Bank (PDB) (75). Unfortunately, the structure for LADH / NAD^+ / pyrazole is not recorded in the PDB; however, a structure, LADH / NAD^+ / p-bromobenzyl alcohol, that is essentially identical to the LADH / NAD^+ / pyrazole structure (H. Eklund, personal communication) is recorded in the PDB, and FDPB calculations for pK's and isoelectric point were performed for this structure; the results are assumed to be the same as for the LADH / NAD^+ / pyrazole structure. (MIEF experiments were not done for p-bromobenzyl alcohol instead of pyrazole because NAD^+ is not as tightly bound in this complex and the costs of providing saturating levels of NAD^+ were prohibitive.)

The results are as follows: the experimental pI for LADH is 8.9; for LADH / NAD^+ / pyrazole the pI is 7.6. Two FDPB calculations were done for each structure, one for dielectric constant $\epsilon = 4$ and one for $\epsilon = 20$. For LADH $\epsilon = 4$ the calculated pI is 7.3; for $\epsilon = 20$ the pI is 8.1. For LADH / NAD^+ /p-bromobenzyl alcohol $\epsilon = 4$ the pI is 6.2; for $\epsilon = 20$ the pI is 7.4. Reviewing these results it is observed that the calculated values are closer to the experimental values for $\epsilon = 20$ rather than for $\epsilon = 4$. Specifically, the calculated pI values for $\epsilon = 20$ are higher than those for $\epsilon = 4$ and therefore closer to the higher experimental values. The lower calculated pI's at $\epsilon = 4$ can be attributed to sizeable downward pK shifts in residues LYS 113 and LYS 323 for both LADH and LADH / NAD^+ / p-bromobenzyl alcohol, and ARG 369 for the latter; these pK shifts are due mainly to desolvation of these residues in the protein which is greater at $\epsilon = 4$ than at $\epsilon = 20$. At $\epsilon = 4$ these residues have effectively less positive charge than at $\epsilon = 20$, and this leads to lower calculated isoelectric points.

Now consider only the change in isoelectric point ΔpI that occurs in forming the LADH / NAD^+ / pyrazole (or p-bromobenzyl

alcohol) complex from apo-LADH, a change that should reflect the addition of charge and pK shifts associated with ligand binding as well as the accompanying well-known conformational change. The calculated isoelectric point change ($\Delta pI = 1.1$ for $\epsilon = 4$; $\Delta pI = 0.7$ for $\epsilon = 20$) is closer to the experimentally measured isoelectric point change ($\Delta pI = 1.3$) for $\epsilon = 4$ rather than for $\epsilon = 20$. The fact that the calculated ΔpI is closer to the experimentally measured ΔpI for $\epsilon = 4$ may be attributed to a pK shift of a single residue. There are no significant shifts in calculated pK's in forming LADH / NAD^+ /p-bromobenzyl alcohol from LADH for either $\epsilon = 4$ or $\epsilon = 20$ except for a sizeable downward shift for ARG 369 (part of a β-sheet of the catalytic domain surrounding the active site zinc) (38) only for $\epsilon = 4$. This downward shift in calculated pK and the associated decrease of positive charge contributes to the decrease in isoelectric point of the LADH / NAD^+ / p-bromobenzyl alcohol complex in addition to the decrease resulting from the addition of negative charge due to ligand binding.

The ΔpI experimental results together with the FDPB calculations suggest that the binding of NAD^+ and substrate

brings about a substantial energy shift for ARG 369 and that the dielectric constant at the position of ARG 369 is closer to 4 than to 20. It should be remembered, however, that FDPB calculations have occasionally resulted in large pK shifts that are not consistent with experiment (65).

A better agreement between theoretical calculations and experiment for the magnitude of isoelectric point shifts as well as the values of isoelectric points might be obtained if the dielectric constant were allowed to vary in the protein. The dielectric constant could be set at values closer to ϵ = 4 in the vicinity of ARG 369 and at higher values in the vicinity of other residues that affect isoelectric points. For example, the dielectric constant in the vicinity of residues LYS 113 and LYS 323 could be raised to 20. This would raise the isoelectric points of both LADH and LADH / NAD^+ / p-bromobenzyl alcohol from values calculated at ϵ = 4 throughout the protein, bringing them closer to experimental values. Effects on the calculated ΔpI's would be negligible. (It may be helpful to refer back to table 1.)

Finally, the slopes of the FDPB calculated titration curves, which range from 3 to 5 charges per pH unit in the range of the isoelectric point, agree reasonably well with the experimental results. The addition of four charges that accompany the binding of NAD^+ and substrate results in an experimental isoelectric point shift of the order of one pH unit as expected from the calculated slopes of the titration curves. The contribution to the pI shift attributable to the conformational change upon binding ligand is not expected to change the charge by large amounts because this conformational change involves only a slight rotation of one domain relative to the other about a narrow neck (38). This order of magnitude agreement of calculated pI shifts with experimental shifts supports the calculated finding that all cysteine and tyrosine residues are substantially desolvated in the protein so that their pK's have large upward shifts thus preventing them from being titrated in the range of the isoelectric point. The null model which assumes that cysteine and tyrosine residues have pK's that allow these residues to be titrated in the range of the isoelectric point give slopes of the order of 20 charges per pH unit in this range.

LADH / Salicylate and pH-Dependent Conformational Change

It can be concluded from previous studies that two molecules of salicylate bind to the LADH dimer. Studies of competitive inhibition by salicylate of NADH binding to LADH (53) as well as x-ray crystallographic studies of LADH / salicylate analog complexes (53) have confirmed that salicylate binds at the adenosine site of the coenzyme binding pocket. The equilibrium dissociation constant has been found to be close to 1.25 mM over the pH range 7 to 10. However, results of MIEF runs with glycine buffer including close to saturating levels of salicylate (figure 21) do not show a downward shift of isoelectric point when compared with MIEF runs with glycine but without salicylate. From the FDPB calculated slopes of the titration curves for LADH a downward shift of the order of 0.5 pH units would be expected for the addition of two negative charges associated with the binding of two salicylate molecules. The absence of a significant shift in isoelectric point in the presence of salicylate suggests that the binding of salicylate is accompanied by proton uptake by the protein. Proton uptake has been shown to accompany the binding of reduced coenzyme NADH to the protein (48); proton uptake also

accompanies the binding of ADP-ribose as well as the heavy metal anion $Pt(CN)_4^{2-}$ which has been shown to bind to the same site as the pyrophosphate of coenzyme (48). The binding of adenosine, however, is not accompanied by proton uptake (48).

It is of interest to consider the FDPB calculated isoelectric point shifts in forming the LADH / ADP-ribose complex from LADH as presented in a previous section. This isoelectric point shift ΔpI is 0.7 at $\epsilon = 4$. If this isoelectric point shift can be corrected for the contribution due to the two additional charges for ADP-ribose relative to salicylate (ADP-ribose brings four negative charges to the LADH dimer; salicylate brings two), it may be meaningfully compared with experimentally measured shifts in forming salicylate complexes. Using the calculated slope of the titration curve of 4 charges per pH unit, the isoelectric point shift in forming the LADH / ADP-ribose complex may be corrected by subtracting 0.5. That is, if ADP-ribose had the same negative charge as salicylate, the FDPB calculated isoelectric point shift would be $0.7 - 0.5 = 0.2$. This is substantially less than the pI shift of 0.5 expected for the addition of two negative charges to the complex. As discussed in a previous

section, this diminished pI shift is attributable to a pK shift for GLU 267 from 4.9 in apo-LADH to 8.5 in LADH / ADP-ribose (for ϵ = 4). This pK shift may also occur in forming the salicylate complex, and it may be the mechanism for proton uptake that prevents the isoelectric point from shifting downward when salicylate binds.

Results of MIEF experiments with a bicine buffer including close to saturating levels of salicylate (figure 22) in which the protein is allowed to approach its isoelectric point from low pH values (protein applied at anode edge of focusing gel) reveals a low pH isoelectric point for what should be the LADH / salicylate complex. This isoelectric point, 8.09, is substantially lower than the isoelectric point measured with glycine, and somewhat lower than what would be expected (from the FDPB calculations) for the addition of the two negative charges of two salicylate molecules to the protein. The fact that the LADH / salicylate complex exhibits two widely separated isoelectric points strongly suggests that this complex undergoes a pH-dependent conformational change; from the theory of titration curves (78) a protein of a given conformation has only one isoelectric point. It appears that

for this low pH conformation a compensating proton uptake does not occur.

For the protein to exhibit the low isoelectric point, the presence of salicylate is required. This is demonstrated with MIEF experiments with bicine but without salicylate, in which the protein is again allowed to approach its isoelectric point from low pH values (figure 23). These experiments show that LADH without salicylate exhibits the same high isoelectric point (within experimental error) as in the glycine experiments, even when the approach is from low pH values. Since the same high isoelectric point is found with both glycine and bicine buffers, it is very probable that there are no significant effects due to change of buffer.

These experiments provide evidence that supports the hypothesis that LADH undergoes a pH-dependent conformational change. This conformational change has been proposed to account for the pH-dependence of the association rates of coenzyme binding (45). As discussed above, the association rates for both NAD^+ and NADH decrease with increasing pH. The conformation at higher pH was proposed to have a more

restricted access to the binding site. From the pH dependence of the association rates it has been suggested that this conformational change is triggered by the ionization of a group with a pK of 9.2 (45,46). If LADH undergoes a pH-dependent conformational change in a range about a pH of 9.2, it is likely that a complex of LADH and a low molecular weight ligand such as salicylate would also undergo a conformational change in a similar pH range. The present MIEF experiments indicate that the LADH / salicylate complex does undergo such a pH-dependent conformational change in a pH range close to 9.2.

Finally, it is of interest to consider the efforts to focus the LADH / NAD^+ complex (figure 20), and their relationship with a pH-dependent conformational change in LADH; the results were anomalous. As was previously discussed, the formation of the LADH / NAD^+ complex involves the addition of negative charge and a conformational change. The structural realignments in the LADH / NAD^+ complex are substantially the same as those that lead to the conformation of the LADH / NAD^+ / pyrazole complex (62); NAD^+, however, is more tightly bound in this ternary complex. As with the LADH / NAD^+ / pyrazole

complex, a substantial shift in isoelectric point for the LADH / NAD^+ complex may be expected. It is reasonable to expect that the isoelectric point of the LADH / NAD^+ complex might be somewhere between that of LADH and that of the LADH / NAD^+ / pyrazole complex, i.e., between 8.9 and 7.6. The focusing of the LADH / NAD^+ complex was carried out in this pH range. The salicylate experiments suggest that LADH undergoes a pH-dependent conformational change in the range 8.1 to 8.9. Hence, the difficulty in focusing the LADH / NAD^+ complex may be due to the fact that this complex has several isoelectric points in a pH range over which pH-dependent conformational change occurs.

It is believed that the experiments with LADH that are presented here are the first to confirm a pH-dependent conformational change in a protein with isoelectric focusing that are not complicated by the ambiguities that may be attributed to carrier ampholytes. Previous studies of pH-dependent conformational change, although sparse, include ampholyte focusing of the 12 s protein of foot-and-mouth disease virus (85). Also, ampholyte focusing experiments with

t-RNA's (86) have suggested pH-dependent conformational change.

Part 3. Conclusions and Future of MIEF

Conclusions

First, I have demonstrated the feasibility of an isoelectric focusing method in which stable pH gradients are established with simple buffer systems. Numerous laboratories have attempted to develop such an isoelectric focusing system (22,87 - 90); among these are the laboratories of A. Kolin (20) and H. Svensson (Rilbe) (21) who are recognized as pioneers in the fields of electrophoresis and isoelectric focusing.

Second, low concentrations of LADH focused with MIEF exhibit a single band. Consequently, the complex banding patterns obtained for LADH (EE isozyme) focused with carrier ampholytes by others and in this work are most likely due to either binding of ampholytes or protein-protein interactions.

Third, from the example of LADH it may be concluded that the FDPB approach for calculating isoelectric points does not give accurate results when compared to experiment. It remains

unclear which dielectric constant, 4 or 20, gives results that are closer to experimental results. Isoelectric point values agree better with experimental values for a dielectric constant of 20. However, a calculated isoelectric point shift in forming a complex is closer to an experimental value for a dielectric constant of 4. The pK's of certain specific residues, calculated using the higher dielectric constant, account for the better agreement between predicted and experimentally determined isoelectric point values. By contrast, the pK of a different residue, calculated using the lower dielectric constant, accounts for the better agreement between theory and experiment for an isoelectric point shift. This suggests that there might be an improvement in theoretical models if the dielectric constant were allowed to vary from one position to another in the protein.

Finally, evidence has been obtained that supports the hypothesis that LADH undergoes a pH-dependent conformational change. Two isoelectric points have been measured for the LADH / salicylate complex. This observation is consistent with a pH-dependent conformational change that occurs in a narrow pH range near its isoelectric point. Anomalous results in

focusing the LADH / NAD^+ binary complex suggest that this complex has multiple isoelectric points, which also is consistent with the hypothesis that LADH undergoes a pH-dependent conformational change.

Future of MIEF

Improvements

Although the present configuration for MIEF provides a practical method for establishing a pH gradient with simple buffers for analytical purposes, improvements may be made. By far, the largest contributions to error in determining the isoelectric point come from uncertainties in gel harvesting and pH measurement. As a result, much of the advantage of high resolution isoelectric focusing is lost. To recapture some of this advantage, investments may be made in hardware to harvest gel sections more precisely. Alternatively, spectrophotometric methods may be applied to measure gel pH in situ, for example, through the use of pH sensitive dyes. An additional approach, which is in principle quite simple, is as follows. A set of marker peptides with closely spaced isoelectric points may be selected that focus in the same range as the protein of interest. These peptides may be individually tagged with a set of covalently attached chromophores. Measuring isoelectric points and isoelectric point shifts for a protein becomes a

simple matter of including the marker peptides in the applied protein sample and determining the position of each focused protein relative to the marker peptides. Of course, it would be necessary to insure that these marker peptides do not interact with the protein of interest. A test for this interaction might be through the use of fluorescent chromophores for the marker peptides; interactions may be revealed through fluorescence anisotropy measurements (91).

Another improvement would be providing a means to record protein concentrations in the gel during the protein focusing process. This could be accomplished, for example, by irradiating the gel with high intensity UV pulses and recording the intensity of fluorescence emission from tryptophan and tyrosine residues (92) as a function of position in the focusing gel. With this capability isoelectric focusing with MIEF could be used to study kinetics of protein-protein interactions. A theoretical analysis of protein concentration distributions that would be expected for steady-state and transient isoelectric focusing of proteins that interact has been presented (34). Early studies of protein-

protein interactions with carrier ampholyte isoelectric focusing have been carried out for hemoglobin isoforms (6).

Protein Purification

The MIEF system should make a significant contribution in the area of protein purification. Carrier ampholyte isoelectric focusing has not been used widely for preparative purposes in the past for several reasons. In addition to providing a low ionic strength environment in which many proteins are insoluble, the cost of carrier ampholytes would be prohibitive for large scale purifications. Also, removal of the carrier ampholytes from the final product adds additional cost and may not be complete leaving the product contaminated with ill-defined high weight molecules. Binding of ampholytes to proteins may further complicate this removal procedure. The immobilized pH gradient methods are also costly; they provide a low ionic strength environment, and are complicated by the possibility of proteins binding to the charged gel matrix. Additionally, residual reactive products formed during gel polymerization may modify proteins being purified (18).

In addition to eliminating problems discussed above, the MIEF method has a capability that should have a substantial impact

on protein purification: this is the capability of forming pH gradients in the presence of salts other than those used for buffering. This attribute may be exploited as follows: in a first isoelectric focusing run a crude protein extract is focused in a pH gradient with only buffering salts, and a focused fraction containing the protein of interest is harvested. This fraction is then subjected to a second isoelectric focusing run; however, in this second run a concentration of a charged ligand that binds specifically to the protein of interest is included in the pH gradient gel. This need not be a tightly binding ligand since relatively high concentrations of it may be included. The first isoelectric focusing run isolated proteins focusing in a very narrow pH interval. The included charged ligand in the second run shifts the isoelectric point of the protein of interest (in a complex with ligand) away from those of the other proteins; this should accomplish a substantial purification in just two steps. The feasibility of shifting the isoelectric point of a protein by including charged ligands in the focusing environment has been demonstrated for tightly binding ligands with the focusing of LADH versus LADH complexed with NAD^+ and pyrazole, and for weakly binding ligands with LADH

versus LADH complexed with salicylate. This procedure should be applicable to a wide range of proteins including receptors and ligands and enzymes and substrates. It may also be possible to apply this procedure to solubilized membrane proteins. In preliminary experiments MIEF pH gradients have been established with gels containing glycerol and lubrol, a non-ionic detergent; both components help to keep membrane proteins solubilized. Several membrane proteins of the rat cytochrome P-450 system have been focused.

Analytical Applications

MIEF also has a bright future as an analytical tool. As previously discussed, this methodology may be applied to problems involving weak ligand binding and conformational changes in addition to evaluating theoretical procedures for calculating important protein parameters. A most interesting future application of MIEF would be to further refine the theoretical methods for approaching problems in electrostatics as related to protein structure and function. Until very recently theoretical calculations assumed a dielectric constant that was held at a fixed value throughout the protein interior. A dielectric constant of 20 has been found to work well for calculating pK's of titratable groups. This value is higher than what might be expected from the composition of proteins and takes into account the flexibility of protein structure. In particular, this takes into account the fact that under the influence of electric fields the dipolar groups in the protein can change their positions to a limited extent; this raises the effective dielectric constant. The results of the comparison of theoretical isoelectric points with

experimental values as presented in this work suggest that in theoretical models the dielectric constant should vary from position to position in the protein. A new theoretical approach to determining a variation in dielectric constant has taken into account the conformational flexibility of amino acid side chains as constrained by the overall protein structure (92). To justify this approach a detailed comparison of predicted and experimental results is needed. Having measured shifts in isoelectric point would allow this comparison. Specifically, replacing a charged residue at a certain position in the protein with a neutral residue using site directed mutagenesis techniques should shift the isoelectric point of the protein by an amount directly dependent upon the local dielectric constant; this experimental result may be compared with a theoretically calculated result to suggest which aspects of the theoretical model are valid and which are not. This procedure could be repeated for many residues in, for example, a certain element of secondary structure, or throughout the protein. In this way it may be possible to answer questions such as: what is the dielectric constant in various types of secondary structure, α-helix, β-sheet, etc. containing amino acid side chains that

are either polar or non-polar, charged or neutral? It may also answer questions like: by what mechanisms do certain kinds of residues in certain types of secondary structure affect the local dielectric constant? These are important considerations because electrostatic interactions depend very heavily upon dielectric constant, and the biological function of proteins depends very heavily upon electrostatic interactions.

References

1. B. Lee, et al (1971) *J. Mol. Biol.* 55, 379.
2. A. Kolin (1954) *J. Chem. Phys.* 22, 1628.
3. H. Svensson (1961) *Acta Chem. Scand.* 15, 325.
4. O. Vesterberg (1969) *Acta Chem. Scand.* 23, 2653.
5. N. Ui (1971) *Biochim. Biophys. Acta* 229, 582.
6. C. Park (1973) *Ann. N.Y. Acad. Sci.* 209, 237.
7. H. Bunn (1973) *Ann. N.Y. Acad. Sci.* 209, 345.
8. N. Ngyuyen, et al (1976) *Anal. Biochem.* 74, 145.
9. B. Radola (1973) *Biochim. Biophys. Acta* 295, 412
10. P. Righetti, et al (1971) *Biochim. Biophys. Acta* 236, 17.
11. G. Baumann (1975) *Anal. Biochem.* 64, 530.
12. L. Kaplan (1971) *Biochem.* 10, 630.
13. K. Wallevik (1973) *Biochim. Biophys. Acta* 322, 75.
14. P. Righetti, et al (1974) *J. Chrom.* 98, 271.
15. M. Jonsson (1980) *Electrophoresis* 1, 3.
16. B. Bjellqvist, et al (1982) *J. Biochem. Biophys. Meth.* 6, 317.
17. P. Righetti, et al (1983) *Electrophoresis* 4, 393.
18. P. Righetti, et al (1984) *J. Chromatogr.* 291, 31.
19. C. Cuono (1982) *Electrophoresis* 3, 65.

20. S. Luner, et al (1970) *Proc. Nat. Acad. Sci. USA* 66, 898.

21. H. Rilbe (1978) *J. Chromatogr.* 159, 193.

22. P. Wenger, et al (1986) *J. Biochem. Biophys. Meth.* 13, 259.

23. P. R. Bergethon, et al (1989) *Biophysical Chemistry*, Springer Verlag, New York.

24. R. Ward, et al (1971) *Biochem. Biophys. Res. Comm.* 45, 1444.

25. T. Laue, et al (1989) *Anal. Biochem.* 182, 377.

26. N. Lakshminarayanaiah (1965) *Chem. Rev.* 65, 491.

27. B. Radola (1973) *Biochim. Biophys. Acta* 295, 412.

28. R. Aschaffenburg, et al (1957) *Nature* 180, 376.

29. S. Timasheff, et al (1964) *Nature* 203, 517.

30. O. Vesterberg (1967) *Acta Chem. Scand.* 21, 206.

31. H. Gregor, et al (1964) *J. Phys. Chem.* 68, 2201.

32. O. Vesterberg, et al (1966) *Acta Chem. Scand.* 20, 820.

33. H. Svensson (1961) *Acta Chem. Scand.* 15, 325.

34. D. Stimpson, et al (1977) *Biophys. Chem.* 7, 115.

35. J. Matthew, et al (1982) *Biochem.* 21, 4989.

36. W. Smythe (1968) *Static and Dynamic Electricity*, McGraw-Hill, New York.

37. R. Pietruszko (1980) *Current Topics in Biol. Med. Res.* 4, 107.

38. C. Branden, et al (1975) *The Enzymes*, 3rd Ed. 11, 103.

39. H. Sund, et al (1963) *The Enzymes*, 2nd Ed. 7, 25.

40. U. Lutstorf, et al (1970) *Eur. J. Biochem.* 17, 497.

41. A. Akeson (1964) Biochem. *Biophys. Res. Comm.* 17, 211.

42. H. Eklund, et al (1981) *J. Mol. Biol.* 146,561.

43. D. C. Anderson, et al (1982) *Biochem.* 21, 3569.

44. I. Ohlsson, et al (1974) *J. Mol. Biol.* 89, 339.

45. J. Kvassman, et al (1979) *Eur. J. Biochem.* 100, 115.

46. M. Eftink, et al (1986) *Biochem.* 25, 6624.

47. S. Subramanian, et al (1979) *J. Biol. Chem.* 254, 7827.

48. P. Andersson, et al (1980) *Eur. J. Biochem.* 108, 303.

49. M. Hennecke, et al (1983) *Biochem.* 22, 3721.

50. W. Laws, et al (1978) *J. Biol. Chem.* 253, 8593.

51. R. Dworschack, et al (1977) *Biochem.* 16, 2716.

52. J. Mani, et al (1971) *Biochemie* 53, 355.

53. R. Einarsson, et al (1974) *Eur. J. Biochem.* 49, 41.

54. P. Gunnarsson, et al (1974) *FEBS Lett.* 43, 289.

55. P. Gunnarsson, et al (1974) *Eur. J. Biochem.* 43, 479.

56. B. Vallee, et al (1957) *J. Biol. Chem.* 225, 185.

57. T. Boiwe, et al (1977) *Eur. J. Biochem.* 77, 173.

58. H. Theorell, et al (1961) *Acta Chem. Scand.* 15, 1811.

59. H. Eklund, et al (1979) *J. Biol. Chem.* 254, 3458.

60. A. Winer, et al (1960) *Acta Chem. Scand.* 14, 1729.

61. H. Theorell, et al (1963) *Biochem. Z.* 338, 537.

62. E. Eklund, et al (1982) *Biochem.* 21, 4858.

63. H. Theorell, et al (1969) *Acta Chem. Scand.* 23, 255.

64. J. Matthew (1985) *Ann. Rev. Biophys. Biophys. Chem.* 14, 387.

65. J. Antosiewicz, et al (1994) *J. Mol. Biol.* 238, 415.

66. J. Ribeiro, et al (1991) *Comput. Biol. Med.* 21, 131.

67. K. A. Sharp (1990) *Ann. Rev. Biophys. Biophys. Chem.* 19, 301.

68. E. L. Mehler, et al (1991) *Protein Engineering* 4, 903.

69. M. Bucher, et al (1986) *J. Phys. Chem.* 90, 3406.

70. T. J. Webb (1926) *J. Am. Chem. Soc.* 48, 2589.

71. L. B. Richards, et al (1971) *J. Mol. Biol.* 55, 379.

72. C. Tanford (1972) *Biochem.* 11, 2192.

73. A. Yang, et al (1993) *Proteins Struct. Func. Gen.* 15, 252.

74. D. Bashford, et al (1991) *J. Phys. Chem.* 95, 9556.

75. F. C. Bernstein, et al (1977) *J. Mol. Biol.* 55, 379.

76. B. R. Brooks (1983) *J. Comp. Chem.* 4, 187.

77. Catalog (1993) *Biosym Technolgies, Inc.* San Diego, CA

78. C. Tanford (1961) *Phys. Chem. of Macromolecules*, John Wiley & Sons, New York.

79. K. Moser, et al (1968) *Enzym. Biol. Clin.* 9, 447.

80. K. Dalziel (1957) *Acta Chem. Scand.* 11, 397.

81. K. van Holde (1985) *Physical Biochemistry*, Prentice Hall, Englewood Cliffs, N.J., 139.

82. C. Long, ed. (1961) *Biochemists' Handbook*, E. and F. N. Spon, London, 320.

83. P. Serwer, et al (1982) *Electrophoresis* 3, 80.

84. J. Ross (1979) *Biophys. Chem.* 10, 217.

85. P. Talbot (1975) *Isoelectric Focusing*, J. Arbuthnott, et al, eds. Butterworths, London, 270.

86. J. Drysdale, et al (1972) *Biochem.* 11, 4044.

87. P. Lundahl (1973) *Ann. NY Acad. Sci.* 209, 94.

88. A. J. P. Martin (1978) *J. Chromatogr.* 159, 101.

89. F. Hampson (1983) *Electrophoretic Techniques*, C. F. Simpson, et al eds. Academic Press, New York, 231.

90. R. A. Mosher (1984) *Electrophoresis '84*, V. Neuhoff, ed., Verlag Chemie, Weinheim, 79.

91. C. Cantor et al (1980) *Biophysical Chemistry*, W. H. Freeman, New York.

92. T. J. You et al (1995) *Biophys. J.* 69, 1721.